

**Experimental Evaluation of Axial, Shear, and Moment Forces of
Double Angle Connections when Subjected to Unanticipated Loading**

by

Max A. Morache

A Report Submitted to the Faculty of the
Milwaukee School of Engineering
in Partial Fulfillment of the
Requirements for the Degree of
Master of Science in Architectural Engineering

Milwaukee, Wisconsin

May 2019

Abstract

Double angle shear connections are commonly found in steel frame buildings because of their ease of design, fabrication and installation. While these connections are normally designed for only vertical shearing force, previous research has proven that these connections can resist an interaction of shear, axial, and moment forces. There exists a need for further research concerning the behavior of these connections due to their abundant use throughout the engineering and construction industries.

The purpose of this thesis was to observe and quantitatively measure the interaction of forces in double angle connections. Results from this research illustrate the behavior of these connections during an unanticipated loading event: the compromising and collapse of the center support in a steel frame building. In this study, robustness, redundancy and structural integrity of the connection were considered. Test results were used to establish the level of flexural capacity and presence of catenary action of various double angle connections.

To study and analyze the performance of these connections, physical testing was commenced on nine double angle connections, mounted in a testing frame, consisting of 3-, 4-, and 5-bolt configurations. Data collected during this testing were used to calculate forces, including axial, shear, and moment, at the connection and along the length of a supported beam within the testing frame. Further analysis explored failure modes and overall test assembly performance.

Testing showed that double angle shear connections possess a level of flexural resistance, and catenary action occurred in the test assembly beyond the flexural resistance range of this connection. Every tested double angle connection exhibited high levels of ductility, and aside from angle unfolding, did not pose a risk of brittle failure under the limitations present during testing. Excessive rotation of the member, interaction of shear, axial and moment, combined with the unfolding of the connecting angles and eminent binding of the beam flanges with the column flanges indicates that while double angle connections provide a certain level of robustness, they are incapable of supporting full design loads due to the additional shear and moment introduction.

Acknowledgments

Many people and organizations contributed to the completion of this thesis. First and foremost, I would like to thank Milwaukee School of Engineering for funding this project and providing testing equipment. I would also like to thank Germantown Iron and Steel for their gracious donation of testing materials and specimens.

Undoubtedly, this project would not have been possible without the guidance, wisdom and patience of my advisor, Chris Raebel, Ph.D. Thank you to Douglas Stahl, Ph.D. and Todd Davis, Ph.D. for assisting with the data collection technology. Thank you also to Jeff MacDonald, who assisted with material acquisition and testing.

This work would not have been possible without the support of Michelle Van Buskirk, who has contributed significant amounts of time and effort towards the success of this thesis as she worked concurrently on her thesis project.

Finally, I am grateful for the everlasting support of my family and friends, who have been understanding of the time that I had to spend away from them to complete this thesis. I look forward to spending more time with you soon.

Table of Contents

| | |
|---|----|
| List of Figures | 8 |
| List of Tables | 13 |
| Nomenclature | 14 |
| Glossary | 16 |
| Chapter 1: Introduction | 17 |
| Chapter 2: Literature Review | 19 |
| 2.1. AISC Provisions on Robustness | 19 |
| 2.2. Behavior of Steel Shear Connections under Column-Removal Demands by Oosterhof and Driver..... | 20 |
| 2.2.1. Testing Setup | 20 |
| 2.2.2. Specimen Geometry..... | 21 |
| 2.2.3. Experimental Results | 22 |
| 2.2.4. Column Bolt Line Failure Characteristics | 24 |
| 2.3. Test, Modeling and Design of Bolted-Angle Connections Subjected to Column Removal by Yanglin Gong..... | 26 |
| 2.3.1. Testing Configuration | 27 |
| 2.3.2. Experimental Results | 29 |
| 2.3.3. Mechanical Properties in Tension..... | 30 |
| 2.3.4. Mechanical Properties in Compression | 33 |
| 2.3.5. Conclusions..... | 34 |

| | |
|---|----|
| 2.4. Modeling of Double-Angle Connections for Robustness Evaluation of Steel Gravity Frames by Weigand, Liu and Main..... | 34 |
| 2.4.1. Modeling Approach | 35 |
| 2.4.2. Model Evaluation..... | 37 |
| 2.4.3. Geometry of Deformed Angle | 38 |
| 2.4.4. Load-Deformation Relationship | 39 |
| 2.4.5. Angle Fracture at Ultimate Load | 41 |
| 2.4.6. Comparisons with Experimental Data | 43 |
| 2.4.7. Conclusions..... | 44 |
| 2.5. Integrity of Bolted Angle Connections Subjected to Simulated Column Removal by Weigand and Berman..... | 44 |
| 2.5.1. Bolted Angle Assemblages | 45 |
| 2.5.2. Experimental Setup..... | 48 |
| 2.5.3. Equipment and Instrumentation..... | 49 |
| 2.5.4. Connection Response Quantities | 50 |
| 2.5.5. Fiber Displacements from Experiments..... | 51 |
| 2.5.6. Experimental Results | 52 |
| 2.5.7. Influence of Connection Parameters on the Bolted Angle Connection Responses | 61 |
| 2.5.8. Effect of Angle Thickness on Connection Response..... | 62 |
| 2.5.9. Absolute Connection Strength and Connection Performance | 63 |
| 2.5.10. Staggering of Bolt Holes..... | 64 |
| 2.6. Building Code of the City of New York..... | 67 |

| | |
|--|-----|
| 2.7. Steelwork Connections – The Robustness of Simple Connections by Owens and Moore | 67 |
| Chapter 3: Experimental Program | 70 |
| 3.1. Introduction..... | 70 |
| 3.2. Test Specimen Overview | 70 |
| 3.3. Test Assembly Overview | 73 |
| 3.4. Test Procedures..... | 78 |
| 3.4.1. Assembling of Testing Frame..... | 78 |
| 3.4.2. Pre-Test Procedure..... | 78 |
| 3.4.3. Test Procedure | 80 |
| 3.4.4. Post-Test Procedure | 82 |
| Chapter 4: Experimental Results | 84 |
| 4.1. Introduction..... | 84 |
| 4.2. Determination of Forces | 84 |
| 4.2.1. Determination of Connection Forces | 85 |
| 4.3. Determination of Bolt Forces..... | 88 |
| 4.4. Results of Experimental Tests | 88 |
| 4.4.1. Three-Bolt Double-Angle Tests..... | 89 |
| 4.4.2. Four-Bolt Double-Angle Tests | 101 |
| 4.4.3. Five-Bolt Double-Angle Tests..... | 113 |
| 4.5. Summary of Test Results | 125 |
| 4.6. Verification of Data Results..... | 127 |

| | | |
|------------|---|-----|
| Chapter 5: | Discussion and Conclusion | 130 |
| 5.1. | Introduction..... | 130 |
| 5.2. | Conclusions..... | 130 |
| 5.3. | Comparisons of Test Results with Results in Literature..... | 132 |
| 5.4. | Future Research | 134 |
| References | 136 | |

List of Figures

| | |
|--|----|
| Figure 2.2-1: Experimental setup..... | 20 |
| Figure 2.2-2: Testing configuration for double angle specimens. | 21 |
| Figure 2.2-3: Development of plastic hinges in double angles..... | 22 |
| Figure 2.2-4: Tear propagation near the heel..... | 24 |
| Figure 2.2-5: Tear propagation near column bolts..... | 24 |
| Figure 2.2-6: Load development plot of a double angle test. | 25 |
| Figure 2.2-7: Propagation of tears along the column bolt line. | 26 |
| Figure 2.3-1: Testing frame. | 27 |
| Figure 2.3-2: Group C and D configurations.. | 27 |
| Figure 2.3-3: Testing frame. | 28 |
| Figure 2.3-4: Specimen C1 failure..... | 30 |
| Figure 2.3-5: Specimen C2 failure..... | 30 |
| Figure 2.3-6: Tear along C3 specimen..... | 30 |
| Figure 2.3-7: D1 specimen..... | 32 |
| Figure 2.3-8: Compressive load on angle. | 33 |
| Figure 2.4-1: Schematic assembly overview and symmetry boundary constraints..... | 37 |
| Figure 2.4-2: (a) Horizontal reaction versus chord rotation for varying beam spans, and (b) average horizontal deformation of angle versus chord rotation. | 38 |
| Figure 2.4-3: (a) Initial angle geometry, and (b) deformed angle geometry. | 38 |
| Figure 2.4-4: Load-deformation relationship for angle. | 40 |
| Figure 2.4-5: Two-hinge idealization of angle's column leg at ultimate load: (a) geometry and (b) free-body diagram. | 41 |

| | |
|---|----|
| Figure 2.4-6: Comparisons of component-based model with experimental measurements for a double-angle connection with three bolt rows (uncertainty is estimated at +/- 0.5% based on repeated instrument calibration). | 44 |
| Figure 2.5-1: Typical bolted-bolted configuration..... | 46 |
| Figure 2.5-2: Load frame assembly. | 48 |
| Figure 2.5-3: Free body diagram of testing frame. | 49 |
| Figure 2.5-4: Method for computing fiber displacements. | 52 |
| Figure 2.5-5: Phases of vertical and horizontal force-displacement behavior for ba3b 34 14 | 53 |
| Figure 2.5-6: Phases of vertical and horizontal force-displacement behavior for ba3b 34 14 | 53 |
| Figure 2.5-7: Phases of vertical and horizontal force-displacement behavior for ba3b 34 12 | 54 |
| Figure 2.5-8: Phases of vertical and horizontal force-displacement behavior for ba3b 34 12 | 55 |
| Figure 2.5-9: Plastic hinge formation in 1/4-in. angles (top) and 1/2-in. angles (bottom). | 56 |
| Figure 2.5-10: Specimen ba3b 34 14 post-test. | 57 |
| Figure 2.5-11: Specimen ba3b 34 12 post-test. | 58 |
| Figure 2.5-12: Normalized vertical responses of 1/4-in. 3- and 5-bolt specimens. | 62 |
| Figure 2.5-13: Extreme column warping of specimen ba3b 1 34 | 63 |
| Figure 2.5-14: Staggered angle configuration. | 65 |
| Figure 2.5-15: Specimen ba3b 34 14 HConfig compared to ba3b 34 14 | 66 |

| | |
|--|----|
| Figure 2.5-16: Specimen ba3b 34 12 HConfig compared to ba3b 34 12 | 66 |
| Figure 2.7-1: Critical sections in double-angle connections..... | 69 |
| Figure 3.2-1: Naming convention example. | 70 |
| Figure 3.2-2: Angle configurations for testing with (a) 3 bolt lines, (b) 4 bolt lines, and (c) 5 bolt lines. | 71 |
| Figure 3.3-1: Test assembly overview..... | 73 |
| Figure 3.3-2: Test assembly overview..... | 74 |
| Figure 3.3-3: Bolt naming convention for (a) 2L3, (b) 2L4, and (c) 2L5 configurations. | 74 |
| Figure 3.3-4: Hydraulic cylinder assembly..... | 75 |
| Figure 3.3-5: Strain gage placement on beam. | 76 |
| Figure 3.3-6: Strain gage placement for (a) 2L3, (b) 2L4 and (c) 2L5 specimens. | 77 |
| Figure 3.4-1: Plaster application on 2L3 specimen. | 79 |
| Figure 3.4-2:Lateral torsional buckling of test assembly..... | 80 |
| Figure 3.4-3: Measurement of LTB behavior. | 81 |
| Figure 3.4-4: 2L3-2 test following completion..... | 82 |
| Figure 4.4-1: Typical 2L3 assembly before testing. | 90 |
| Figure 4.4-2: Typical LTB behavior of a 2L3 series specimen during testing. | 91 |
| Figure 4.4-3: Typical 2L3 series specimen post-test. | 91 |
| Figure 4.4-4: Typical post-test layout of 2L3 series specimen..... | 92 |
| Figure 4.4-5: Typical left-hand side of a 2L3 series specimen following testing..... | 92 |
| Figure 4.4-6: Typical right-hand-side of a 2L3 series specimen following testing..... | 93 |
| Figure 4.4-7: Enlargement of plaster application on test specimen 2L3-2, typical of 2L3 series tests. | 93 |

| | |
|--|-----|
| Figure 4.4-8: Load versus displacement for 2L3 series of tests. | 96 |
| Figure 4.4-9: Load versus rotation for 2L3 series of tests with respect to DWT1 (US units). | 97 |
| Figure 4.4-10: Load versus rotation for 2L3 series of tests with respect to DWT1 (Metric units). | 98 |
| Figure 4.4-11: Load versus rotation for 2L3 series of tests with respect to DWT2 (US units). | 99 |
| Figure 4.4-12: Load versus rotation for 2L3 series of tests with respect to DWT2 (Metric units). | 100 |
| Figure 4.4-13: Typical 2L4 assembly before testing. | 101 |
| Figure 4.4-14: Typical LTB behavior of 2L4 series specimen during testing. | 102 |
| Figure 4.4-15: Typical 2L4 specimen post-test. | 103 |
| Figure 4.4-16: Typical underside view of specimen post-test showing angle deformation. | 104 |
| Figure 4.4-17: Typical post-test layout of 2L4 series specimen. | 104 |
| Figure 4.4-18: Typical left hand-side of a 2L4 series specimen following testing. | 105 |
| Figure 4.4-19: Typical right hand-side of a 2L4 series specimen following testing. | 105 |
| Figure 4.4-20: Plaster flake on specimen 2L4-1. | 106 |
| Figure 4.4-21: Force versus displacement for 2L4 series of tests. | 108 |
| Figure 4.4-22: Load versus rotation for 2L4 series of tests with respect to DWT1 (US units). | 109 |
| Figure 4.4-23: Load versus rotation for 2L4 series of tests with respect to DWT1 (Metric units). | 110 |

| | |
|--|-----|
| Figure 4.4-24: Load versus rotation for 2L4 series of tests with respect to DWT2 (US units). | 111 |
| Figure 4.4-25: Load versus rotation for 2L4 series of tests with respect to DWT2 (Metric units). | 112 |
| Figure 4.4-26: Typical 2L5 assembly before testing. | 113 |
| Figure 4.4-27: Typical LTB behavior of 2L5 series specimen during testing..... | 114 |
| Figure 4.4-28: Typical 2L5 specimen post-test. | 115 |
| Figure 4.4-29: Typical post-test layout of 2L5 series specimen. | 116 |
| Figure 4.4-30: Typical left hand-side of a 2L5 series specimen following testing..... | 117 |
| Figure 4.4-31: Typical right hand-side of a 2L5 series specimen following testing. | 117 |
| Figure 4.4-32: Plaster flake on specimen 2L5-1. Typical for 2L5 series of tests. | 118 |
| Figure 4.4-33: Force versus displacement for 2L5 series of tests..... | 120 |
| Figure 4.4-34: Load versus rotation for 2L5 series of tests with respect to DWT1 (US units). | 121 |
| Figure 4.4-35: Load versus rotation for 2L5 series of tests with respect to DWT1 (Metric units). | 122 |
| Figure 4.4-36: Load versus rotation for 2L5 series of tests with respect to DWT2 (US units). | 123 |
| Figure 4.4-37: Load versus rotation for 2L5 series of tests with respect to DWT2 (Metric units). | 124 |
| Figure 4.6-1: Free body diagram for statics evaluation as seen in Friedman (2009)..... | 127 |

List of Tables

| | |
|---|-----|
| Table 2.5-1: Connection sub-assemblages (Weigand & Berman, 2016)..... | 47 |
| Table 2.5-2: Bolted angle connection sub-assemblage force and deformation quantities at failure (Weigand & Berman, 2016). | 60 |
| Table 3.2-1: Double-Angle Connection limit state strength (without safety factors)..... | 72 |
| Table 4.5-1: Test Values at Maximum Moment, US units. | 125 |
| Table 4.5-2: Test Values at Maximum Moment, metric units..... | 126 |
| Table 4.6-1: Static Check Percent Error for 2L Tests..... | 129 |

Nomenclature

Symbols

A – area

B – resultant force acting on one bolt

C – coefficient for eccentrically loaded bolt group

E – modulus of elasticity

F_u – ultimate stress of material, ksi

F_y – yield stress of material, ksi

H – normalized shear force

I – moment of inertia

L_{beam} – length of beam

L_{eh} – horizontal edge distance

M – bending moment, kip-in or kip-feet

P – axial load, kips

R – nominal shear strength of one bolt at deformation

V – applied shear force, kips

e – eccentricity

t – thickness of material

y – distance from neutral axis

ε – strain

Δ – deflection, inch

θ – angle of rotation, radians

ϕ – factor of safety

σ – stress

μ – micro

Abbreviations

ACI – American Concrete Institute

AISC – American Institute of Steel Construction

Avg – Average

DTI – Direct Tension Indicator

DWT – Draw Wire Transducer

ft – feet

HSSL – Horizontally short-slotted bolt hole

IBC – International Building Code

ICOR – instantaneous center of rotation

in. – inches

ksi – kips per square inch

lbs or lb – pounds

psi – pounds per square inch

SG – strain gage

2L – double angle configuration

Glossary

catenary – curve described by a rope hanging from two points on the same horizontal plane

catenary action – tensile force acting along the geometry of a catenary

kips – 1000 pounds

progressive collapse – failure in adjoining structural elements that originated from failure in a primary structural element

Chapter 1: Introduction

Structural robustness, or the ability of a building to resist progressive collapse that is disproportionate to the causative event, is of increasing importance in engineering design. Robustness has become of increased concern especially following events such as the Ronan Point apartment collapse of 1968 and especially the World Trade Center Terrorist Attacks. In each of these cases, a collapse was initiated by an unanticipated loading event but perpetuated by a lack of robustness in the design of the structural system. Catastrophic events similar to those aforementioned occur to this day, sometimes accompanied by significant occupant casualty.

Proper specification and design of structural connections between framing members is a method to ensure adequate provision of structural robustness. Understanding the behavior of simple shear connections under unanticipated loading scenarios is therefore crucial toward the proper specification and design, given their widespread use in steel framed buildings. Examples of unanticipated loading scenarios may include the compromising of a structural element due to vehicle impact, material strength reduction resulting from extreme temperature increase during a fire, concussive force emanating from an explosive blast, and localized overburdening of a framing member among countless others.

There are many types of simple shear connections, namely: shear tab; extended plate; end plate; seated; single angle; tee; and double angle. While these connections are typically designed solely to resist vertical shearing force, these connections have the capability of resisting a simultaneous combination, or interaction, of shear, axial, and moment forces. The capability for these connections to resist this interaction is

advantageous during an instance of unanticipated loading, however, varying levels of ductility among those mentioned result with different levels of deformation and failure modes.

The AISC Steel Construction *Manual* and *Specification* (AISC, 2017) is of limited help in the design of steel connections for robustness, requiring designers to look elsewhere for guidance. However, ACI 318-14 (ACI Committee 318, 2014) allows for reductions in load due to the inherent robustness of concrete. Following the 9/11 terrorist attacks, the International Building Code (International Code Council, 2019) has incorporated requirements relating to structural integrity and robustness.

The purpose of this research is to both qualitatively and quantitatively evaluate the robustness of bolted-bolted double-angle connections. Nine all-bolted double-angle specimens of 3-, 4- and 5-bolt configurations were tested in a manner consistent with a central column-loss scenario, upon which excessive rotation is developed in the connection. This excessive rotation and column loss event imparted an interaction of shear, axial and moment forces through the double-angle connection, and these forces were measured through strain gages applied to a testing beam and connection bolts themselves.

Chapter 2: Literature Review

Significant research is in progress relating to the robustness of framing connections. This research is important toward understanding behavior of various connection geometry performance while under unanticipated loading scenarios. However, there lacks a significant amount of research relating to double angle connection behavior under shear, axial and moment interaction. Several existing researchers propose models to anticipate rotation, while others perform finite element modeling of double-angle connections. There are few examples of full-scale testing that have been performed. A summary of past and current research and practices are included herein. Note that units are reported in US Customary and may have been converted from their original format.

2.1. AISC Provisions on Robustness

Section J1.4 (b) in the AISC *Specification* (AISC, 2017) relates to robustness explicitly in column splices, requiring designers to anticipate a tensile force in the connecting elements for 50% of the axial tensile force on the compression element, or to proportion 2% of total column axial load capacity as a transverse load. According to the Commentary, the intent of this procedure is to provide additional robustness to the design of compression members. However, this section does provide guidance in the design of shear connections. Generally, there lacks specific language in the specification relating to, or how to achieve, a robust design.

2.2. Behavior of Steel Shear Connections under Column-Removal Demands by Oosterhof and Driver

Oosterhof and Driver (2015) conducted full scale experiments on 35 steel shear connections, consisting of shear tab, welded-bolted single angle, bolted-bolted single angle, and bolted-bolted double-angle connections. The bolted-bolted double-angle connections will be the focus of this section. A testing frame was designed to apply independent levels of moment, shear, and axial force to beam-column connections shown in Figure 2.2-1.

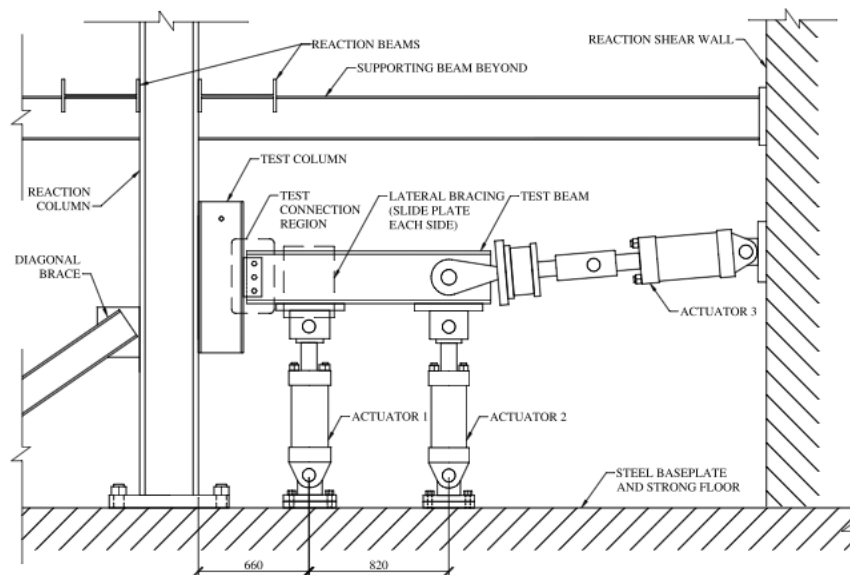


Figure 2.2-1: Experimental setup (Oosterhof & Driver, 2015).

2.2.1. Testing Setup

The use of two vertical actuators, Actuator 1 and 2, allowed for any combination of moment and shear desired, while Actuator 3 was oriented to apply primarily axial load on the connection. All actuators were pinned to their support, allowing free rotation in the plane of the beam about their end. A load cell within each actuator provided loading

information, a clinometer measured axial rotation of each actuator, and a cable transducer measured axial stroke of each actuator. These instruments provided data used to calculate the magnitude, direction, and location of force applied to the test beam by each actuator explicitly throughout the test. In turn, an accurate representation of the three applied forces into their orthogonal components for the calculation of shear, moment and axial force applied to the connection, was possible. Beam rotation was measured using clinometer mounted to the centerline of the beam web, while strains and displacements in the connection region were measured using a digital image correlation system.

2.2.2. Specimen Geometry

The double-angle specimens were $2L3\frac{1}{2} \times 3\frac{1}{2} \times \frac{1}{4}$ with a yield strength of 50 ksi, with either three or five bolt holes spaced at 3.15 inches. Testing bolts were $\frac{3}{4}$ -in. A325 bolts, mounted in all standard holes, fastened to a snug tight condition. Connection geometry is shown in Figure 2.2-2.

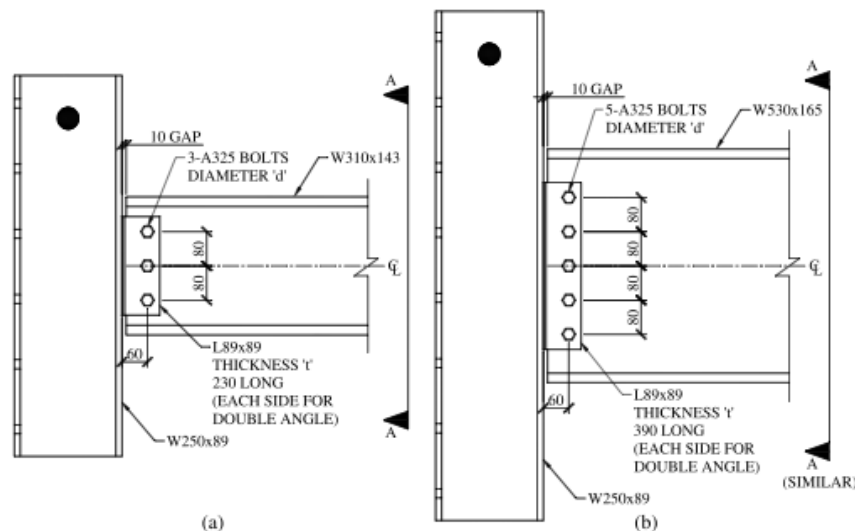


Figure 2.2-2: Testing configuration for double angle specimens (Oosterhof & Driver, 2015).

2.2.3. Experimental Results

Oosterhof and Driver observe that bolted-bolted angle connections exhibit significantly different failure mechanisms than welded-bolted angles, primarily the development of plastic hinges near the bolt line of the heel. The proposed location of these plastic hinges is shown in Figure 2.2-3. Throughout testing, it was found that plastic hinges formed first in location 1 and 3.

It is noted that the unfolding of the angle material results with significantly lower axial and rotational stiffness and higher ultimate rotation values than shear tabs and welded-bolted single-angles with like geometries.

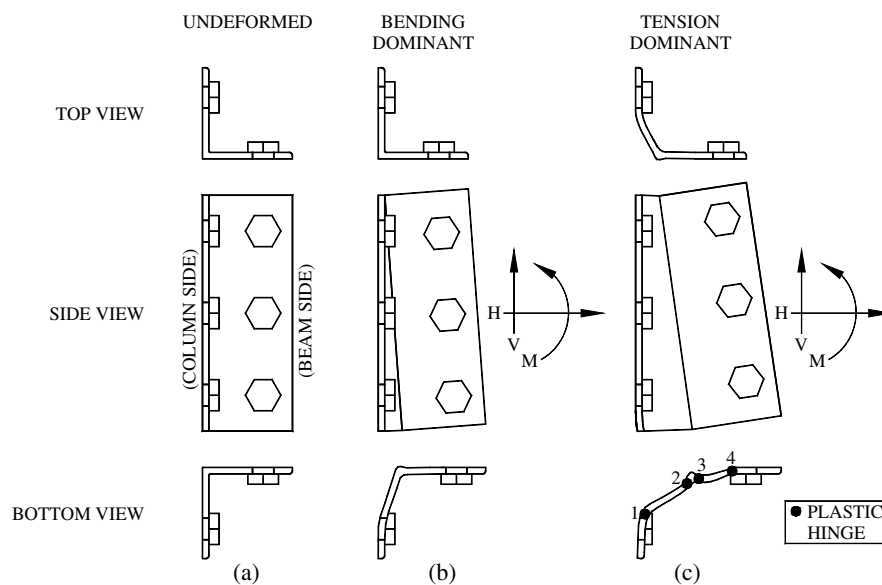


Figure 2.2-3: Development of plastic hinges in double angles (Oosterhof & Driver, 2015).

Oosterhof and Driver do acknowledge that, because the test setup used a three-pin arrangement for Actuator 3, the level of compressive axial force developed during testing was limited. For each test, compressive arching action was observed only at early stages of the loading history: after these early stages, it was found that the developing catenary action resulting from large rotations dominated connection behavior. Bolt bearing

deformation, while visible, never progressed to bolt tear-out or localized block shear rupture failure modes. Bearing deformations at the extreme bolt on the beam-side connection were measured to be less than 3 mm in each test, a relatively small contribution toward the overall ductility when compared to the deformation resulting from angle unfolding.

All angle connections failed by the propagation of a tear initiating from either the bottom heel of the angle, as shown in Figure 2.2-4, or along the length of the column-side connection bolts nearest to the beam web as shown in Figure 2.2-5. Tearing of the gross section near the angle heel, while not commonly observed, was found to be unstable; any increase in rotation caused the tear to continue along the length of the angle with an accompanied decrease in load. This failure mode at times occurred suddenly, with immediate formation of tears across the entire depth of the angle. This type of failure, because it resulted in complete connection failure, may be considered brittle failure mode most akin to tensile rupture. This failure mode typically occurred at the beam side of the angle heel.



Figure 2.2-4: Tear propagation near the heel (Oosterhof & Driver, 2015).



Figure 2.2-5: Tear propagation near column bolts (Oosterhof & Driver, 2015).

2.2.4. Column Bolt Line Failure Characteristics

Tears forming at the column bolt line was the most common type of failure. These tears would follow a jagged path from bolt to bolt but would be arrested before reaching a subsequent bolt hole. This arrest allowed the connection to find new load paths. Upon examination of connection bolts used in one of these types of failures it was found that no shear deformation had occurred and bolt bearing deformation at the beam-side connection of the angle was limited to less than 1 mm. Figure 2.2-6 shows a load development plot typical of a double angle test failing along a plastic hinge which developed at the column bolt line.

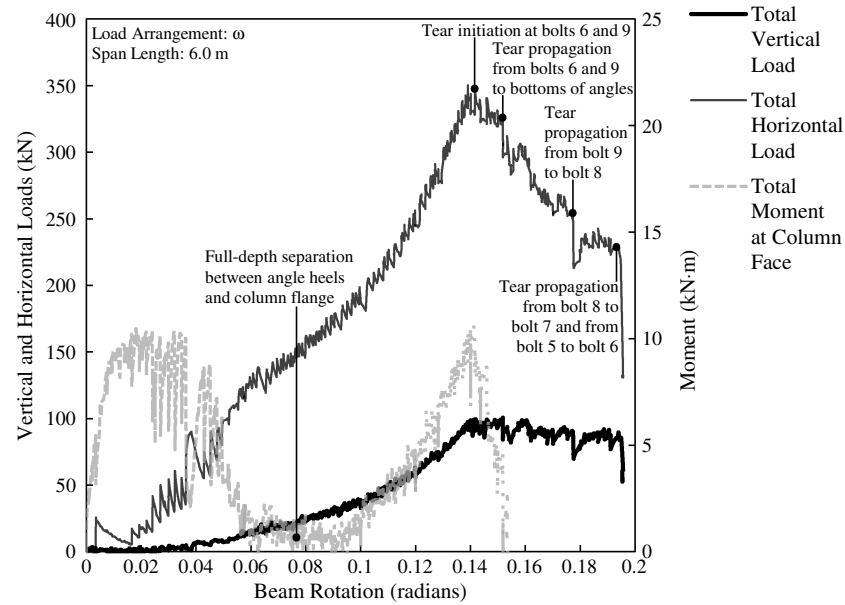


Figure 2.2-6: Load development plot of a double angle test (Oosterhof & Driver, 2015).

Photographs of the angles during this test are shown in Figure 2.2-7. In the test shown, a tear is propagating along the heel of the angle, following a jagged path from bolt hole to bolt hole. The maximum horizontal load was recorded immediately prior to tear initiation at the bottom column bolt hole. A stepwise decrease in load capacity is observed, and results from the initiation and progression of tears along the depth of the angle leg along the column flange. The plateau in the total vertical loading data indicates

a significant presence of residual capacity in the connection despite the progression of these tears along the depth of the angle.

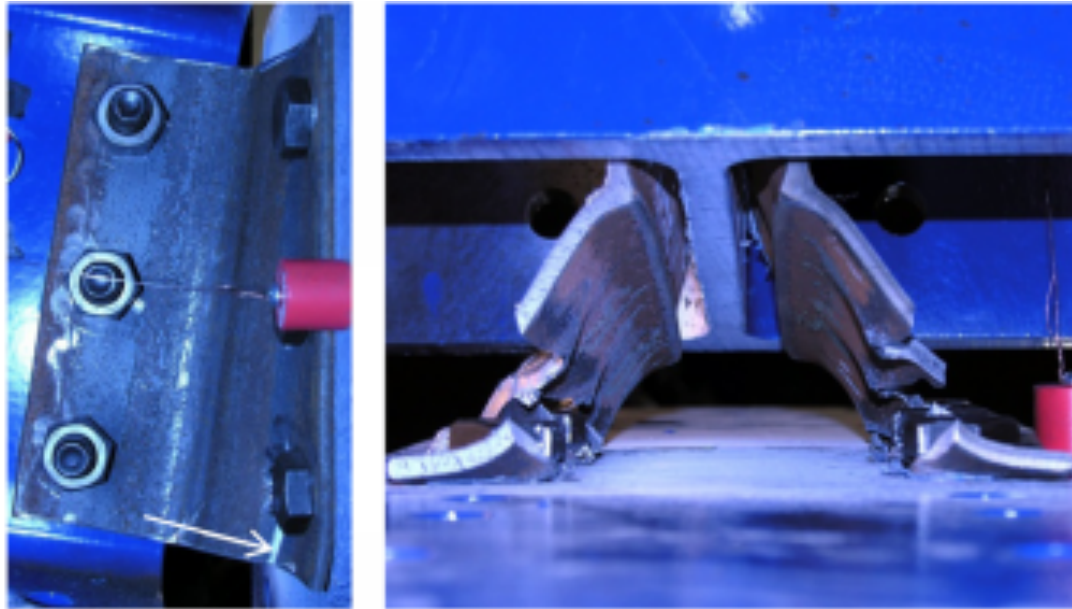


Figure 2.2-7: Propagation of tears along the column bolt line (Oosterhof & Driver, 2015).

2.3. Test, Modeling and Design of Bolted-Angle Connections Subjected to Column Removal by Yanglin Gong

Gong (2017) performed full-scale tests on six specimens of double-angle connections within a testing frame. The specimens were divided into two groups: one group consisting of only double web angles and another group which incorporated both double web and flange angles into the connection. Double web angles will be the primary focus of this review. The testing frame configuration is shown in Figure 2.3-1; note, however, that this figure depicts flange angles.



Figure 2.3-3: Testing frame (Gong, 2017).

The test beams were W12x136 beams composed of Grade 50 material. A large member was chosen to ensure reusability throughout testing and to better match the span-to-depth ratio of common practice, given the laboratory's span limitations during testing. To provide lateral stability to the testing assembly as well as to balance the catenary action, a pair of HSS5x5x5/16 tubes flanked the column as shown in Figure 2.3-4.

Two linear displacement sensors were placed under the middle of the column to provide deflection readings, and a load cell was used to record the load applied to the assembly. Strain gages were installed at the half-length point of each testing beam to record strains to calculate axial force and bending moment. A dial gage was used to monitor the horizontal displacement of each reaction column.

Gong employed a quasi-static test procedure which used a jack to slowly apply load to the assembly at a rate of no greater than 20 mm per minute while the readings from the strain gages, linear displacement sensors and load cells were recording. A block was inserted between the piston of the jack and the load cell if the maximum stroke of the jack was reached, and loading was subsequently resumed. Testing was terminated once continued loading was not possible.

2.3.2. Experimental Results

Gong recognized that among the variety of specimens tested, connection configurations using only web angles exhibited much lower levels of stiffness than configurations which incorporated flange angles. As a result, the maximum stroke of the jack was reached for each double-angle connection, requiring Gong to block the jack to increase assembly deformation. For each specimen tested, failure was always asymmetric about the centerline of the middle column, despite the symmetrical nature of the double-angle connections.

For test C1, the first angle rupture occurred on the left-side beam of the assembly on one angle only. Loading continued until the other angle on the same beam ruptured. These ruptures occurred at the gross section of the angle as shown in Figure 2.3-4. Specimen C2 failed by one of the right-side angles. Because of this failure, the central column tilted dramatically and therefore the testing was terminated immediately. The failure also occurred at the gross section of the angle, along the yield line near the heel of the angle. This location of failure agrees with the plastic hinge locations proposed by Oosterhof and Driver (2015). For C3, the first failure was a partial tear located along the bolt line of the column-side leg of the angle, which was followed by a complete tear along an identical bolt line on the other angle as shown in Figure 2.3-5. The partial tear of the other angle during the C3 test is shown in Figure 2.3-6.



Figure 2.3-4:
Specimen C1
failure (Gong,
2017).



Figure 2.3-5:
Specimen C2
failure (Gong,
2017).



Figure 2.3-6: Tear
along C3 specimen
(Gong, 2017).

2.3.3. Mechanical Properties in Tension

From testing, Gong works toward the development of a spring-model of behavior for the angles tested, which is written as the summation of the deformations from three sources to achieve the total deformation capacity of an angle-spring model, Δ_u . Thus:

$$\Delta_u = \Delta_{au} + \Delta_s + \Delta_{bm}, \quad (2.3-1)$$

where

Δ_{au} is the deformation from the unfolding mechanism of the angle legs,

Δ_s is the bolt slip, and

Δ_{bm} is the deformations between the connected beam and the column.

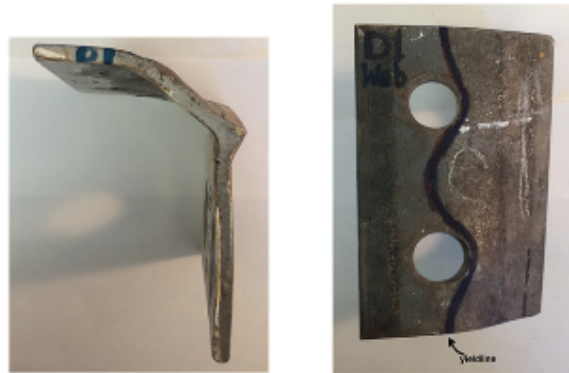
The quantification of deformation resulting from each of these sources is complex and varies with many factors, such as steel strength, angle size, bolt gages, stiffness and strength ratios between the angle and the bolt, and the interaction of shear, moment and catenary force exhibited on the connection assembly. While the purpose of this review is

to focus on experimental behavior, it is useful to consider the contributions of various components and how they may be applicable to connection behavior in general.

A significant source, if not the most significant source of deformation resulting from testing performed by Gong, is the failure of angle material. From testing, the primary failure mode of angles loaded with a significant catenary force and shear is gross rupture near the heel. Gong acknowledges that this contradicts the common perception that the net section at the bolt-line is weaker and would thus fracture first. While Oosterhof and Driver (2015) propose that the shift of this failure location is due to a developed plastic hinge at several locations along the angle, Gong attributes this failure to the constraint that the bolt heads introduce on the bending of the angle leg.

It is argued that among thinner angles which deform more significantly under catenary action, the bearing of the unfolding angle material against the bolt head contributes greatly to the formation of a yield line along the angle. Figure 2.3-7 shows a web angle from a Group D test, with the yield line of the angle being shown in Figure 2.3-7(b). This yield line is not straight; the yield line starts at the bottom of the angle

along a line drawn through the bolt group, but then begins to wrap around the location the bolt heads in a zig-zag fashion, increasing the yielding area of steel.



(a) bending of web angle of D1 (b) the web angle of specimen D1

Figure 2.3-7: D1 specimen (Gong, 2017).

Gong suggests that the yield line would move closer to the toe of the angle (away from the heel) as angle thickness is increased or bolt diameter is decreased. Since the thickness of specimen C3 was much higher than that of D1, the bending yield line was effectively along the net section, and therefore the net section fractured as shown in Figure 2.3-6. In Oosterhof and Driver's (2015) specimens, angle ruptures were observed only along the gross section at the heel when 7/8-in. diameter bolts were used but occurred along the net section when 3/4-in. diameter bolts were used.

Rupture at the net section of the bolt line was more likely to occur when a specimen was subjected to a combination of catenary tension and shear. The web specimens of test C3 were subjected to this combination of forces and experience rupture at the net section, while the same angles experienced rupture of the gross section when subjected to pure tension. However, when under a shear load, the net section is always the critical section irrespective of the constraints introduced by the bolts on the bending of the angle leg.

For the maximum deformation capacity of a double-angle connection to be achieved, the bolts must possess an equal or higher strength than the angles. The bolt slip between plies is also important, especially when considering bolt holes that are larger than standard, such as oversize or slotted holes. Movement of bolts within these holes may allow the connection to rotate before a bolt fully engages and begins to impart a force on the connection.

2.3.4. Mechanical Properties in Compression

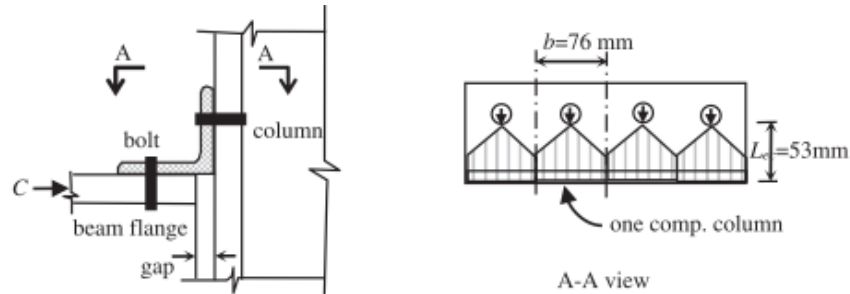


Figure 2.3-8: Compressive load on angle (Gong, 2017).

The capacity of an angle in compression, as shown in Figure 2.3-8, is relatively unknown. Gong proposes that an angle under a compressive load as shown may be analyzed by considering the outstanding leg a rectangular column with the imparted compressive load spanning outward from the bearing of a bolt by a 45-degree angle to yield the width of the column, w_{ec} . Therefore:

$$w_{ec} = \left(\left(\frac{1}{L_{ec}} - \frac{b}{2} \right) b + \left(\frac{b}{2} \right)^2 \right) \text{ and } w_{ec} \leq b, \quad (2.3-2)$$

where L_{ec} is the length of the equivalent column and b is the spacing of the bolts. The column stiffness, K_{bc} , may then be found using a spring model. Thus:

$$K_{bc} = \frac{EA}{L_{ec}} = \frac{E(w_{ec})t}{L_{ec}}, \quad (2.3-3)$$

where t is the angle thickness. The compressive yielding strength, B_y , is calculated using the yield strength of the material as:

$$B_y = (w_{ec})tF_y, \quad (2.3-4)$$

which is smaller than the bearing strength at the bolt holes, B_n , calculated per the Canadian steel code as:

$$B_n = 3.0tF_u d_b, \quad (2.3-5)$$

where d_b is the diameter of the bolt holes and F_u is the ultimate strength of the angle.

2.3.5. Conclusions

It was found that Group C angles were able to undergo much higher rotations than Group D before failure. The primary mode of failure for Group D angles was flange angle failure at the bottom flange, as that angle is furthest from the center of rotation and consequently sees the highest load. Group C angles developed little to no arching action but developed large catenary forces. It is suggested that beam length and angle sizes are coordinated to prevent binding between the beam and column flange so as to prevent the introduction of additional force; that flange angles be used to increase the load carrying capacity of the connection and prevent unfolding of the web angles; and to use slotted holes in the beam leg of the angle to allow for rotation before bolt engagement.

2.4. Modeling of Double-Angle Connections for Robustness Evaluation of Steel Gravity Frames by Weigand, Liu and Main

Weigand, Liu and Main (2017) developed component-based models of bolted double-angle beam-to-column gravity frame connections. Development of these models resulted from high-fidelity finite-element models which used solid elements to model the

bolts, angles and wide-flange sections, with friction and contact modeled explicitly. Fracture and reduced ductility at the “k-area” of the angle were also included in the model. These high-fidelity analyses were used to investigate the relationship between span length and the unfolding mechanisms of the angle and overall connection failure, including angle deformations at fracture. Plastic hinge formation, angle leg straightening and tearing of the angle near the heel were able to be analyzed from the model. This model was then compared to experimental data for double-angle connections that were subjected to an interaction of rotation and catenary force like that which would be seen during a column-loss event.

2.4.1. Modeling Approach

High-fidelity finite-element models were analyzed and validated by comparison to experimental testing. The modeling was performed in the LS-DYNA finite-element software package, and the components modeled included the double angles, bolts and wide flange sections, with each component modeled using 8-node solid elements. The element sizes for each component were chosen to best capture plastic-hinging mechanisms and fracture. The radius of the fillet of the angle was explicitly modeled. All components were modeled in contact with one another, with a static and dynamic coefficient of friction of 0.3 used, matching the coefficient for slip-critical class A connections.

A piecewise linear plasticity material model calibrated to match material tensile coupons was used to model the various steel elements. The plastic strain limit for each material was matched to its corresponding coupon test, and measures were made within the modeling process to ensure that the engineering stress-strain curves corresponded to

the test data. Steel fracture was simulated by element erosion at a certain plastic strain limit.

Ductility reductions were made in the k-area of the heel to correspond to previous tests as proposed by Liu et al. (2016). This ductility reduction in the k-area is attributed to the rotary straightening process conducted in the mill during the rolling of the angle material.

The span conditions used during the test was a two-span beam assembly with exterior pin supports and an interior column stub that would be vertically loaded to force rotation upon the connections. However, the actual model used was only one half of this assembly; symmetry conditions were used to simulate the other half of the model about the centerline of the column.

The beams and columns were A992 Grade 50 material, and the sections used for the beams and the column were W16x26 and W10x49 shapes, respectively. The angles were modeled as L4x3½x5/16 with A572 Grade 50 material and had a depth of 8.5 inches. Three rows of ¾ inch F1852 tension-control bolts were placed in standard holes at a gage of 3 inches on the column-leg and a 2 ½ inch gage on the beam-leg. A horizontal edge distance of 2 inches was used on the beam. The top bolt was located 5 inches from the top of the beam. A schematic overview of the testing setup is shown in Figure 2.4-1.

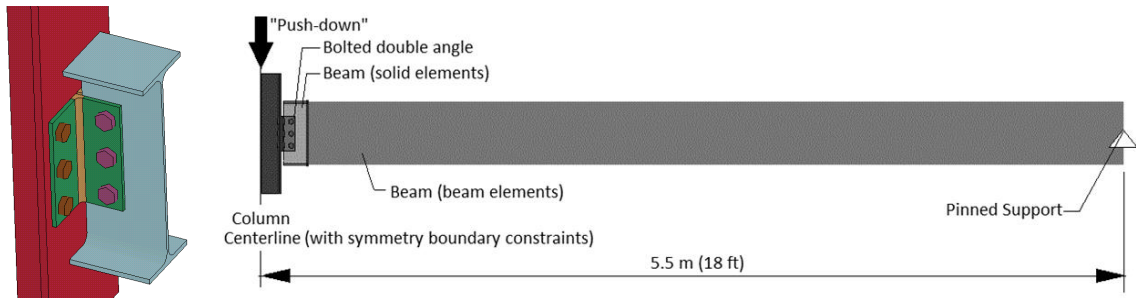


Figure 2.4-1: Schematic assembly overview and symmetry boundary constraints (Weigand, Liu, & Main, 2017).

2.4.2. Model Evaluation

Results from model analysis indicated that the length of beam span played a role in the robustness of the connection, with fracture occurring at a lower rotation when a longer beam was used. It is mentioned that a longer beam span results with a greater elongation at the connection for identical beam chord rotations when compared to shorter beams. It was found, however, that horizontal deformation at failure was only slightly affected by the beam span length. The first fracture at the connection occurred at the bottom of the angle near the k-area of the column leg of the angle and then propagated upward through the angle as loading continued. This is consistent with other research (Gong, 2017; Oosterhof & Driver, 2015; Weigand & Berman, 2016). Horizontal deformation of the angle increased with varying magnitude in relation to a decrease in span length, but the angle deformation at first fracture was nearly constant across tests. The relationship of chord rotations to the horizontal reaction at the connection and the deformation of the angle is shown in Figure 2.4-2(a) and Figure 2.4-2(b).

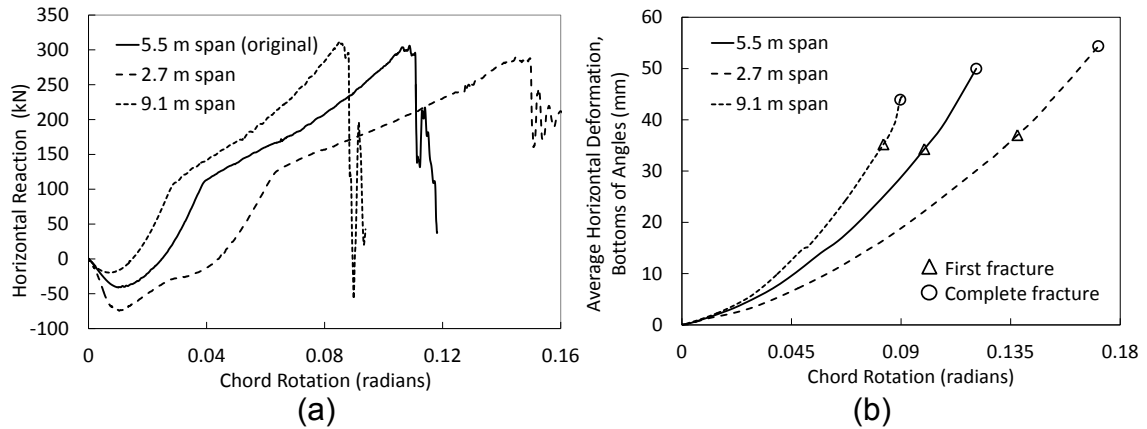


Figure 2.4-2: (a) Horizontal reaction versus chord rotation for varying beam spans, and (b) average horizontal deformation of angle versus chord rotation (Weigand, Liu, & Main, 2017).

2.4.3. Geometry of Deformed Angle

Results from testing and the use of a high-fidelity finite-element model under specific loading and restraint conditions is shown in Figure 2.4-3. Note that the angle legs were truncated at the bolt locations and the angles were modeled as fully fixed at these locations.

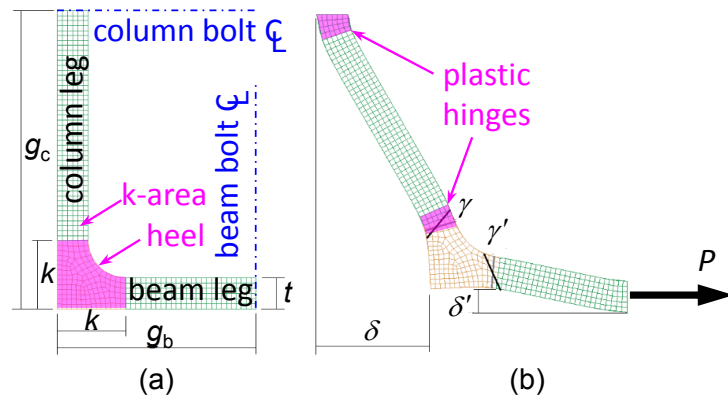


Figure 2.4-3: (a) Initial angle geometry, and (b) deformed angle geometry (Weigand, Liu, & Main, 2017).

Notation used in Figure 2.4-3 is significant for the development of a component-based model, and therefore is worthy of definition: g_c is the column gage length of the angle, g_b is the beam leg gage length of the angle, and t is the thickness of the angle, δ is

the deformation along the beam axis, δ' is the lateral deformation along the beam leg, and γ and γ' are the curvatures at the ends of the k-area in the column and beam legs, respectively.

Like testing performed by other researchers, it was found that plastic hinges formed at several locations along an angle leg as it unfolds with continued loading. Results of the high-fidelity analysis allows relationships to be established between the curvatures and strains near the k-area of the angle, therefore facilitating the development of a component-based model.

2.4.4. Load-Deformation Relationship

A piecewise-linear relationship was established to represent the behavior of the angle while undergoing various levels of loading. This relationship is based on the axial load P and the angle deformation δ . A single angle was considered with a component width of b which was found by dividing the total angle depth by the number of bolts. The load corresponding to one bolt row of the double angle connection was found by simply doubling the load P . The yield capacity P_y corresponds with the development of plastic hinges at the column leg of the angle, and the ultimate capacity P_u is associated with fracture of the angle near the k-area. The load deformation relationship is shown in Figure 2.4-4.

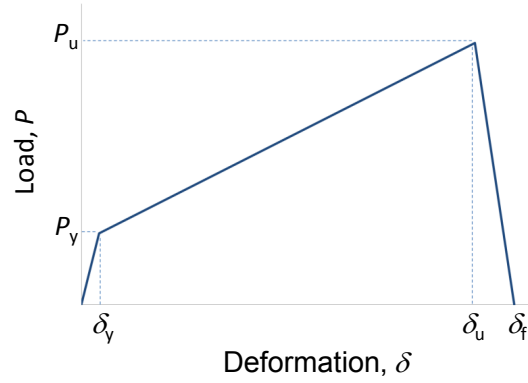


Figure 2.4-4: Load-deformation relationship for angle (Liu, Main, & Sadek, 2016).

The yield load P_y which corresponds to the formation of the two plastic hinges in the column leg of the angles as reflected in Figure 2.4-3 is found by:

$$P_y = \frac{2M_p}{g_{eff}}, \quad (2.4-1)$$

where

$$M_p = \left(\frac{bt^2}{4} \right) F_y,$$

F_y = yield strength of the angle,

$$g_{eff} = g_c - k - \frac{d_h}{2}, \text{ and}$$

d_h = diameter of column-leg bolt holes.

The angle deformation following the formation of plastic hinges, δ_y , is calculated as:

$$\delta_y = \frac{P_y}{K_i}, \quad (2.4-2)$$

where K_i is the initial stiffness of the angle segment. The initial stiffness is based on a derivation from Shen and Astanteh-Asl (Shen & Astanteh-Asl, 1999) which centers on the geometry of the angle section between the beam-leg bolt and the column-leg bolt assuming elastic bending of the leg. Thus:

$$K_i = \frac{12EI}{g_c^3} \left[1 - \frac{3g_b}{4(g_c + g_b)} \right], \quad (2.4-3)$$

where

E = modulus of elasticity of steel,

$I = bt^3/12$ = moment of inertia of the angle.

2.4.5. Angle Fracture at Ultimate Load

The geometry of a deformed angle was simplified and used to develop expressions for the ultimate load P_u and the corresponding angle deformation δ_u . This simplified geometry is shown in Figure 2.4-5. The angle's column leg was modeled as a straight-line segment with plastic hinges at its ends and was subjected to axial tension T_u , shear force V_u , and bending moment M_u . The lengths of the plastic hinges were assumed equal to the thickness of the angle, t .

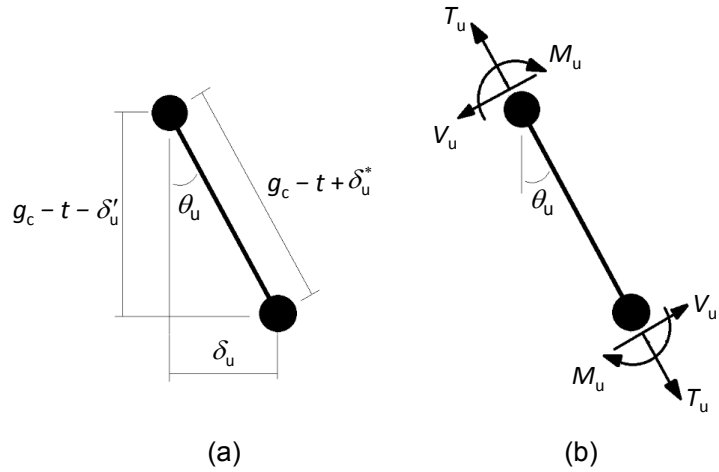


Figure 2.4-5: Two-hinge idealization of angle's column leg at ultimate load: (a) geometry and (b) free-body diagram (Weigand, Liu, & Main, 2017).

Equilibrium of the forces along the beam axis returns an expression for P_u :

$$P_u = V_u \cos \theta_u + T_u \sin \theta_u, \quad (2.4-4)$$

in which the chord rotation of the angle's column leg, θ_u , is found by the expression:

$$\theta_u = \cos^{-1} \left(\frac{g_c - t - \delta_u'}{g_c - t + \delta_u^*} \right), \quad (2.4-5)$$

where δ_u^* is the elongation of the column leg of the angle at ultimate load. The shear and axial tension in the column leg of the angle is calculated by:

$$V_u = \alpha P_y, \text{ and} \quad (2.4-6)$$

$$T_u = \frac{\alpha b t F_y}{3}, \quad (2.4-7)$$

where $\alpha = 1.2$ and is a strain hardening coefficient. Liu, Main and Sadek mention that the expression for T_u in Equation (2.4-7) assumes that:

the cross section of the angle is fully yielded with a linear strain profile based on observations from high-fidelity models, in which the tensile and compressive strains at the faces of the angle's column leg at fracture (at the toe of the angle radius) were found to be ϵ_{uk} and $\frac{1}{2}\epsilon_{uk}$, respectively, where ϵ_{uk} is the elongation at fracture at the k-area. This observed strain profile can be decomposed into a bending strain of $\frac{3}{4}\epsilon_{uk}$ and an axial strain of $\frac{1}{4}\epsilon_{uk}$, from which the column leg elongation can be calculated as $\delta_u^* = \frac{1}{2}t\epsilon_{uk}$, assuming that axial elongation occurs only at the plastic hinges, with plastic hinge lengths of t . As proposed by (Liu, Main, & Sadek, 2016), in the absence of test data for the k-area, 60% of the reported elongation from certified mill test reports or tests of coupons from the leg of the angle is recommended for ϵ_{uk} . (Weigand, Liu, & Main, 2017)

The lateral deformation of the beam leg, δ' , first introduced in Equation (2.4-5), is calculated from the geometry:

$$\delta' = (g_b - t) \sin\left(\frac{\gamma_u'(k-t)}{2}\right) \approx \frac{\gamma_u'(g_b-t)(k-t)}{2}. \quad (2.4-8)$$

The curvature of the angle's column leg at the end of the k-area may be calculated as:

$$\gamma_u = \frac{3\epsilon_{uk}}{2t}. \quad (2.4-9)$$

The curvature of the angle's beam-side leg at the end of the k-area, γ_u' in Equation (2.4-8), can be related to the curvature of the column-side leg of the angle in Equation (2.4-9), which is expressed as γ_u , through an empirical equation which is based on the results of high-fidelity finite-element analysis. The empirical equation is evaluated as:

$$\gamma_u/\gamma'_u = r + (r^3 - 1) \left(t - \frac{5}{16} \right) + (r^5 - 1) \left(t - \frac{5}{16} \right)^2, \quad (2.4-10)$$

where

$r = g_c/g_b$, the ratio of the angle's gage lengths. Equation (2.4-10) is applicable for angles with a thickness t of 0.25 inches to 0.63 inches and gages g_b and g_c of 2.0 inches to 3.0 inches. In addition, g_c should be greater than or equal to g_b . The ultimate deformation of the angle can be calculated as:

$$\delta_u = (g_c - t - \delta_b) \tan \theta_u. \quad (2.4-11)$$

The deformation in which failure occurs and the load P drops to zero is taken as:

$$\delta_f = 1.1\delta_u. \quad (2.4-12)$$

2.4.6. Comparisons with Experimental Data

The results from the high-fidelity finite-element model and the component-based model that were developed were compared to experimental data from Weigand and Berman (2016). In Weigand and Berman's study, double-angle connections of various configurations were subjected to combinations of axial and shear load with a rotation to evaluate the robustness properties of connections. This experiment was reviewed in this study and is summarized in Chapter 2.5. Figure 2.4-6 shows a comparison of measured and computed values of the vertical load applied to the center column of the test assembly with the resulting horizontal reactions. Weigand, Liu and Main (2017) summarize this comparison to their test of ba3b|34|14:

For that connection test, the thickness of the angles was $t = 6.4$ mm (0.25 in) and the gages of the column leg and the beam leg were $g_c = 76$ mm (3.0 in) and $g_b = 70$ mm (2.8 in), respectively. The measured yield strength of the angle steel was $F_y = 382$ MPa (55.4 ksi). Initial differences between the measured and computed values, for displacements less than about 300 mm (11.8 in), resulted from frictional resistance of the connection due to pre-tensioning of the bolts, which was not considered in the model. The subsequent response, after frictional slippage and loss of pre-tension, is captured fairly well by the component-based model. The peak vertical load and the peak horizontal reaction from the model exceeded the measured values by 9 % and 0.7 %, respectively.

The model prediction for the center column displacement at the ultimate vertical load was 7 % less than the experimental value.

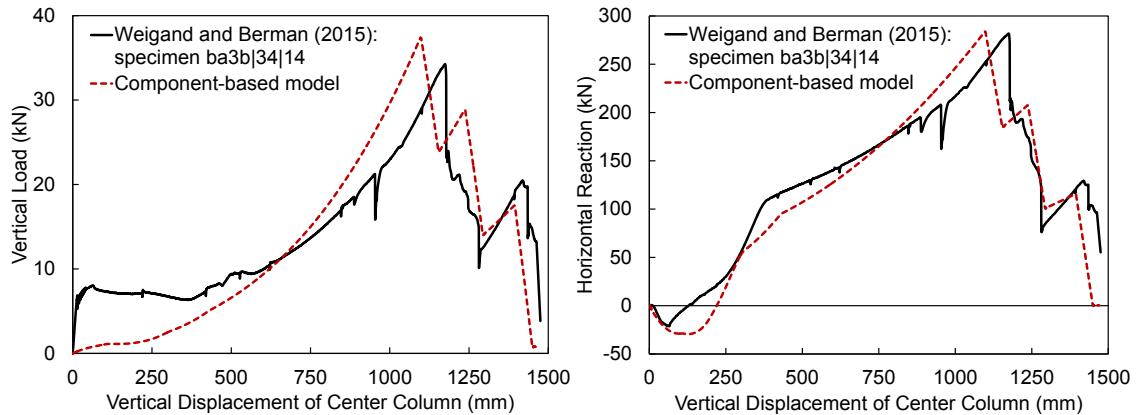


Figure 2.4-6: Comparisons of component-based model with experimental measurements for a double-angle connection with three bolt rows (uncertainty is estimated at $\pm 0.5\%$ based on repeated instrument calibration) (Weigand, Liu, & Main, 2017).

2.4.7. Conclusions

The high-fidelity modeling of double-angle connections provided valuable insights into the initiation of tears in angle material as load was applied. Equations were developed to estimate the applied load which would cause the development of plastic hinges and the curvature of the angle legs resulting from angle deformation. Comparisons between the component-based model which was developed to experimental testing shows that the developed model does capture key features of connection response.

2.5. Integrity of Bolted Angle Connections Subjected to Simulated Column

Removal by Weigand and Berman

Weigand and Berman (2016) performed 17 full-scale bolted angle connection sub-assemblages subjected to loading interactions consistent with a column-loss scenario. Key attributes of the connection responses, such as the force and deformation capacities, were quantified. Additionally, the influences on a number of variables within the

connection detailing, such as the number of bolts, diameter of bolts and the thicknesses of the angles were studied and quantified. A novel approach to determine the deformations of fibers used to discretize the connections is then used to calculate component-level deformation capacities at failure, which is useful for analysis of floor systems in practice.

2.5.1. Bolted Angle Assemblages

Specimens were chosen to represent angles commonly used in practice today and also to provide a variation of connection parameters such as angle thickness, bolt size and number of bolts. A summary of the specimens used in this test are shown in Table 2.5-1. The parameters in the table include number of bolts (n_b), bolt diameter (d_b), angle leg thickness (t_L), and whether the connection is welded or bolted to the supports. Each connection assemblage was fastened to a W12x72 column stub and a W21x50 beam stub.

Most connection assemblages were bolted-bolted configurations with 3/4-in. bolts and either 1/4-in. or 1/2-in. thick angle legs; these configurations are shown in Figure 2.5-1. These two angle thicknesses were chosen to investigate the differences in connection performance with respect to the limit states of angle leg rupture and bolt prying rupture when the angle is subjected to a tensile catenary force. The thinner angle specimens were also chosen to isolate damage to the angles rather than the supported beams, ensuring that they could be re-used without significant damage or introduction of imperfection.

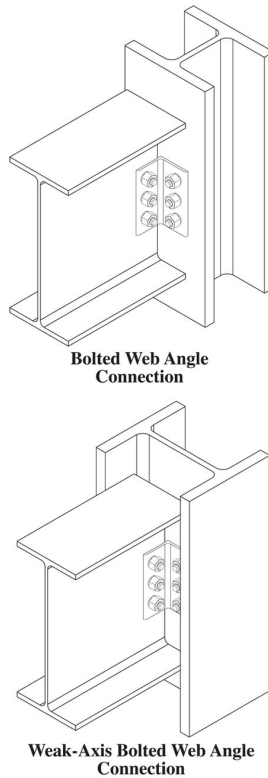


Figure 2.5-1: Typical bolted-bolted configuration (Weigand & Berman, 2016).

All angles tested were ASTM A36 L4x4x1/4, L4x4x1/2 or L6x4x3/4 hot rolled angle stock with a specified minimum yield strength of 36 ksi and ultimate strength of 58 ksi. Bolts were all A325, and all wide flange sections were ASTM A572 Grade 50. Fillet welds were welded with an E71T-8-D electrode with a nominal ultimate strength of 70 ksi.

Table 2.5-1: Connection sub-assemblages (Weigand & Berman, 2016).

Bolted angle connection sub-assemblage configurations

| Specimen Name | Connection Properties | | | |
|----------------------------------|-----------------------|--------------------------------------|--------------------------------------|--------------------------------------|
| | n_b | C _{LEG} d_b mm (in.) | B _{LEG} d_b mm (in.) | t_L mm (in.) |
| ba3bl34l14l | 3 | 19.1 (³ / ₄) | 19.1 (³ / ₄) | 6.35 (¹ / ₄) |
| ba3bl34l12l | | | | 12.7 (¹ / ₂) |
| ba5bl34l14l | 5 | 19.1 (³ / ₄) | 19.1 (³ / ₄) | 6.35 (¹ / ₄) |
| ba5bl34l12l | | | | 12.7 (¹ / ₂) |
| ba3bl1l34l | 3 | 25.4 (1) | 25.4 (1) | 19.1 (³ / ₄) |
| ba3bl34l14lOffset ¹ | 3 | 19.1 (³ / ₄) | 19.1 (³ / ₄) | 6.35 (¹ / ₄) |
| ba3bl34l12lOffset ¹ | | | | 12.7 (¹ / ₂) |
| ba3bl34l14lGap ² | 3 | 19.1 (³ / ₄) | 19.1 (³ / ₄) | 6.35 (¹ / ₄) |
| ba3bl34l12lGap ² | | | | 12.7 (¹ / ₂) |
| ba3bl34l14lTopSeat ³ | 3 | 19.1 (³ / ₄) | 19.1 (³ / ₄) | 6.35 (¹ / ₄) |
| ba3bl34l12lTopSeat ³ | | | | 12.7 (¹ / ₂) |
| ba3bl34l14lHConfig ⁴ | 3 | 19.1 (³ / ₄) | 25.4 (1) | 6.35 (¹ / ₄) |
| ba3bl34l12lHConfig ⁴ | | | | 12.7 (¹ / ₂) |
| ba3bl34l14lBlegWeld ⁵ | 3 | 19.1 (³ / ₄) | - | 6.35 (¹ / ₄) |
| ba3bl34l14lClegWeld ⁶ | 3 | - | 19.1 (³ / ₄) | 6.35 (¹ / ₄) |
| ba3bl34l14lWeak ⁷ | 3 | 19.1 (³ / ₄) | 19.1 (³ / ₄) | 6.35 (¹ / ₄) |
| ba3bl34l12lWeak ⁷ | | | 19.1 (³ / ₄) | 12.7 (¹ / ₂) |

¹ Angles offset 76.2 mm (3.0 in.) from beam centerline.² Reduced gap of 6.35 mm (¹/₄ in.) between beam flange and column flange.³ Top-and-seat angle configuration.⁴ Angles had three 19.1 mm (³/₄ in.) bolts on column legs and two 25.4 mm (1 in.) bolts on beam legs.⁵ Angles bolted to column face and welded to beam web.⁶ Angles welded to column face and bolted to beam web.⁷ Weak-axis configuration that frames into column web.

2.5.2. Experimental Setup

The sub-assemblages were tested using a self-reacting frame at the University of Washington Structural Research Laboratory. This frame is shown in Figure 2.5-2.

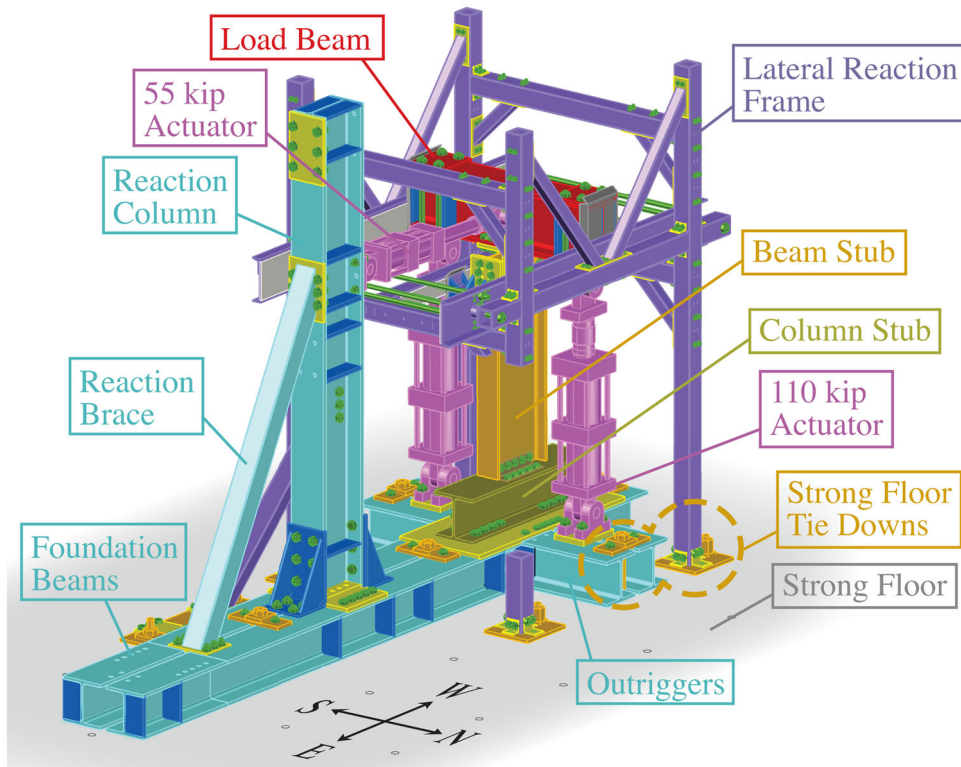


Figure 2.5-2: Load frame assembly (Weigand & Berman, 2016).

The frame was rigidly connected to the floor system, and the column stub was positioned horizontally across the base of the frame. The test beam, spanning vertically, was connected to this column stub using a testing assemblage. A loading beam was then connected to the other end of the test beam and would impart load on the test beam via three actuators: two to apply an axial load on the testing beam and another to apply a lateral load. The combination of these loadings would produce a catenary force and a shear on the connection being tested and would rotate to remain in-line with the test beam and load beam, respectively. The loading was simulated for a 30-foot beam that had

undergone a column-removal scenario in a double span condition. The loading was applied quasi-statically over a time span of approximately 60 minutes. A free body diagram of the testing frame, test beam and actuators are shown in Figure 2.5-3.

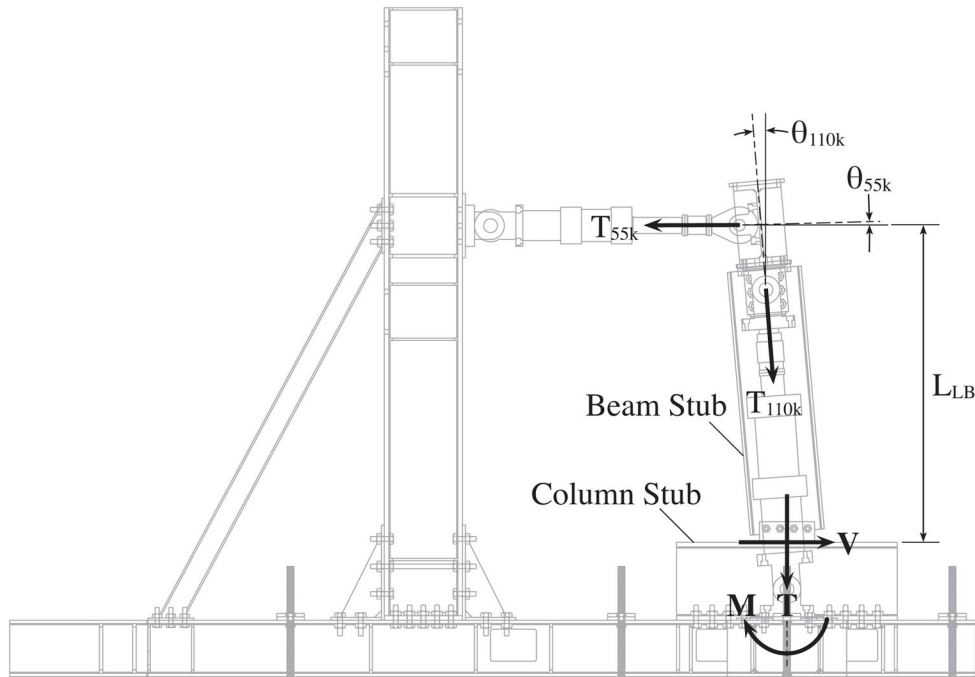


Figure 2.5-3: Free body diagram of testing frame (Weigand & Berman, 2016).

2.5.3. Equipment and Instrumentation

Photographs were taken at regular time intervals with DSLR cameras to observe the rotation and behavior of the connection over the length of each test. Each actuator was equipped with a 110-kip load cell to measure the applied force to the assembly. Wire potentiometers and electronic axis inclinometers monitored the displacements and rotations of the specimen beam stub, load beam and actuators throughout the test. Local to the connections, displacements were acquired using a dense grid of LED targets which were fixed to the angles, bolts and beam and column stubs. This LED displacement

measurement system had an estimated uncertainty of $\pm 1\%$, which is based on repeated calibration over the course of testing.

Three separate units were used to collect data from the actuators, potentiometers and inclinometers, and the LED targets, respectively. For the actuators, a FlexTest 60 controller and optical cable were used to transmit data to the LabView Hub. Signals from the potentiometers and inclinometers were recorded directly by the LabView Hub, and a Northern Digital Inc. Certus HD Position Tracker (NDI OptoTrak) system with two sets of three cameras natively triangulated the positions of the LED grids.

2.5.4. Connection Response Quantities

Because the assembly rotated throughout testing, the connection displacement and force quantities are presented in coordinates that are aligned with axes parallel to the column and beam longitudinal axis prior to testing. Figure 2.5-3 shows a free body diagram of the system under a rotational and axial load. Actuator loads are assumed to intersect at the center of the load beam and are assumed to act through the actuator head swivel pins. Each of the two 110-kip actuators were considered separately in the calculation of forces, with one actuator being designated as North (N) and one as south (S). The shear, tension and moment forces V , T and M , respectively, at the connection were determined from the summation of the actuator loads with the sign convention as tension positive. Thus:

$$V = T_{55k} \cos \theta_{55k} - (T_{110kN} \sin \theta_{110kN} + T_{110kS} \sin \theta_{110kS}), \quad (2.5-1)$$

$$T = -T_{55k} \sin \theta_{55k} - (T_{110kN} \cos \theta_{110kN} + T_{110kS} \cos \theta_{110kS}), \quad (2.5-2)$$

$$M = T_{55k} L_{LB} \left(\cos \theta_{55k} + \sin \theta_{55k} \tan \left(\frac{\theta_{110kN} + \theta_{110kS}}{2} \right) \right), \quad (2.5-3)$$

where T_{55k} , T_{110kN} , and T_{110kS} were the 55 kip north and south actuator loads, respectively. Data from inclinometers fixed to each actuator updated the direction of the loads, θ_{55k} , θ_{110kN} , and θ_{110kS} .

2.5.5. Fiber Displacements from Experiments

Weigand and Berman suggest that connection displacements such as simulated vertical displacement or connection rotation are not sufficient to demonstrably compare the deformation capacities of connections with varying spans. In a prior research project, Weigand and Berman developed a technique to compute fiber displacements from experimental data. This technique accounts for combined contributions to bolt and single angle deformations resulting from any combination of rotation and axial extension demands. While the testing presented in this review consisted only of 30-ft simulated spans and were therefore subjected to the same rotation and displacement demands, the fiber displacement technique remains beneficial for the calibration of the fiber connection models that are used to simulate connections in the analysis of gravity frames in which a disproportionate collapse has occurred.

Summarily, in this technique, the connection sub-assemblages are discretized into fibers, with each fiber representing a characteristic width segment of a connector component such as a bolt, weld, angle or beam web. The locations of these fibers were determined before load application. One node of the fiber was assumed to be rigidly attached to the column stub and the other node rigidly attached to the beam stub, as shown in Figure 2.5-4. The motions of the beam web fiber-nodes were computed by best-fitting a rigid-link frame structure onto the grid of OptoTrak LED targets attached to the web of the test beam. In the undeformed state before load application, the two nodes

exactly coincide and the length of each of the two fibers is zero. After load application and consequent deformations, the fiber displacements were computed as the distance between the undeformed and the deformed locations of the fiber nodes and were then decomposed into axial and shear components.

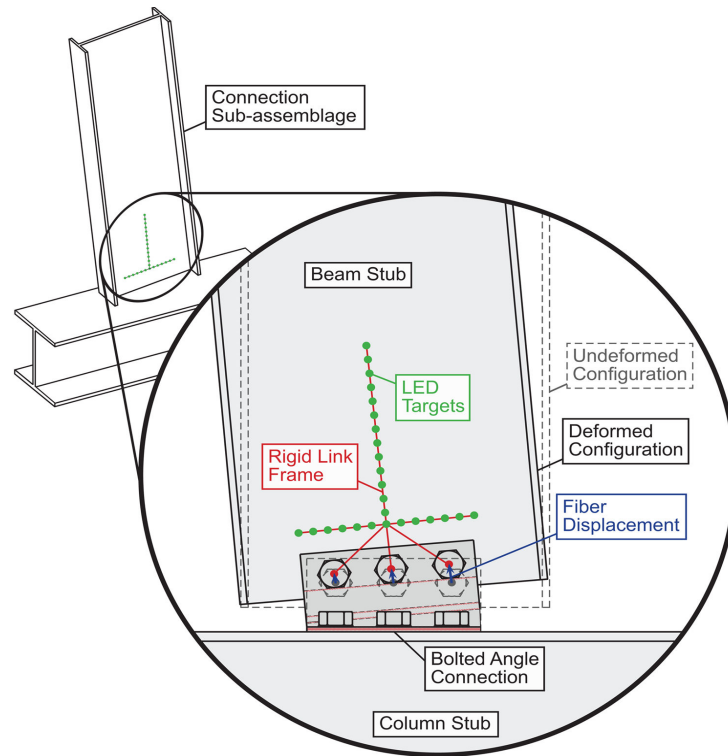


Figure 2.5-4: Method for computing fiber displacements (Weigand & Berman, 2016).

2.5.6. Experimental Results

The behavior of the bolted connection sub-assemblages varied with the angle thickness, with the 1/4-in. specimens deforming with little to no prying action in the column leg bolts. With 1/2-in. angles, however, the increased angle strength was sufficient to induce prying into the bolts at the column leg of the angle as the primary mechanism of deformation and ultimate failure.

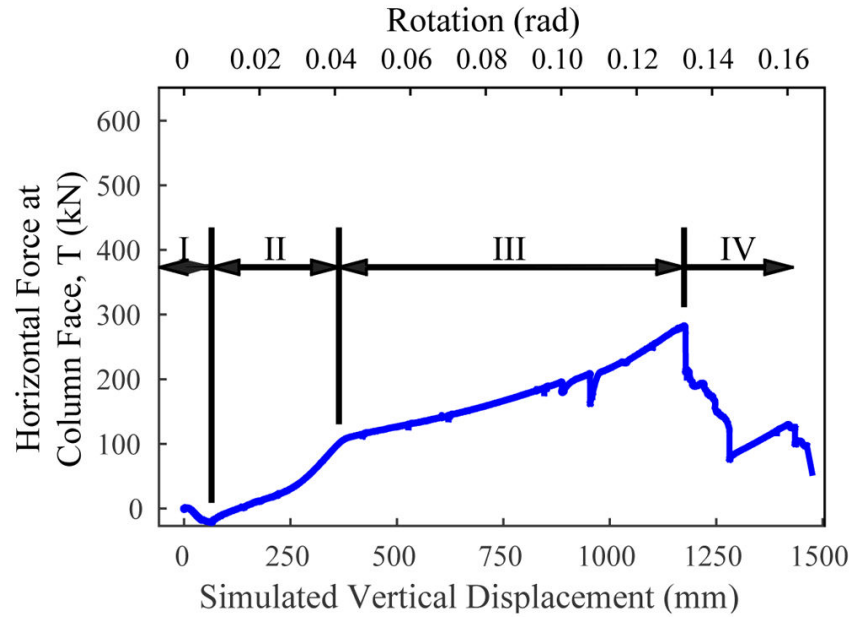


Figure 2.5-5: Phases of vertical and horizontal force-displacement behavior for ba3b|34|14| (Weigand & Berman, 2016).

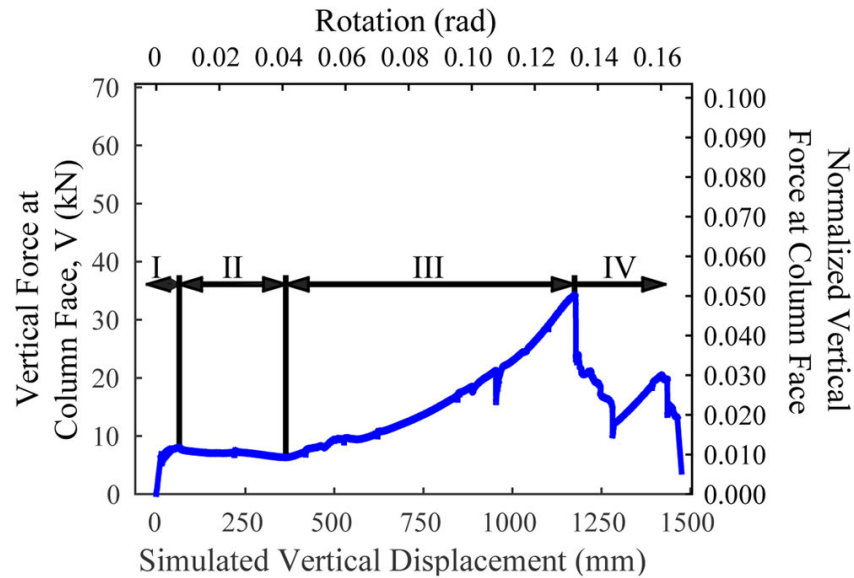


Figure 2.5-6: Phases of vertical and horizontal force-displacement behavior for ba3b|34|14| (Weigand & Berman, 2016).

Each angle test underwent four primary phases of behavior, illustrated in Figure 2.5-5 and 2.6-6 for ba3b|34|14| and 2.5-7 and 2.5-8 for ba3b|34|12|. In Phase I the

connection vertical force-displacement response was characterized by large initial stiffness as the beam leg bolts resisted moments through dissipation of their pretension forces. Because of the relatively large compression stiffnesses of the angles to their tension stiffnesses, an amount of compression was initially developed in the horizontal force-displacement responses and the centers of rotation for the angles were predisposed toward the compressive sides of the connections.

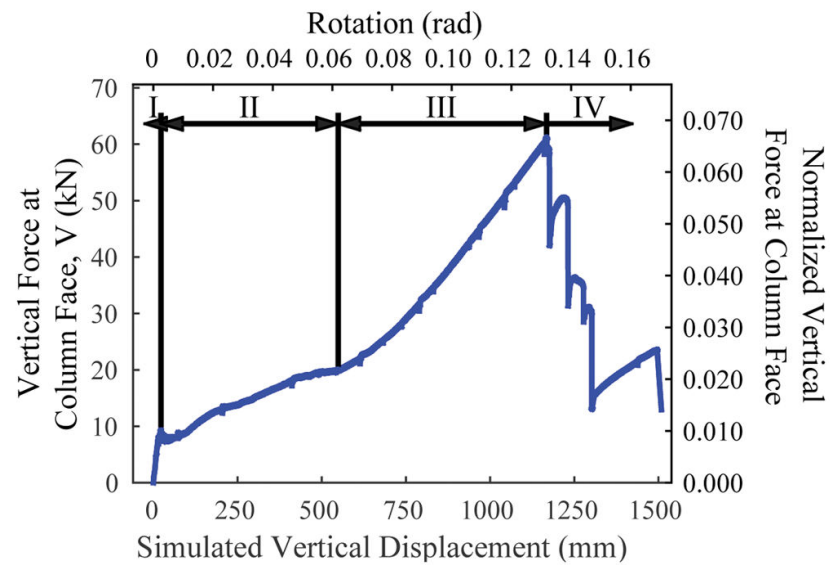


Figure 2.5-7: Phases of vertical and horizontal force-displacement behavior for ba3b|34|12| (Weigand & Berman, 2016).

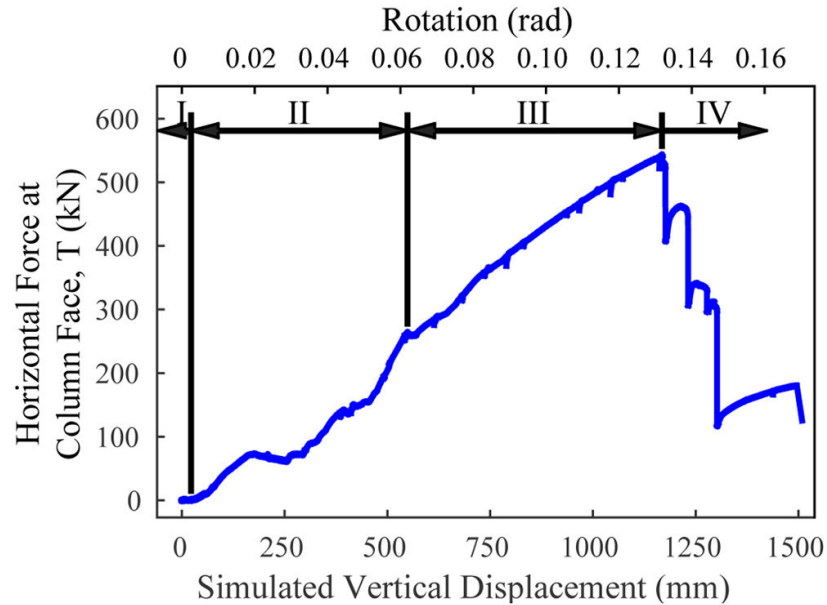


Figure 2.5-8: Phases of vertical and horizontal force-displacement behavior for ba3b|34|12 (Weigand & Berman, 2016).

Phase II of the response may be attributed to the slip of the beam's web between the angles. This occurred as the beam rotated until contact was established between the bolt shanks and the bolt holes. The rotation of the beam within the connection induced flexural deformations in the angle column legs that resulted with a separation of the angle heel from the column face along the length of the angle. Phase III began when the entire lengths of the angle heels had separated from the column face, after which the angles underwent increasingly high levels of deformation. As the angles move from Phase II to Phase III, they transition to a tension-dominated behavior, rather than flexure dominated behavior, as occurred in Phase II. Weigand and Berman remark that the largest portion of the connection resistance to vertical and horizontal load was in Phase III.

Similar to Oosterhof and Driver (2015), Weigand and Berman suggest that plastic hinges developed in the angle as loading progressed and deformations became extreme. These plastic hinge lines were apparent through flaking of mill scale and through the

large concentrations of rotations that were visible on the deformed angle cross-sections. The locations of these plastic hinges varied with the thickness of the angle legs relative to the strengths of the column-leg bolts. The 1/4-in. thick angles developed plastic hinges along the inside edge of the column leg bolts at the toe of the angle leg radius and along the inside edge of the beam leg bolts. One half-inch thick angles, similar to 1/4-in. thick angles, formed plastic hinges at the toes of the angle radius and inside of the beam leg bolts. A difference, however, in the plastic hinge formation is found at the toe of the column bolts, where a hinge formed on the far side of the angle leg relative to the radius. This location of plastic hinge formation and consequent deformation is significant as it introduces a prying action on the column leg bolts. Figure 2.5-9 shows the location of plastic hinges in both 1/4-in. and 1/2-in. specimen.

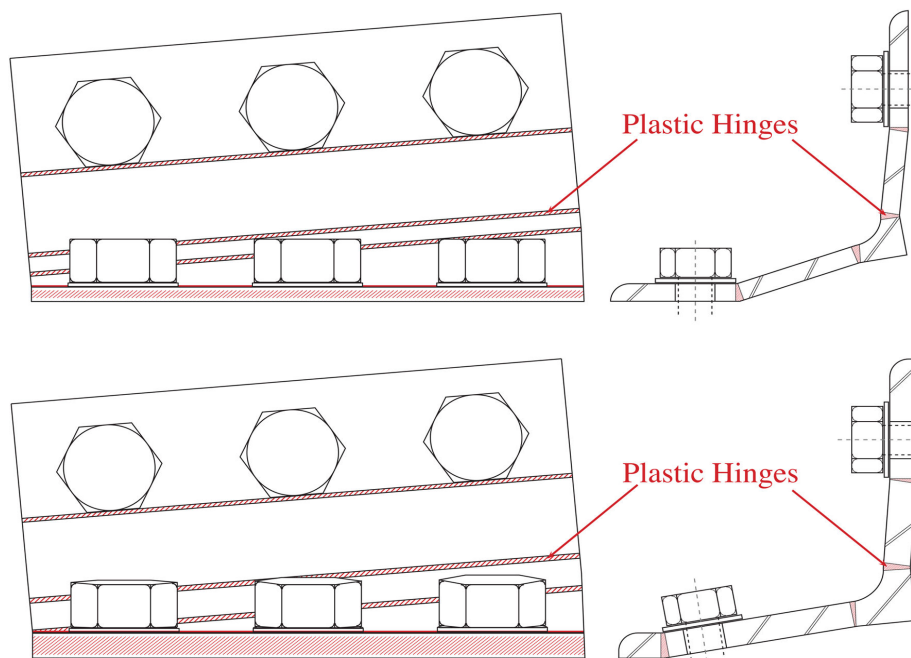


Figure 2.5-9: Plastic hinge formation in 1/4-in. angles (top) and 1/2-in. angles (bottom) (Weigand & Berman, 2016). Column face is along the horizontal. Plastic hinges indicated by hatched regions.

Deformations in the angles increased until failure, at which point the connection moved into Phase IV degradation behavior. In 1/4-in. thick angles, a common failure mechanism was the formation of a crack at one of the plastic hinges in the angle cross section near the angle radius which subsequently tore a length of 30-50% of the total angle depth. This initial tear, with continued loading, would propagate and extend the entire depth of the angle, leading to complete connection failure. Figure 2.5-10 shows damage to the north web angle and column bolts of specimen ba3b|34|14| following test completion. Damage was isolated to the angles instead of the connection bolts, which is typical for the 1/4-in. thick angles. Views (a, b, c) show front and section views of ruptured north web angle beam leg, (d, e, f) show front and section views of ruptured north web and angle column leg, and (g, h, i) show damage to the north web angle column bolts.

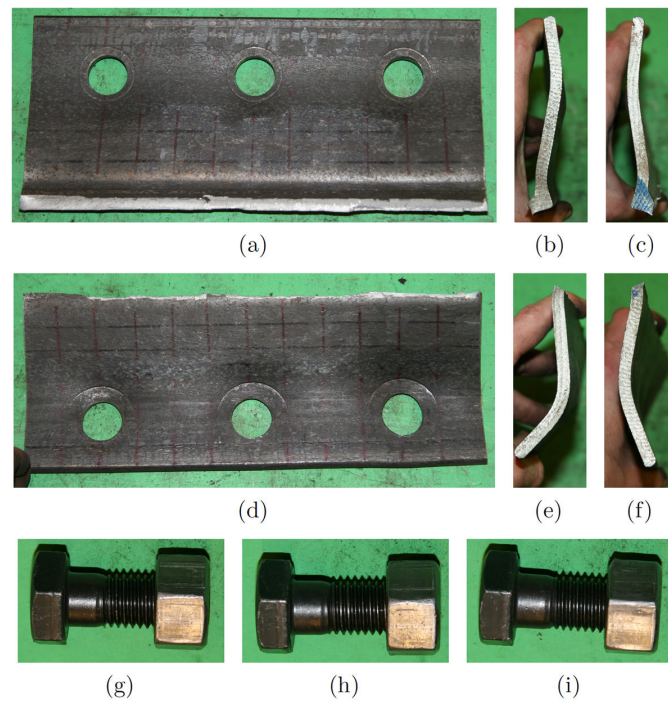


Figure 2.5-10: Specimen ba3b|34|14| post-test (Weigand & Berman, 2016). Representative of 1/4-in. angle behavior.

In connections with 1/2-in. thick angles, bolt rupture at column leg bolts due to prying action was the primary failure mechanism. Bolt ruptures always proceeded sequentially from the tension side of the connection toward the compression side, though ruptures were not always evenly distributed between the web angles. Figure 2.5-11 shows specimen ba3b|34|12| following testing; these results are representative of angles with 1/2-in. thick legs. Views (a, b, c) show front and section views of damage to the north web angle, (d, e, f) show ruptured north web angle column leg bolt heads, and (g, h, i) show ruptured north web angle column leg bolts with the nuts attached.

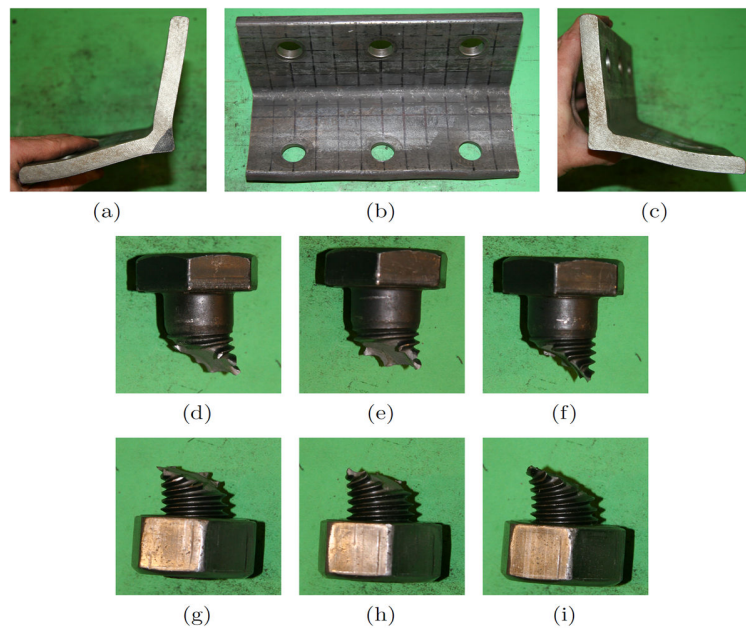


Figure 2.5-11: Specimen ba3b|34|12| post-test (Weigand & Berman, 2016). Representative of 1/2-in. thick angle behavior.

Table 2.5-2 lists critical force and displacement quantities at connection failure.

The quantities Δ_{\max} , θ_{\max} , and δ_{\max} symbolize the simulated vertical displacement, rotation and axial deformation, respectively, while V_{\max} and T_{\max} symbolize vertical and horizontal force at the column face, respectively. The limiting fiber displacement is included under the heading ' $d_{f,\text{lim}}$ '. The normalized vertical resistances, V_{\max}/V_{nom} were

calculated as ratios of the connection vertical resistances at failure to their nominal shear capacity, V_{nom} , using the LRFD design methodology in conjunction with the measured angle and bolt properties. Weigand and Berman did not include horizontal loading in their report because it was believed that current limit states do not accurately represent the capacity of the connections, but rather underestimate the capacity by a considerable margin.

Table 2.5-2: Bolted angle connection sub-assembly force and deformation quantities at failure (Weigand & Berman, 2016).

| Specimen Name | System, Connection Displacement Demands | | | | | Connection Vertical and Horizontal Capacities | | | Normalized Vert. Capacities | |
|--------------------|---|---------------------|-------------------------|---------------------------|--------------------|---|---------------------------|---------------------------|-----------------------------|--|
| | Δ_{max} mm (in.) | θ_{max} rad. | δ_{max} mm (in.) | d_{lim} mm (in.) | V_{max} kN (kip) | T_{max} kN (kip) | $\frac{V_{max}}{V_{nom}}$ | Limit State | | |
| ba3b34i14i | 1175 (46.2) | 0.133 | 37.6 (1.481) | 45.3 (1.782) | 34.2 (7.70) | 282 (63.3) | 0.049 | Angle Rupture | | |
| ba3b34i12i | 1168 (46.0) | 0.132 | 37.2 (1.465) | 41.6 (1.639) | 61.1 (13.74) | 543 (122.0) | 0.067 | Bolt Rupture | | |
| ba5b34i14i | 1033 (40.7) | 0.117 | 29.3 (1.155) | 46.7 (1.839) | 46.4 (10.42) | 373 (83.9) | 0.041 | Angle Rupture | | |
| ba5b34i12i | 1078 (42.4) | 0.118 | 31.9 (1.255) | 47.8 (1.883) | 93.9 (21.10) | 780 (175.3) | 0.059 | Bolt Rupture | | |
| ba3b1134i | 1563 (61.5) | 0.176 | 64.6 (2.544) | 74.6 (2.937) | 134.1 (30.15) | 877 (197.1) | 0.146 | Beam Web Block S Rupture | | |
| ba3b34i14iOffset | 1074 (42.3) | 0.122 | 31.7 (1.249) | 41.1 (1.619) | 33.0 (7.42) | 258 (57.9) | 0.047 | Angle Rupture | | |
| ba3b34i12iOffset | 1086 (42.8) | 0.116 | 32.3 (1.273) | 39.6 (1.559) | 60.5 (13.60) | 533 (119.8) | 0.066 | Bolt Rupture | | |
| ba3b34i14iGap | 1080 (42.5) | 0.122 | 32.0 (1.261) | 40.5 (1.595) | 30.5 (6.85) | 258 (58.0) | 0.044 | Angle Rupture | | |
| ba3b34i12iGap | 1150 (45.3) | 0.122 | 36.1 (1.423) | 41.2 (1.622) | 65.2 (14.66) | 553 (124.2) | 0.071 | Bolt Rupture | | |
| ba3b34i14iTopSeat | 542 (21.3) | 0.062 | 8.3 (0.325) | - | 42.5 (9.55) | 137 (30.8) | 0.077 | Angle Rupture | | |
| ba3b34i12iTopSeat | 557 (21.9) | 0.063 | 8.7 (0.344) | - | 68.9 (15.48) | 46 (10.3) | 0.108 | Bolt Rupture | | |
| ba3b34i14iHConfig | 1328 (52.3) | 0.150 | 47.6 (1.873) | 52.9 (2.082) [/] | 44.5 (10.01) | 322 (72.3) | 0.064 | Angle Rupture | | |
| ba3b34i12iHConfig | 1216 (47.9) | 0.138 | 40.2 (1.582) | 41.7 (1.642) [/] | 57.8 (13.00) | 475 (106.7) | 0.063 | Beam Web Tearout | | |
| ba3b34i14iBlegWeld | 1067 (42.0) | 0.121 | 31.2 (1.229) | - | 27.2 (6.12) | 240 (54.0) | 0.039 | Angle Rupture | | |
| ba3b34i14iClegWeld | 1125 (44.3) | 0.127 | 34.6 (1.363) | 34.1 (1.342) | 15.8 (3.55) | 130 (29.3) | 0.023 | Weld Rupture | | |
| ba3b34i14iWeak | 1100 (43.3) | 0.125 | 33.2 (1.305) | - | 29.5 (6.63) | 231 (52.0) | 0.042 | Angle Rupture | | |
| ba3b34i12iWeak | 1373 (54.1) | 0.155 | 50.6 (1.993) | - | 79.6 (17.90) | 591 (132.9) | 0.087 | Angle Rupture and Rupture | | |

[/] Value corresponds to fiber centered at beam leg bolt.

2.5.7. Influence of Connection Parameters on the Bolted Angle Connection

Responses

When binding of the beam flange against the column flange occurred, it was the result of deliberate detailing by Weigand and Berman to determine the impact that such a scenario would have on connection performance. When binding did occur, the connection rotated about the point of contact, accelerating the progression of deformations at the bolted angle fibers. However, binding seemed to correct itself: as axial extension demands increased as a result of binding, the beam flange was pulled away from the column flange and the assembly continued resisting load. Ultimately, it was concluded that capacities may not be significantly impacted by binding.

The connection vertical resistance increased as the number of bolts increased: for 1/4-in. thick angles, the vertical capacity was increased by 35%, and for 1/2-in. thick angles, the vertical capacity was increased by 54%. However, these increases were less than expected if one were to compare the percentage-increase of vertical shear capacity to their nominal strengths.

Figure 2.5-12 plots the normalized vertical responses of Specimens ba3b|34|14| and ba5b|34|14| which differed only by the number of bolts in the connection. These results, along with those listed in Table 2.5-2, demonstrate that while the measured deformation capacities of the angle fibers were slightly higher in the 5-bolt angles in comparison to 3-bolt angles, their simulated vertical displacement at failure and corresponding normalized vertical and horizontal resistances decreased.

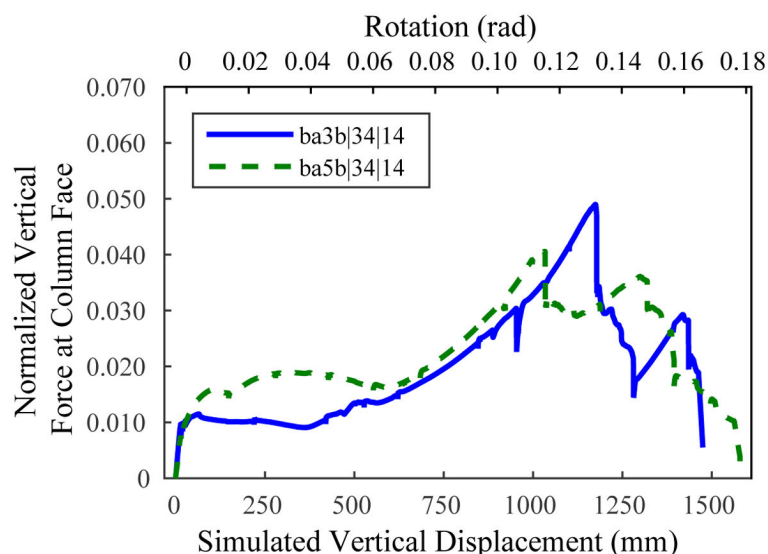


Figure 2.5-12: Normalized vertical responses of 1/4-in. 3- and 5-bolt specimens (Weigand & Berman, 2016).

Weigand and Berman explain this decrease in connection deformation capacity using their fiber displacement technique. While the deformation capacities of angle fibers remained constant between tests, the demands at the outermost fibers due to rotation increased in tests with more bolts. This response caused the demands at the outermost fibers of specimens of 5-bolt angles with 1/4-in. and 1/2-in. thicknesses to exceed their deformation-controlled capacity limits at a smaller simulated vertical displacement than similar specimens with 3-bolt configurations.

2.5.8. Effect of Angle Thickness on Connection Response

For each pair of connections that varied only by angle thickness, i.e., 1/4-in. and 1/2-in. thick 3-bolt and 5-bolt angles, the thicker specimens of 1/2-in. thickness had higher normalized vertical capacities than the thinner specimens of 1/4-in. thickness. The thicker specimens often had higher simulated vertical displacements than thinner specimens as well, which may be attributed to the increased contribution of beam web

and column flange deformation, however. These tests suggest that connections with thicker web angles may perform better than their thinner counterparts. Further testing is required to validate these claims.

2.5.9. Absolute Connection Strength and Connection Performance

Weigand and Berman found that the connection with the highest overall strength was ba3b|1|34| which used 1-in. diameter bolts with a 3/4-in. thick angle. This connection was so strong that it locally deformed the column web and the beam flange, ultimately failing by a brittle mechanism of block shear rupture at the beam web. In addition, the column leg bolts sustained large prying deformations due to angle uplift. This connection was believed to be, of all connections tested, the connection with the most deformation capacity and normalized vertical resistance. Figure 2.5-13 shows the extreme warping of the column flange during the testing.

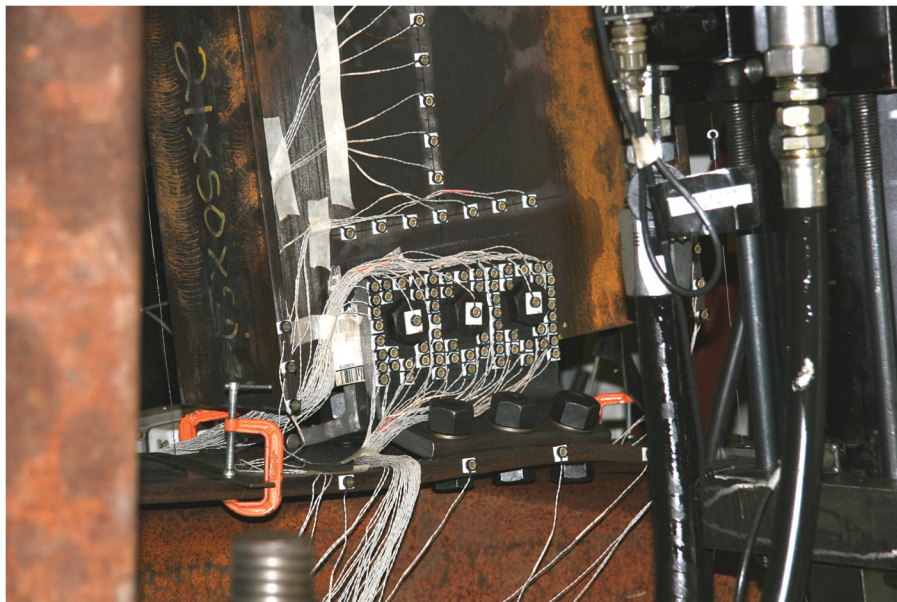


Figure 2.5-13: Extreme column warping of specimen ba3b|1|34| (Weigand & Berman, 2016).

From a global stability standpoint, while the deformation capacity of the connection may appear to be desirably high, the extreme bending of the column flange is bothersome insofar as it may introduce undesirable and destabilizing effects on a structure as a whole. In a column loss event, if a progressive collapse is to be avoided, localizing deformations strictly to the connections, and in this case the double angles, may seem to be more desirable than bending the flanges of the supporting column to introduce higher deformations. While it is unclear whether destabilizing effects have been introduced to the column, further testing should be performed on similarly proportioned assemblies to ensure that the integrity of the structure is not compromised when a supporting member absorbs connection rotation.

2.5.10. Staggering of Bolt Holes

Specimens with staggered bolt holes were tested to establish whether offsetting bolt holes from one another would eliminate localized plastic strains observed while testing standard configuration bolted angle connections. A specimen designated as ba3b|34|14|HConfig was tested to establish a connection response which was compared to the response of ba3b|34|14|, a standard configuration. Figure 2.5-14 shows a staggered angle configuration.

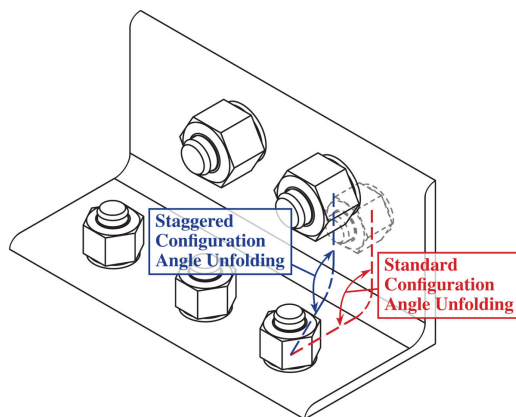


Figure 2.5-14: Staggered angle configuration (Weigand & Berman, 2016).

From testing, it was found that the staggered angle configuration of ba3b|34|14|HConfig had a 30% improvement in strength and 13% improvement in deformation capacity in comparison to its conventionally detailed counterpart. Similarly, a test was run with 1/2-in. thick angles with staggered bolt holes as well, designated as ba3b|34|12|HConfig. However, the test in which these specimens were used failed prematurely during testing due to beam web tear-out, so the extent to which the staggering of bolt holes might improve connection performance with relation to angle prying performance is unclear. However, from the 1/4-in. thick angle tests and the data collected from the 1/2-in. thick angle test, the data do collectively support the conclusion that staggering of the bolt holes may reduce concentrations of deformations at the angle plastic hinge lines, consequently improving connection performance under column removal-type scenarios. Results from these tests are shown in Figure 2.5-15 and 2.5-16.

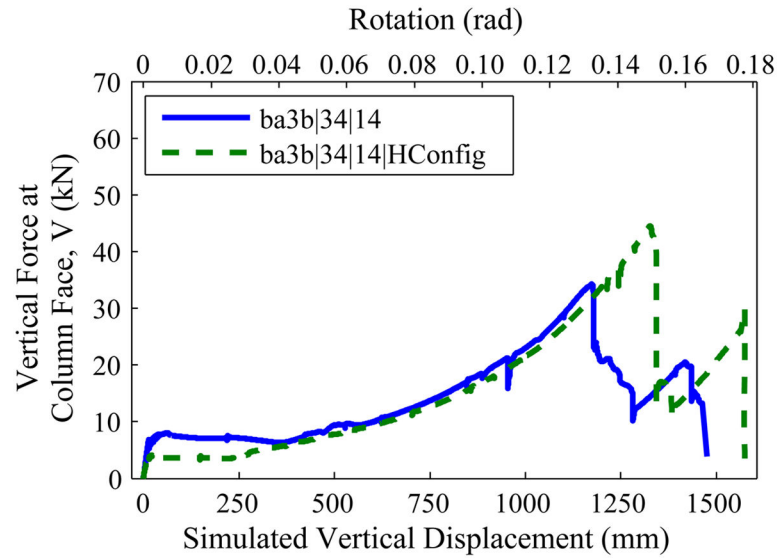


Figure 2.5-15: Specimen ba3b|34|14|HConfig compared to ba3b|34|14| (Weigand & Berman, 2016).

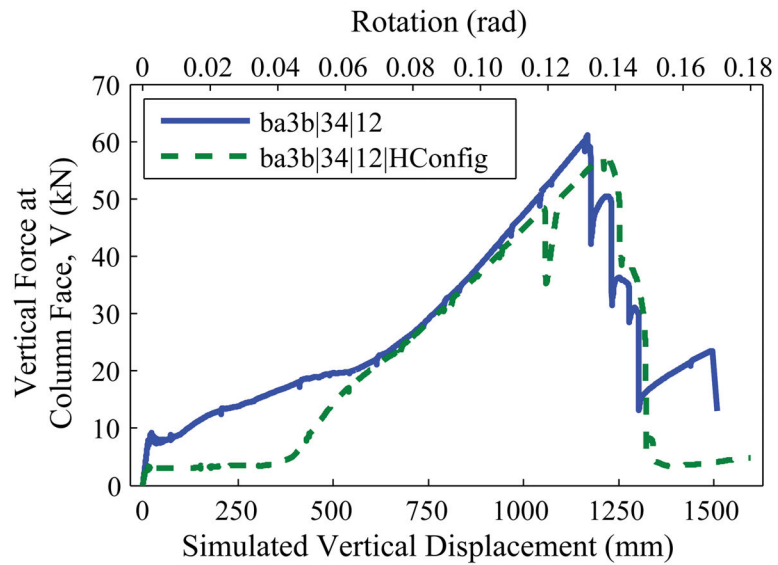


Figure 2.5-16: Specimen ba3b|34|12|HConfig compared to ba3b|34|12| (Weigand & Berman, 2016).

2.6. Building Code of the City of New York

The 2014 NYC Construction Code (City of New York, 2014) specifies requirements for structural integrity in Section 2212. Barring some exceptions, end connections of beams and girders are required to possess a level of tensile capacity even when the member end connection is designed as a simple shear connection.

According to the NYC Construction Code: “End connections of all beams and girders shall have a minimum available tensile strength equal to the larger of the available vertical shear strength of the connections at either end, but not less than 10 kips (45 kN). For the design of the connections, the shear force and the axial force need not be considered to act simultaneously” (City of New York, 2014; Owens & Moore, 2006). Any connection that is designed in accordance with the AISC Steel Construction Manual to meet the required tension force satisfies the requirements of the code.

The NYC Construction Code explicitly states that simple connections must account for unexpected forces but does not require that the connection be checked for simultaneous application of the shear and tensile forces. In many cases, simple shear connections already meet this requirement when the limit state is based on bolt shear or bolt bearing, making it unlikely to cause a connection to fail by application of a pure tension force in comparison to a pure shear force. A requirement to apply varying percentages of maximum shear and maximum tensile force may be more sensible.

2.7. Steelwork Connections – The Robustness of Simple Connections by Owens and Moore

Owens and Moore (2006) studied and tested double-angle and endplate connections subject to tying forces, or axial forces, to establish a set of parameters for

design. The focus of their testing was the ability of simple connections to resist tying forces, and all of the experiments were based on typical connection sizes based on industry use.

The tests were performed by applying a tensile load through the centroid of a load beam, therefore axially loading the end connection. The end connection was typically a one-, three-, five-, or seven-bolt double angle connection.

Results from testing showed that there exists a linear relationship between axial displacement and axial load in the beginning phases of the test, with a gradual decrease in stiffness until failure. These results coincide with the findings of Oosterhof and Driver (2015) and Weigand and Berman (2016). In thin elements, failure occurred by bolt bearing and bolt punching, while fracture of the angle near the heel was the predominant failure mechanism in thicker elements.

An important observation made during testing was the significant amount of deformation that the double-angle connections could undergo before failure. This significant deformation allowed the connection to resist forces in excess of the required capacities for tying forces. This deformation, or “unfolding” of the angle legs, reduced the amount of eccentricity in the legs of the angles within the connection. It was also found that the angles had four critical sections as shown in Figure 2.7-1.

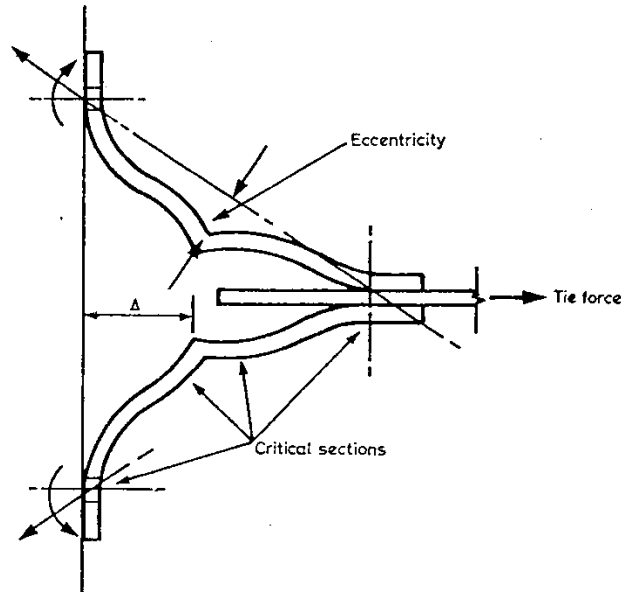


Figure 2.7-1: Critical sections in double-angle connections (Owens & Moore, 2006).

After completion of the experimental tests, comparisons to the expected strength found through design calculations that the connections possessed more capacity than expected, with an over strength factor relative to expectations between 1.5 to 1.89.

It was established from this testing that connections subjected to unexpected loads possess an inherent robustness capable of resisting tying forces and preventing damage from spreading to other areas and subsequently perpetuating a collapse. However, the high deformations in the angle legs against the column face introduced a high prying force against the bolts, which was found by Weigand and Berman (2016) to be an important limit state to consider. Finally, Owens and Moore conclude that the design of double-angle shear connections will not be controlled by tying forces.

Chapter 3: Experimental Program

3.1. Introduction

Testing was conducted in the Construction Science and Engineering Center (CSEC) at the Milwaukee School of Engineering (MSOE) to determine the effectiveness of various double-angle shear connections to resist an interaction of moment, axial and shear loads. The goal of this testing was to gain a better understanding of the interaction of forces in connections of this configuration. Testing was commenced in conjunction with other experimental tests involving WT connections by Van Buskirk (2019).

3.2. Test Specimen Overview

Nine tests of varying double-angle configurations were performed with three bolting patterns: three, four and five rows. Each configuration was tested three times. A naming convention was developed to simplify data presentation and increase convenience of reference; an example of this convention is shown in Figure 3.2-1.

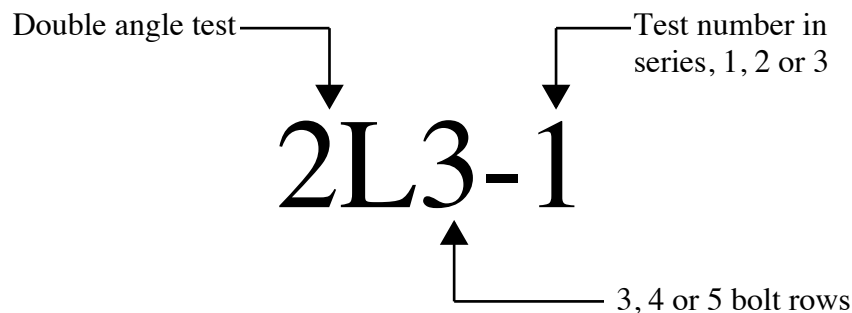


Figure 3.2-1: Naming convention example.

To aid in test assembly erection and fit-up, each configuration was detailed with one angle entirely composed of standard holes, with the other angle on the opposite side of the beam web fabricated with horizontal short-slotted holes on the column leg. This

allowed for some lateral movement of the angle during the erection process. Details of the configurations are shown in Figure 3.2-2. The angle material was tested in a material testing laboratory and mill certifications were provided; these angles were dual certified for ASTM A36 and ASTM A572-Grade 50. Reference Appendix B for these mill certifications and laboratory reports. All angles were L4 x 3 1/2 x 1/4 .

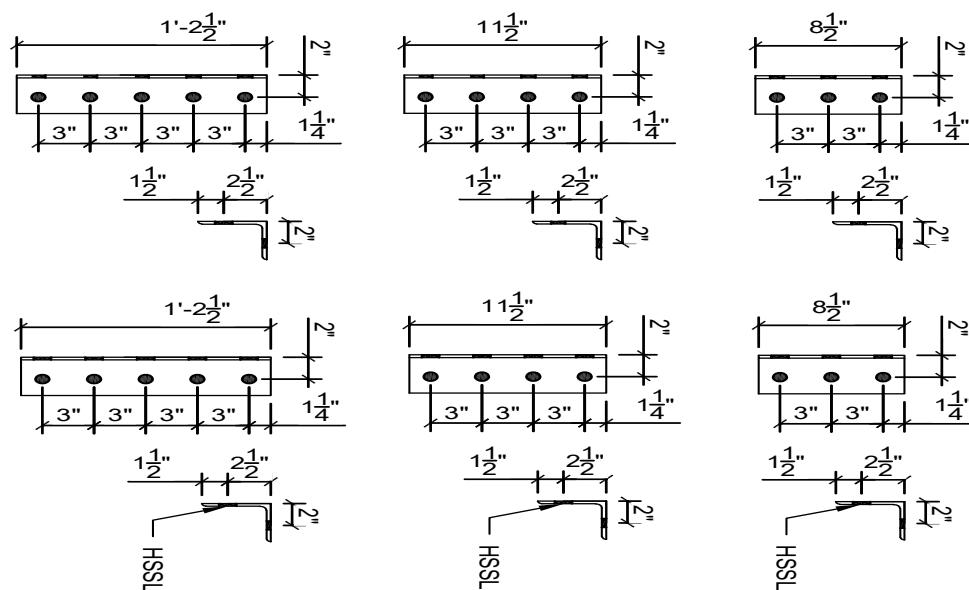


Figure 3.2-2: Angle configurations for testing with (a) 3 bolt lines, (b) 4 bolt lines, and (c) 5 bolt lines.

The double-angle connections adhered to the specification requirements and design considerations of the AISC 15th Edition Steel Construction Manual. Bolt holes were 13/16-in. diameter for use with 3/4-in. diameter A325-X fully-pretensioned bolts between the angle legs and column faces, with 3/4-in. A325-N fully-pretensioned bolts at the beam web. Later in the testing, 3/4-in. diameter F1852-X bolts were used to aid in erection. Holes in one angle leg affixed to the column face were HSSL for fit-up as previously discussed and reflected in Figure 3.2-2. Refer to Appendix A for connection design and capacities. Table 3.2-1 summarizes the ultimate capacities for each connection

based on failure mode. Because each bolt was fully-pretensioned, it is possible that the connections developed slip-critical level capacities.

Table 3.2-1: Double-Angle Connection limit state strength (without safety factors).

| | | Connection Type | | |
|--|---------------------------|-----------------|-------------|-------------|
| Limit State | | 2L3 | 2L4 | 2L5 |
| Shear Checks | Bolt Bearing and Tear Out | 209.8 k | 279.8 k | 349.6 k |
| | Shear Yielding | 148.9 k | 201.5 k | 254.0 k |
| | Shear Rupture | 141.3 k | 192.4 k | 253.3 k |
| | Block Shear Rupture | 149.8 k | 199.4 k | 249.1 k |
| Tension Checks | Bolt Bearing and Tear Out | 153.8 k | 205.1 k | 256.4 k |
| | Tension Yielding | 248.2 k | 335.8 k | 423.4 k |
| | Tension Rupture | 235.5 k | 320.5 k | 405.5 k |
| | Block Shear Rupture | 216.8 k | 298.1 k | 386.8 k |
| Bolt Shear – Type N | | 143.1 k | 190.9 k | 238.6 k |
| Slip Critical Class A | | 57 k | 76 k | 95 k |
| Slip Critical Class B | | 95 k | 127 k | 159 k |
| Bolt Tension and Shear Interaction Maximum Tensile Force per Bolt | | 20.6 k/bolt | 19.9 k/bolt | 18.2 k/bolt |

3.3. Test Assembly Overview

The test assembly was constructed in the existing CSEC test frame at MSOE. The double-angle specimens were centered in the frame and attached to a W18×35 beam. The opposite side of the W18×35 beams were detailed with a pin connection designed to allow free rotation. A two-span system was used to replicate a typical steel building. To allow for reuse of the W18×35 beams, web doubler plates were welded to each side of the beam webs to minimize bolt-hole deformations after repeated testing. Figure 3.3-1 and 3.3-2 show the general arrangement of the testing frame. The components of this test frame were designed during earlier tests by Friedman (2009); as components are identical for this experimental program, structural design calculations may be viewed in the appendix of Friedman's report.

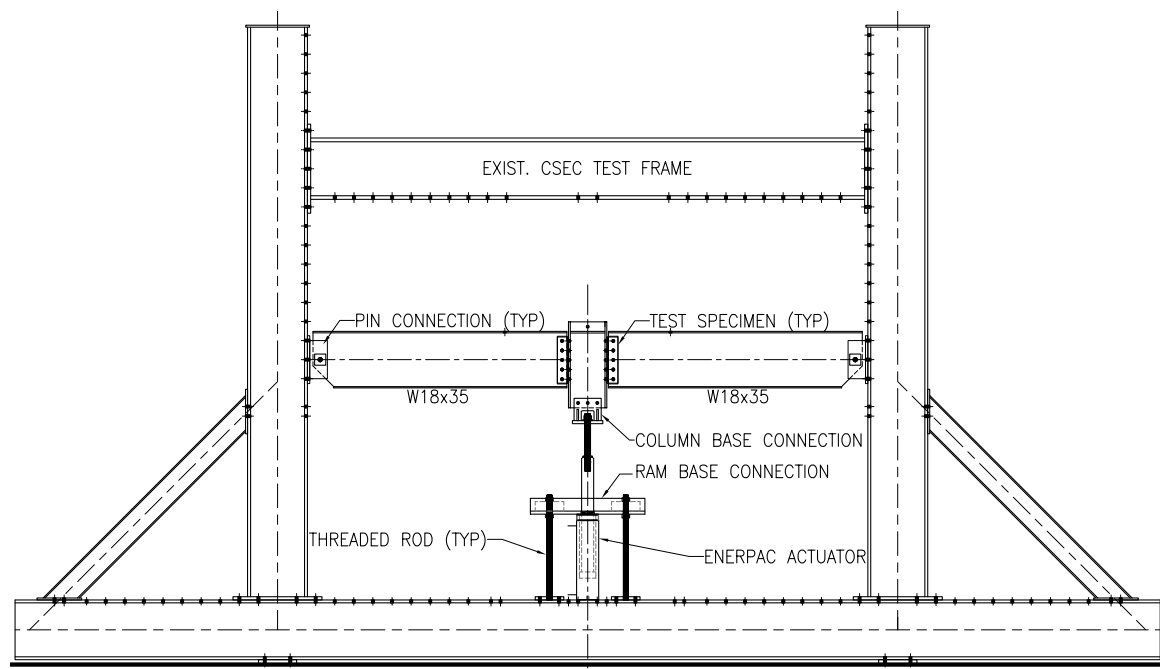


Figure 3.3-1: Test assembly overview.

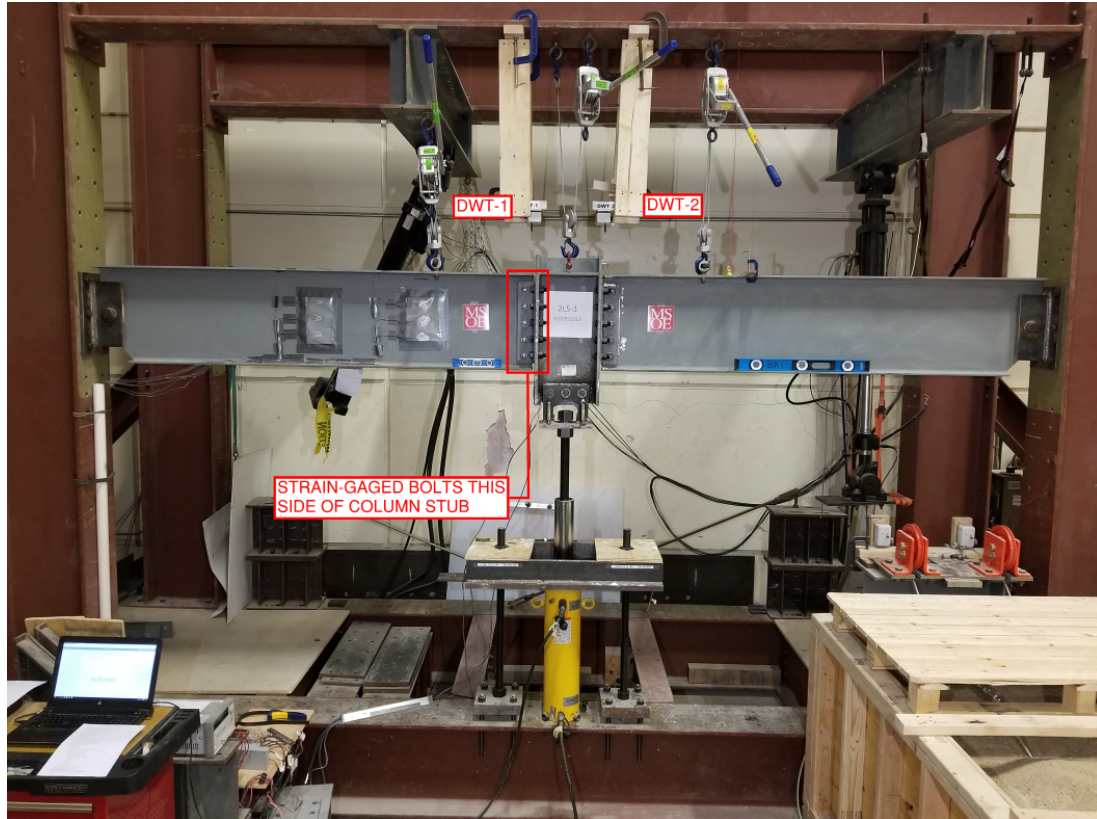


Figure 3.3-2: Test assembly overview.

All bolts were labeled prior to testing. Figure 3.3-3 details the bolt hole labeling, with odd numbered bolts on the left-hand side of the column and even on the right-hand side as an observer would see as they face either side of the column stub.

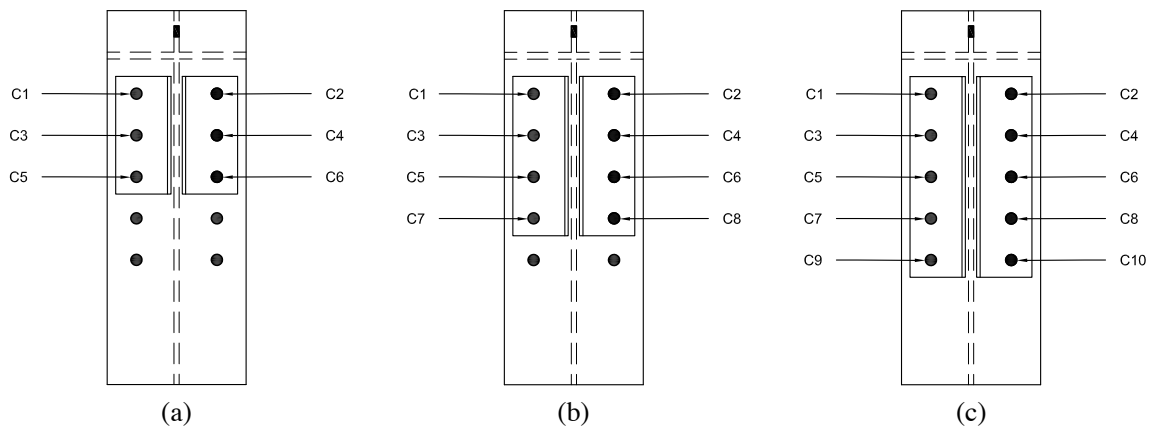


Figure 3.3-3: Bolt naming convention for (a) 2L3, (b) 2L4, and (c) 2L5 configurations.

Specimens were pretensioned in place using a spud wrench and cheater bar, and later on in testing by a TONE shear wrench. Pretensioning force was confirmed for all bolts in all tests through the use of DuraSquirt DTI torque-indicating washers from Applied Bolting Technologies. The test specimens were bolted to a column stub, which was in turn connected to a threaded rod. This threaded rod was threaded directly into the ram of an Enerpac RR-10018 hydraulic cylinder. This hydraulic cylinder assembly is shown in Figure 3.3-4.

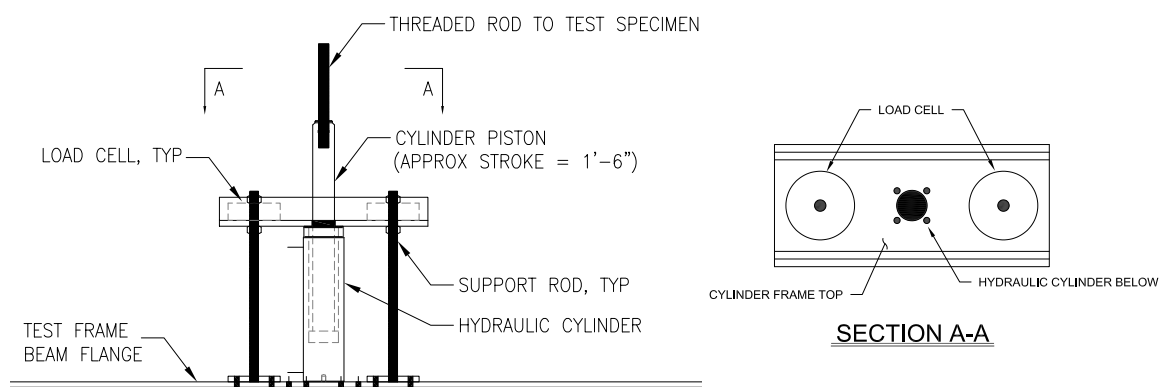


Figure 3.3-4: Hydraulic cylinder assembly.

The hydraulic cylinder assembly held two Sensotec Model 41-A530-01-03 load cells that were connected to a National Instruments NI 9215 cDAQ 9178 connector and signal conditioner, which connected to an HP ZBook 15 G3 mobile workstation with National Instruments “LabView” software for user interface with the data acquisition system. The data acquisition system measured the total amount of applied load to the system by essentially using the two load cells as reactions for the hydraulic cylinder: A heavy built-up channel spanned across the contact point of the hydraulic ram, and this channel was restrained from vertical movement by nuts spun onto the threaded rod until they contacted the load cells. When the hydraulic cylinder was retracted to pull the test

assembly down, the rods flanking it developed a tension force which was resisted against the load cells.

Unimeasure Model PA-30-DS-L5M draw wire transducers (DWT) with an MPJA Model 14601PS DC Power Supply were placed above the specimen, on wooden frames, to measure vertical displacement as load was applied to the assembly. Deflections from the two DWTs used were averaged to determine the deflection of the system. Rotation at the connection was determined based on DWT measurements and assembly geometry.

Ten Texas Measurements FLA-5-11-5LJC strain gages were applied to the left test beam, with five strain gages placed at the $1/4$ point of the beam span, and five placed at the $1/2$ point of the beam span. The beam span used to place the strain gages is the distance from the holes used for the angle connection to the pin connection at the other end. The five strain gages at each of these locations were placed at the top of the flanges, the third points of the beam depth, and at the half point of the beam depth. Figure 3.3-5 shows the strain gage placement on the testing beam.

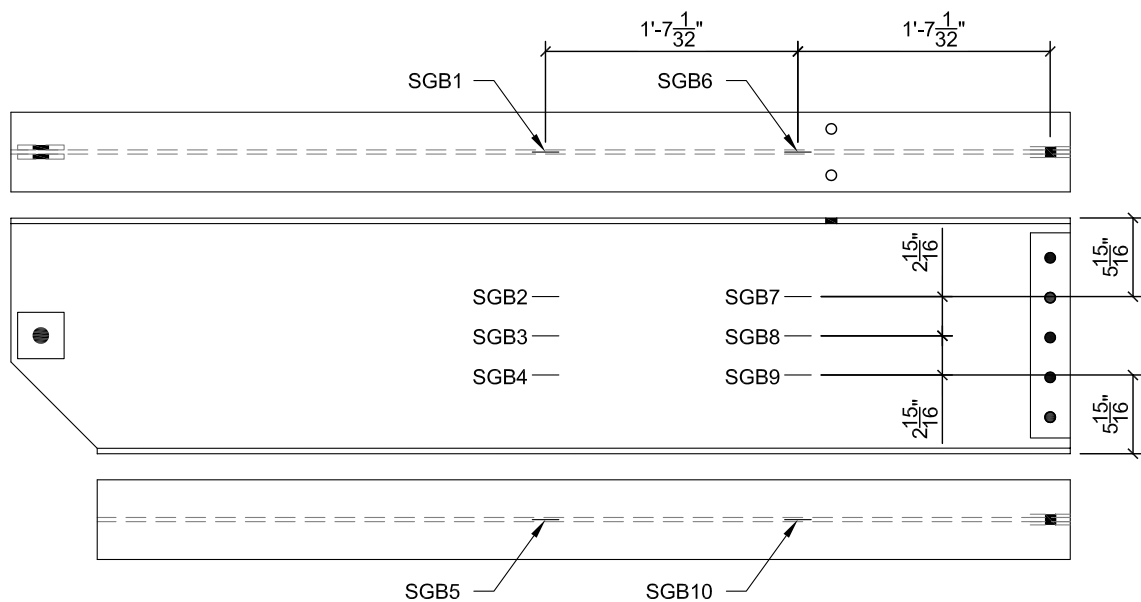


Figure 3.3-5: Strain gage placement on beam.

In addition to the strain gages on the test beam, six bolts were strain gaged with Texas Measurements BTM-6C-1LDA strain gage to provide tensile strains during testing. The two National Instruments NI 9235 input modules limited the number of total strain channels for testing to 16; because 10 were used for the beam, a maximum of six strain gaged bolts could be used at a time. These bolts were used to connect the angles to the column web to measure the catenary tensile force which developed during testing. Figure 3.3-6 details bolt details the placement of each of these strain gaged bolts during testing.

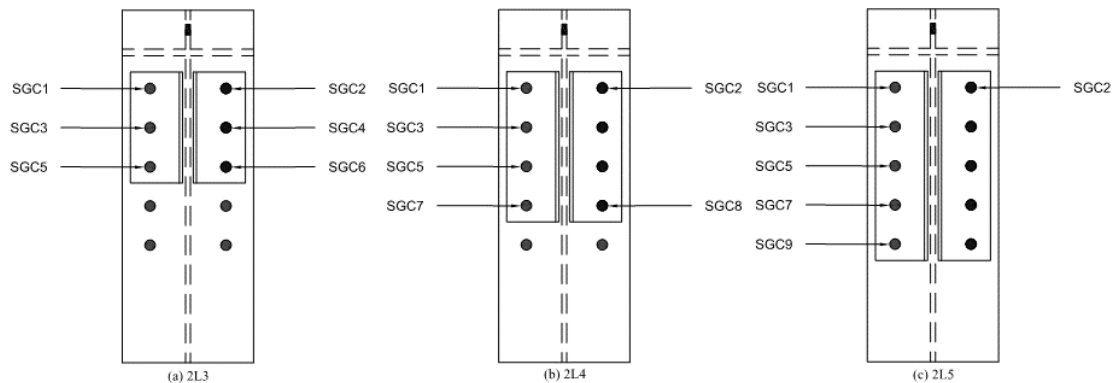


Figure 3.3-6: Strain gage placement for (a) 2L3, (b) 2L4 and (c) 2L5 specimens.

Several safety features were installed and used during testing. Three winches were used to support the test beams and column stub in case of catastrophic failure during testing. These winches were also used to support the test beams while the column stub was being removed after each test for examination of each specimen. Lateral bracing was installed at the actuator assembly to stabilize the hydraulic cylinder. A Lexan safety sheet was hung over the column stub to arrest any projectiles that may result from bolt shear.

3.4. Test Procedures

3.4.1. Assembling of Testing Frame

An initial inspection of the testing frame and actuator assembly components was completed prior to erection of the testing components. All connections on the existing testing frame were inspected and tightened if necessary. Next, the test beams were raised by bridge crane, their pin connections were fixed to the testing frame, and their supporting winches fixed to their free end. Next, the hydraulic actuator assembly was constructed, and a hydraulic pump was connected directly to the hydraulic cylinder. All measurement devices were tested for accuracy and calibrated before the installation of the column stub and test specimens.

3.4.2. Pre-Test Procedure

The installation of multiple components was required for each test. These components included the W12x53 column stub, the coupling connector, and connection elements consisting of four L4 x 3 ½ x ¼ angles: two with all standard holes, and two with HSSL holes on the column-side legs. The angles on the near side of the column stub were loosely installed with bolts and raised to the testing beams. Once column stub reached the proper elevation, the far sides of the angles were installed, and bolts were pretensioned. Strain gaged bolts were installed where appropriate and tightened. Strain gaged bolts were not pretensioned but rather were installed by spud wrench, plus a quarter turn using a cheater bar so that positive contact was made between connected elements. All bolts were then marked with an identifier matching Figure 3.3-3 for normal bolts and Figure 3.3-6 for strain gaged bolts.

After the column stub was connected to the test beams, the hydraulic ram and coupling connector were raised to the column stub. The connector was fastened to the column stub using 3 A490-X bolts to a snug tight condition. Strain gage leads and connections were inspected to ensure proper operation during testing.

Plaster of Paris was applied to the non-strain gaged side of the column to identify stress patterns along the length of the angle. This was allowed to dry completely before testing began. An example of pre-test application of plaster is shown in Figure 3.4-1.



Figure 3.4-1: Plaster application on 2L3 specimen.

Photographs of the test assembly were taken following plaster application; an example of one of these photographs is shown in Figure 3.3-2. Next, Lexan was hung

over the assembly to arrest projectiles should a bolt be sheared. Winches were then loosened to allow for vertical movement of the test assembly, the data acquisition system was started and zeroed, and then load application began.

3.4.3. Test Procedure

Testing was performed by continual load application by retraction of the actuator, with intermittent stops to observe behavior and to ensure safety mechanisms were working properly. In most tests, particularly the 2L5 series of testing, significant out-of-plane displacement similar to lateral torsional buckling (LTB) behavior of the assembly was observed, and load was applied slower out of concern that out-of-plane movement would damage the actuator. An example of this LTB behavior is shown in Figure 3.4-2.

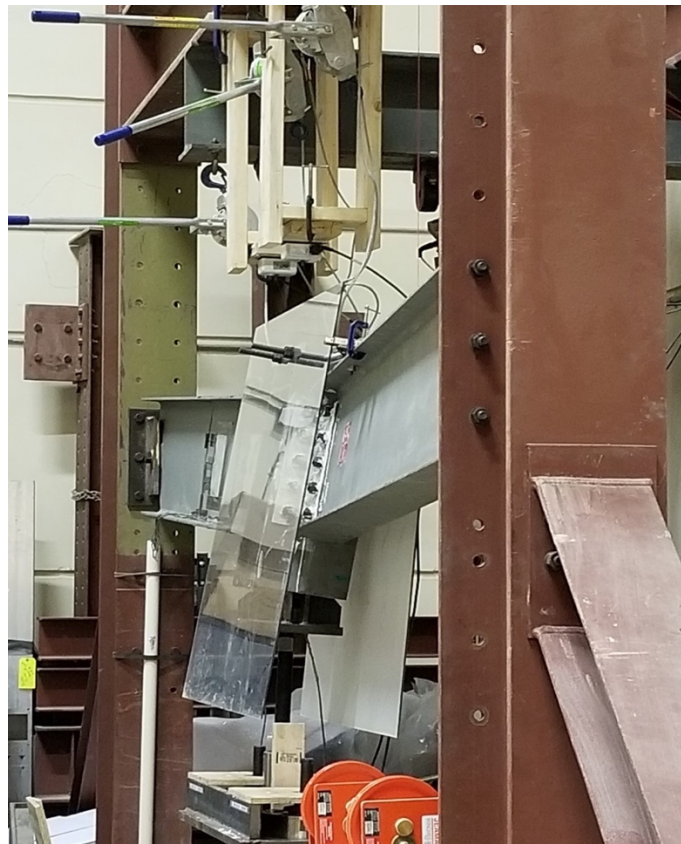


Figure 3.4-2: Lateral torsional buckling of test assembly.

This LTB behavior during testing was rudimentarily measured using a plum-bob hung from the top of the test frame against a measuring stick clamped to the top of a test beam at three-quarters of the test beam length. Testing was stopped once the buckling of the beam reached a certain threshold to avoid damage to the pin connections and actuator of the assembly. A photograph of the plum bob and measuring stick is shown in Figure 3.4-3.



Figure 3.4-3: Measurement of LTB behavior.

3.4.4. Post-Test Procedure

Once testing was completed, either by observation of binding occurrence or exhibition of severe LTB behavior, photographs were taken with an example shown in Figure 3.4-4. The winches were tightened, and the actuator was then extended to reduce the amount of applied load to a safe level. Because the angles had typically deformed and pulled away from the column flange, complete return of the actuator piston to pre-testing levels was not possible without further distortion of connection material. Therefore, to eliminate residual loading, the nuts on top of the load cells were manually loosened to reduce the amount of tensile load in the connecting rods.

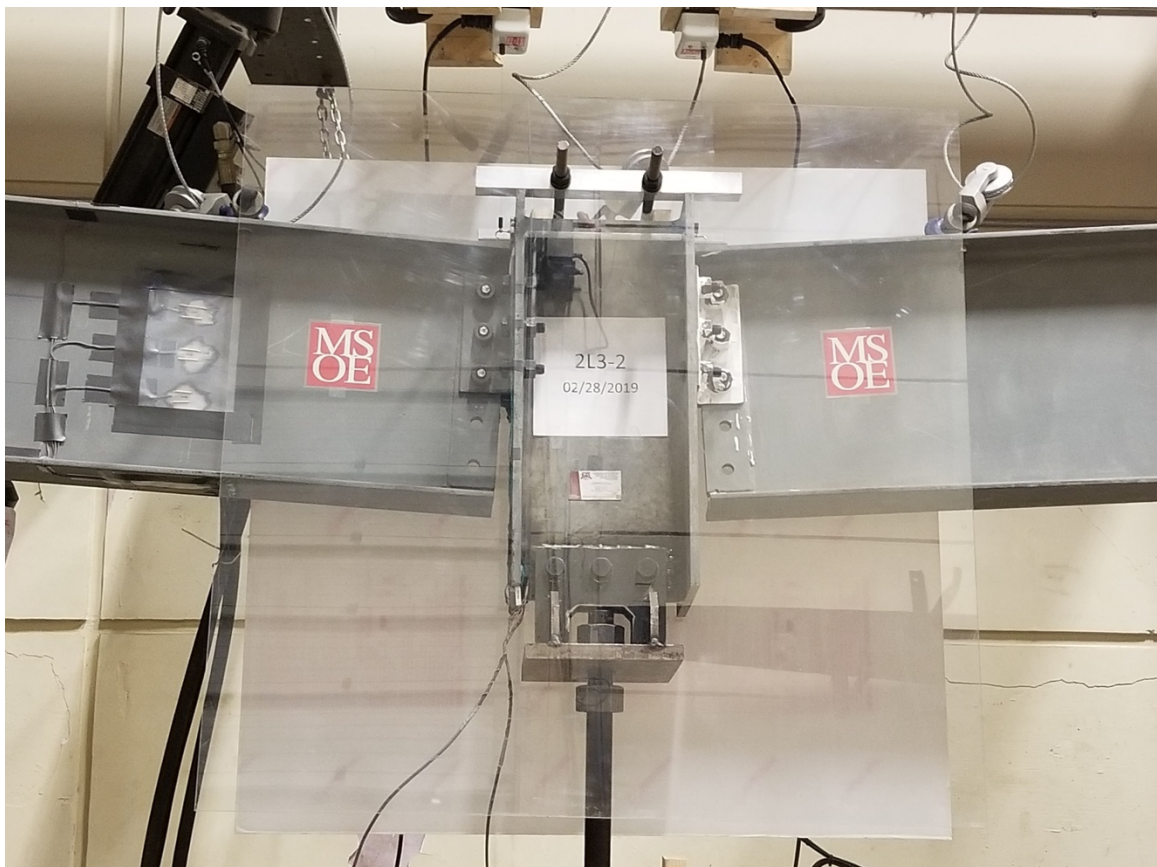


Figure 3.4-4: 2L3-2 test following completion.

Once the residual loading was eliminated, the winches were again tightened and the connection between the actuator rod and the coupling connector to the column stub was disassembled. The actuator piston was then lowered, and the specimen assembly was then disassembled.

Chapter 4: Experimental Results

4.1. Introduction

A total of nine experiments were run in this experimental program. These nine experiments were broken in to three tests each of 3-Bolt, 4-Bolt and 5-Bolt double-angle tests. Each configuration was quasi-static as the loading was applied slowly, at a rate of about one-quarter of an inch per second, with intermittent interruptions to allow for observation. The data collected were then verified through a basic structural analysis procedure, and the results have been summarized to provide means of comparison between different specimens in this experimental program as well as published literature.

4.2. Determination of Forces

The output data from the strain gages, DWTs and load cells were collected through the LabView program which was written specifically for these tests. Strain gages located at the flanges, third points and half points of the beam depth collected strain data throughout the duration of the test. Data were collected at an interval of 0.1 seconds. The strain data points collected from the beam strain gages were used to determine internal forces in the beam, and the strain data collected from the strain gaged bolts in the connection provides a means to determine the distribution of strain throughout the depth of the connection. DWTs measured the amounts of vertical displacement at the top of the column stub. These displacements were used to determine the amount of rotation at the connection for each test. Load cells recorded the applied force in pounds of force.

After testing, the force versus displacement of each particular specimen was plotted, along with load versus strain and load versus rotation.

4.2.1. Determination of Connection Forces

Average deflection was determined by averaging the deflection values recorded by each DWT during testing. Deflection was measured at the midpoint of each column flange, and the DWT connectors were attached at the very end of the column stub. The average deflection, Δ_{ave} , was calculated as:

$$\Delta_{ave} = \frac{DWT1 + DWT2}{2} \quad (\text{inches}), \quad (4.2-1)$$

where $DWT1$ and $DWT2$ are the displacement readings from DWT1 and DWT2, respectively, in inches.

Total load, P_{total} , was determined by summation of the individual load cell values. The resulting value represents the total amount of load imparted into the test assembly by the hydraulic actuator. Thus:

$$P_{total} = LC1 + LC2 \quad (\text{pounds}), \quad (4.2-2)$$

where $LC1$ and $LC2$ are the values from the individual load cells in pounds.

The angle of rotation was determined as the angle perpendicular to the face of the column stub. Using data collected from the DWT1 and DWT2 and the geometry of the testing assembly, the angle of rotation for either side of the assembly is calculated as:

$$\theta_n = \tan^{-1} \left(\frac{\Delta_n}{L_{beam}} \right) \quad (\text{radians}), \quad (4.2-3)$$

where

Δ_n = deflection reading from DWT1 or DWT2 (left or right, respectively)

L_{beam} = 79.81 inches.

Stresses were calculated by multiplying measured strain values by the modulus of elasticity of the testing material as determined from material tests by a laboratory. From these material tests, it was found that the test beam material met the requirements for

classification of ASTM A992 and had a modulus of elasticity of 29,000 ksi (to an accuracy of three significant figures). The stress at the strain gages was calculated as:

$$\sigma = \mu\varepsilon(E), \quad (4.2-4)$$

where

$\mu\varepsilon$ = measured microstrain, and

E = modulus of elasticity, 29,000 ksi.

Axial forces were calculated at the quarter and half span of the beams and were determined using the average of the stresses at the beam flanges calculated by Equation (4.2-4). Refer to Figure 3.3-5 for strain gage numbering on the beam. For the axial load at the half point of the beam, strain gages SGB1 and SGB5 were used. Thus:

$$P_{0.5L} = \left(\frac{\sigma_1 + \sigma_5}{2} \right) A, \quad (4.2-5)$$

where

σ_1 = stress calculated from strain gage SGB1, ksi,

σ_5 = stress calculated from strain gage SGB5, ksi, and

A = cross sectional area of the member, in².

An identical approach was taken to calculate the axial force in the test beam at the quarter point length, with the only difference being the strain gages used to calculate the force. SGB6 and SGB10 were used to calculate the axial force at this location. Thus:

$$P_{0.25L} = \left(\frac{\sigma_6 + \sigma_{10}}{2} \right) A, \quad (4.2-6)$$

where

σ_6 = stress calculated from strain gage SGB1, ksi,

σ_{10} = stress calculated from strain gage SGB5, ksi, and

A = cross sectional area of the member in².

By an application of mechanics of materials, the normal stress may be calculated by using the interaction equation for flexural and axial stress. Because the normal stress at the locations of strain gages is known by the use of Equation (4.2-4), this equation may be rearranged to solve for the moment, M , at the location of any strain gage. Thus:

$$M = \left(\sigma - \frac{P}{A} \right) \frac{I}{y}, \quad (4.2-7)$$

where

σ = stress calculated from a respective strain gage, ksi,

P = axial force calculated by equation 4.2-5 or 4.2-6, kips,

A = cross sectional area of the member, in²,

I = moment of inertia of the member, in⁴, and

y = distance to the neutral axis of the member, in.

The moment at the connection, M_{conn} , was found by scaling the moment at the midpoint of the beam by a factor of length. Because the moment along the beam was assumed to increase in a linear fashion, this scaling factor was 2. Thus:

$$M_{conn} = 2M, \quad (4.2-8)$$

where M is the moment at the midpoint of the beam as calculated by Equation (4.2-7).

The shear applied to the connection was assumed to be one-half of the total load imparted on the assembly by the actuator because there are two identical connections resisting the downward movement of the column stub. Thus:

$$V_{applied} = \frac{P_{total}}{2}, \quad (4.2-9)$$

where

P_{total} = load imparted on the test assembly by the hydraulic ram, kips.

4.3. Determination of Bolt Forces

Axial forces in the bolts were found by first determining the stress in the bolt by use of Equation (4.2-4) and multiplying this stress by the cross-sectional area of the bolt.

Thus:

$$P_{bolt} = \mu\sigma A, \quad (4.2-10)$$

where $\mu\sigma$ is the microstrain measured from the strain gage and A is the cross-sectional area of the bolt, which is 0.442 in^2 .

4.4. Results of Experimental Tests

The following sections are organized by bolting configuration and include a description of the tests, pictures before and after failure, and graphs of the calculated forces and moment at the connection based on measured strains. For all tests, significant LTB behavior was observed immediately upon loading of the column stub, with rotation of the top of the column stub out of the plane of the testing frame clearly visible. This behavior was not expected, and as such, loading was applied at a more gradual pace, with numerous periods of load application and non-application throughout the course of each test.

It is hypothesized that the entire assembly behaved as a large beam spanning from one end of the frame to the other because of force transfer through the frictional forces between the angle legs and the beam web resulting from bolt pretensioning. In effect, if this theory is correct, the connection behaved somewhat similarly to a partially restrained moment connection, or at least as a connection incorporating slip critical bolts of either class A, class B, or somewhere between class A and class B capacity. As will be discussed more thoroughly in their respective sections, 2L3, 2L4 and 2L5 tests each

underwent insignificant levels of bolt and bolt hole deformation, indicating that it is likely that slip resistance of the connection was high and that bearing of the bolts against the edge of their respective holes did not occur.

Binding occurred between the beam flange and column flange faster in loading than expected, and due to fear of equipment damage, loading was terminated upon beam binding. No brittle failure modes were reached during testing as a result of this premature binding, but rather ductile behavior was observed in the form of angle unfolding. The most predominant behavior of the connection, however, was the drastic level of LTB that occurred as load was applied to the column stub.

4.4.1. Three-Bolt Double-Angle Tests

Three three-bolt tests were conducted with naming conventions of 2L3-1, 2L3-2 and 2L3-3. Every three-bolt test was halted before a rupture failure mode occurred due to binding between the beam flange and column flange. There were minor levels of angle deformation, with no apparent bolt deformation. Figure 4.4-1, 4.4-2 and 4.4-3 show pictures before, during, and after testing, respectively. Figures 4.4-4, 4.4-5, 4.4-6 and 4.4-7 show enlargements of testing components following testing.



Figure 4.4-1: Typical 2L3 assembly before testing.



Figure 4.4-2: Typical LTB behavior of a 2L3 series specimen during testing.

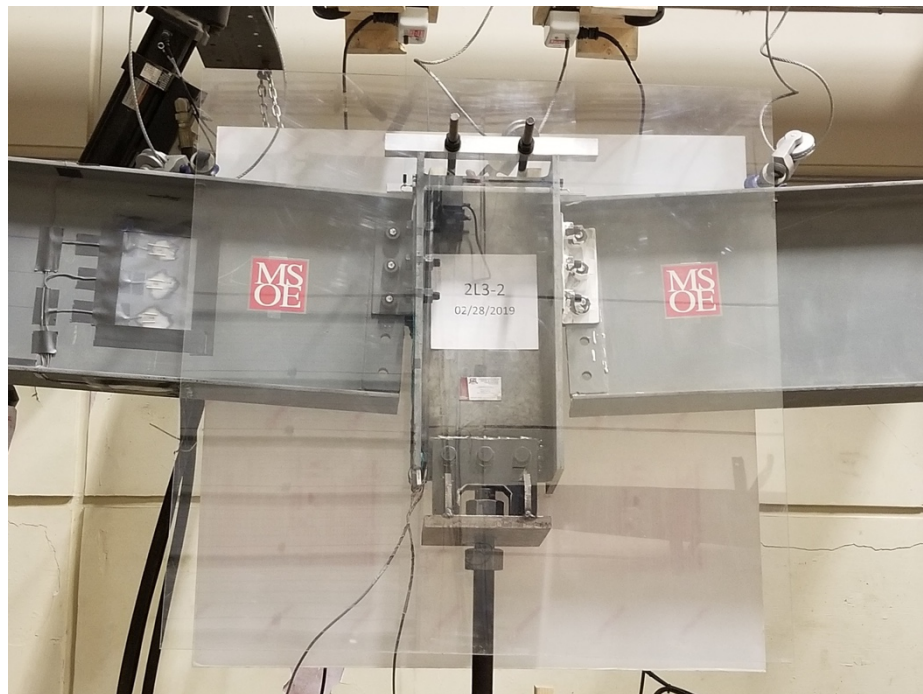


Figure 4.4-3: Typical 2L3 series specimen post-test.

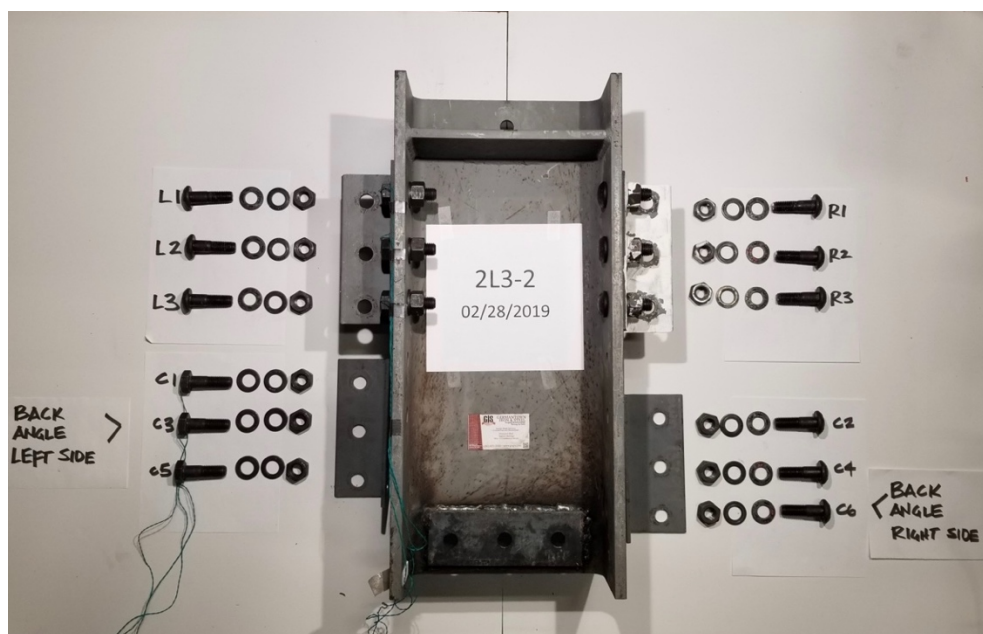


Figure 4.4-4: Typical post-test layout of 2L3 series specimen.

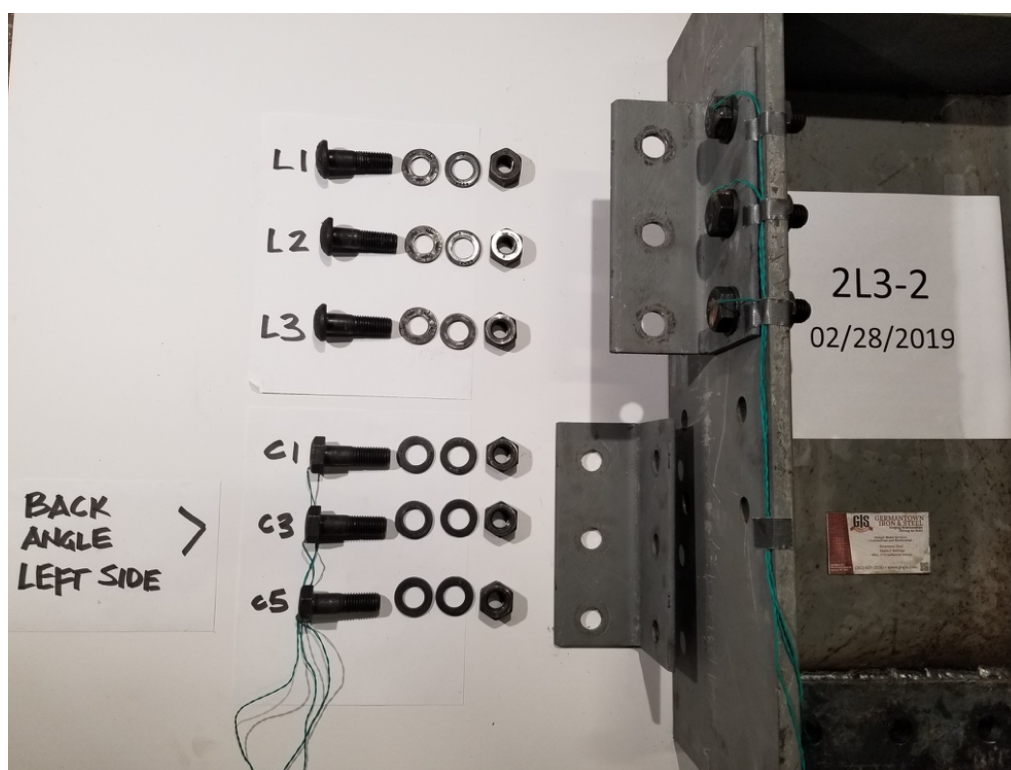


Figure 4.4-5: Typical left-hand side of a 2L3 series specimen following testing.

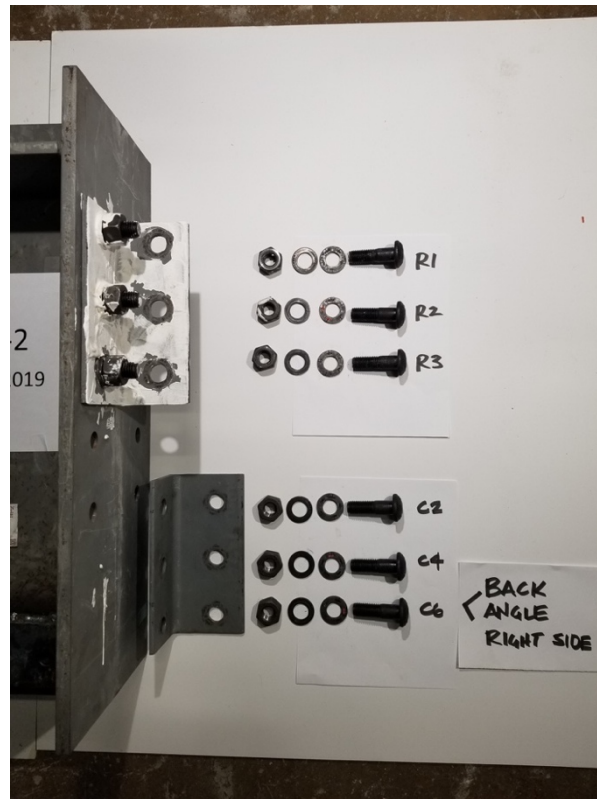


Figure 4.4-6: Typical right-hand-side of a 2L3 series specimen following testing.



Figure 4.4-7: Enlargement of plaster application on test specimen 2L3-2, typical of 2L3 series tests.

It is clear that no 2L3 specimen had undergone even a moderate level of plastic deformation following load application. In Figure 4.4-7, for example, the only visible flaking of plaster was around column bolt C3 (the bottom bolt on the plastered angle) and the web bolts. From this plaster flaking, it appears that center of rotation for the connection was somewhere between the bottom and middle bolt of the connection, making the top two bolts in either angle undergoing a reduction of tensile force due to bearing out of the angle legs against the column stub, with the bottom bolts resisting tensile forces.

Bolt hole deformations were so insignificant that they could not be accurately measured. Deformations of the bolts themselves were also insignificant, especially due to the double shear condition of the bolts at the beam web. It is also likely that the possibility of a slip-critical behavior of the connection eliminated bearing of the bolts against their respective holes, eliminating deformation until the slip-critical capacity is exceeded. Figure 4.4-8 shows the Force-Displacement plot of the 2L3 series of tests. Figures 4.4-9 and 4.4-10 show the load-rotation plots for 2L3 series of tests with respect to DWT1 in US and metric units, respectively. Figures 4.4-11 and 4.4-12 show the load-rotation plots for 2L3 series of tests with respect to DWT2 in US and metric units, respectively.

It is noteworthy that all tests shown in Figure 4.4-8 follow a similar curve. Maximum deflection for each test was about 6 inches with approximately 11 kips (49 kN) of applied load, with the exception of test 2L3-3 which was halted earlier.

From Figures 4.4-8 through 4.4-12, the maximum moment developed at the double angle tests was approximately 11 kip-ft (14 kN-m) at a shear load of 3 kips (13

kN). What is particularly interesting in the behavior of the 2L3 series of tests, however, is that the axial loads as measured by the beam were predominantly compressive rather than tensile as would be expected with the development of a catenary force. Rotations were limited to just over 0.07 radians.

Some unusual behavior was recorded by a strain gaged bolt which impacted the calculations of total bolt tensile load as evidenced by the spiking indicated on Figures 4.4-9 through 4.4-12. However, aside from the test that had been impacted by this strain gage failure, the sum of the bolt axial loads, as were expected, were all tensile.

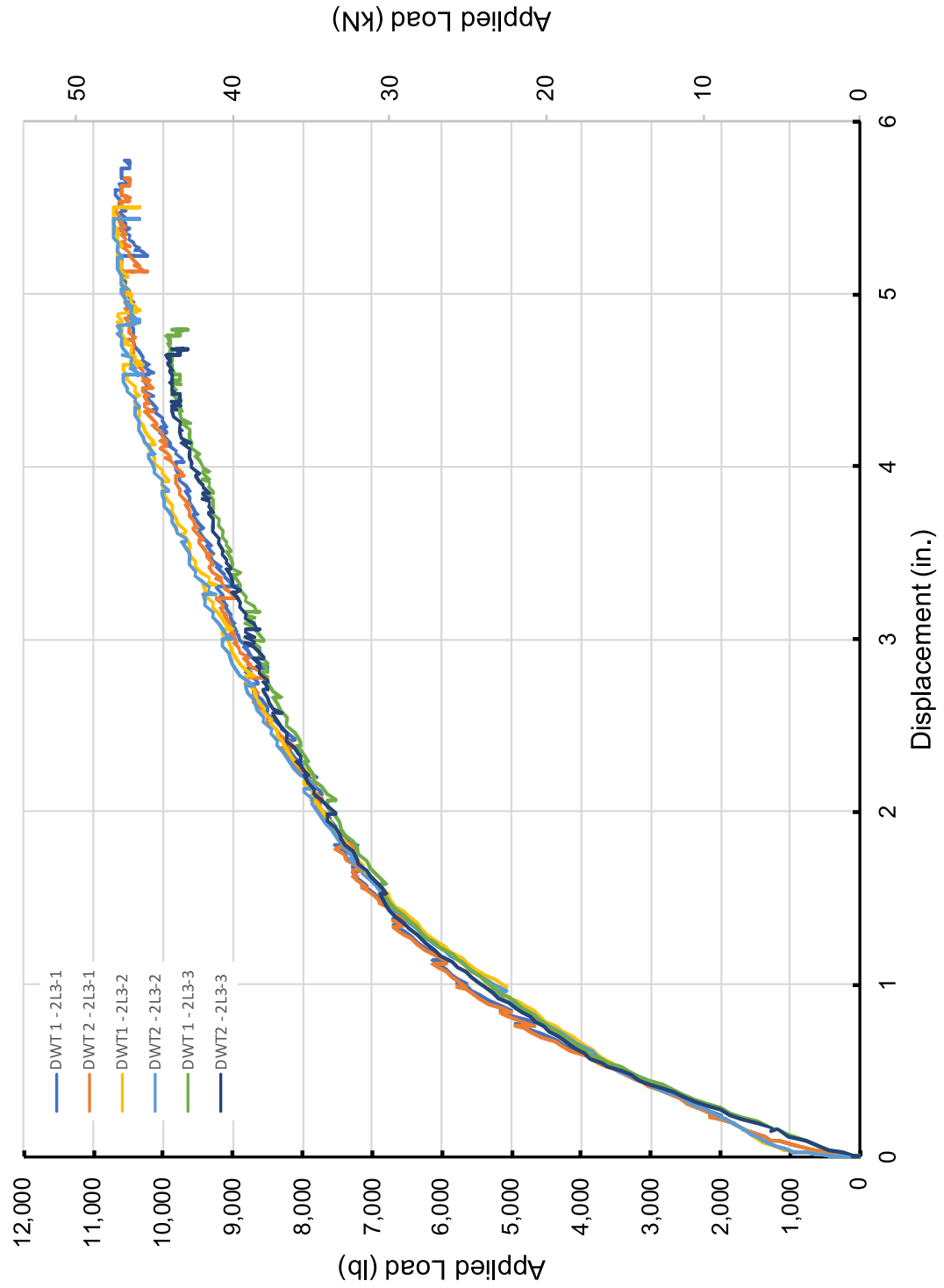


Figure 4.4-8: Load versus displacement for 2L3 series of tests.

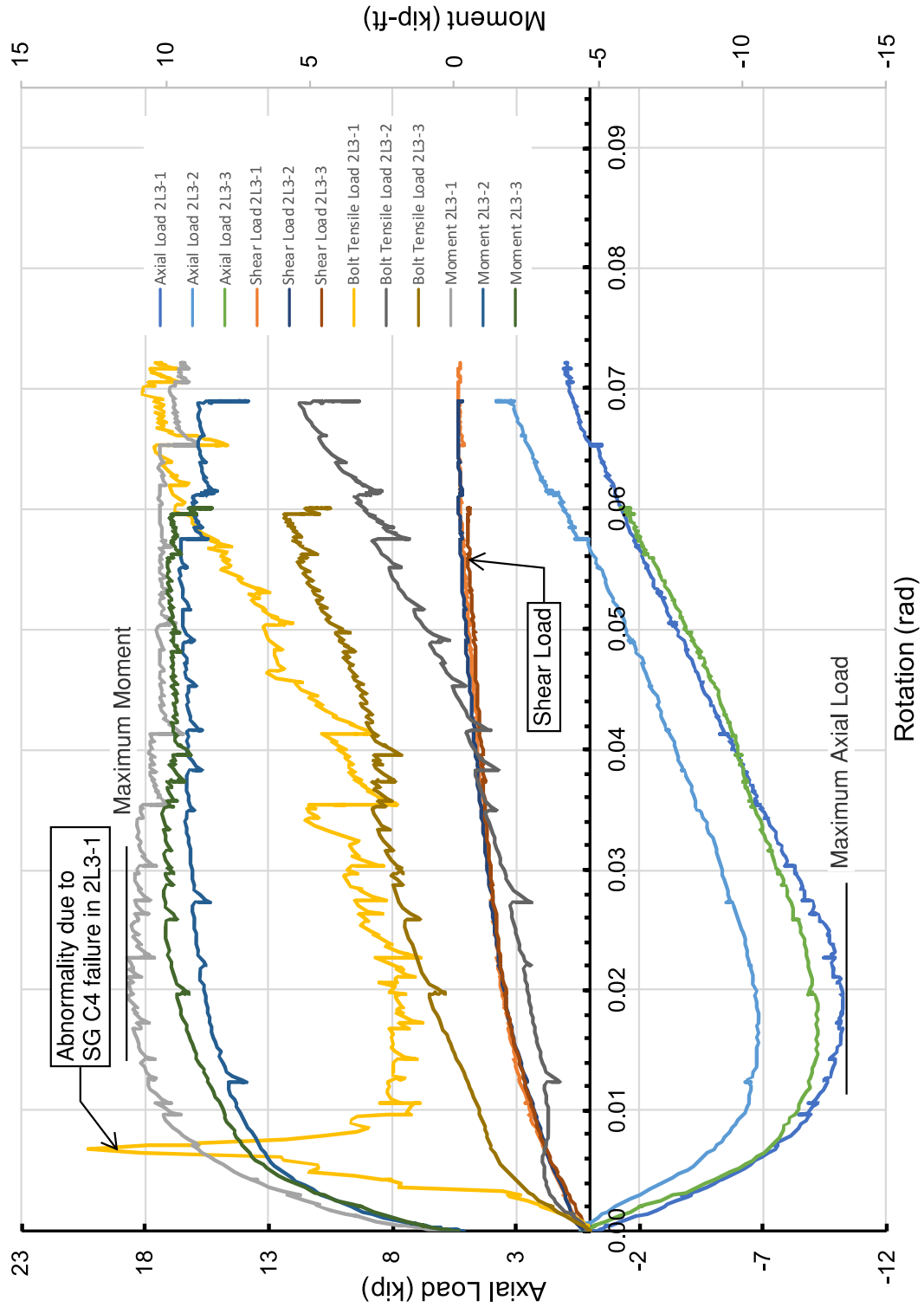


Figure 4.4-9: Load versus rotation for 2L3 series of tests with respect to DWT1 (US units).

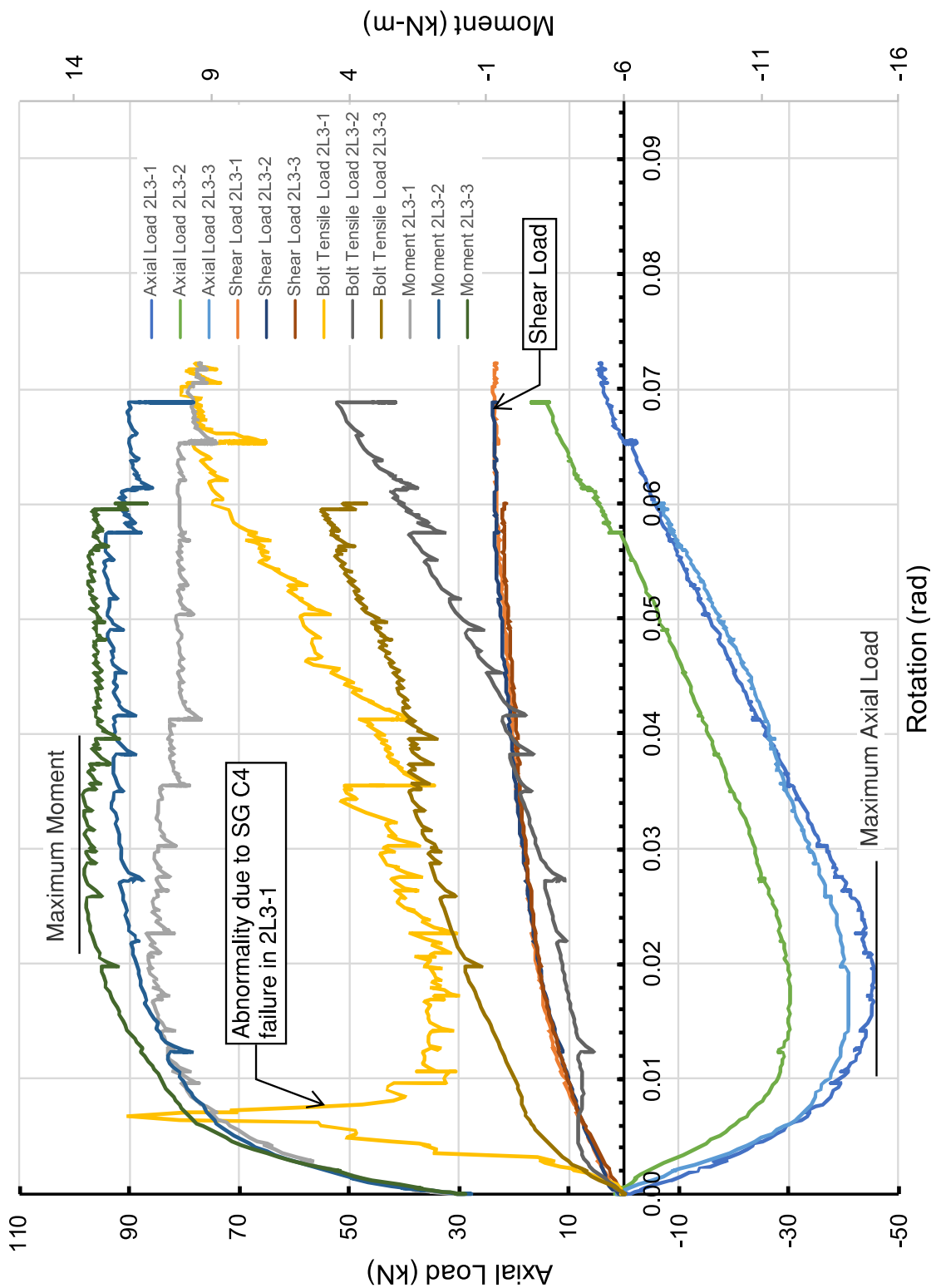


Figure 4.4-10: Load versus rotation for 2L3 series of tests with respect to DWT1 (Metric units).

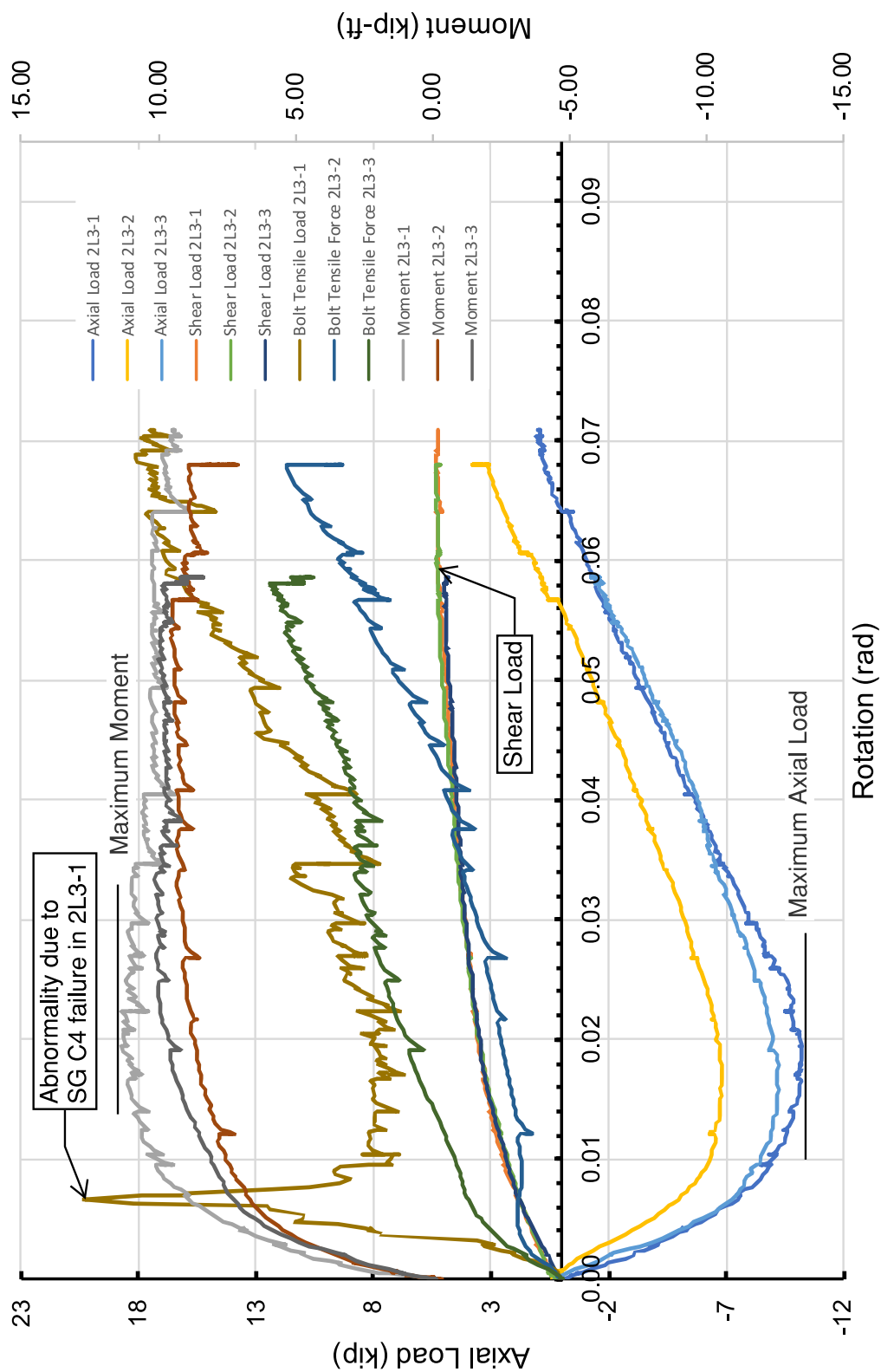


Figure 4.4-11: Load versus rotation for 2L3 series of tests with respect to DWT2 (US units).

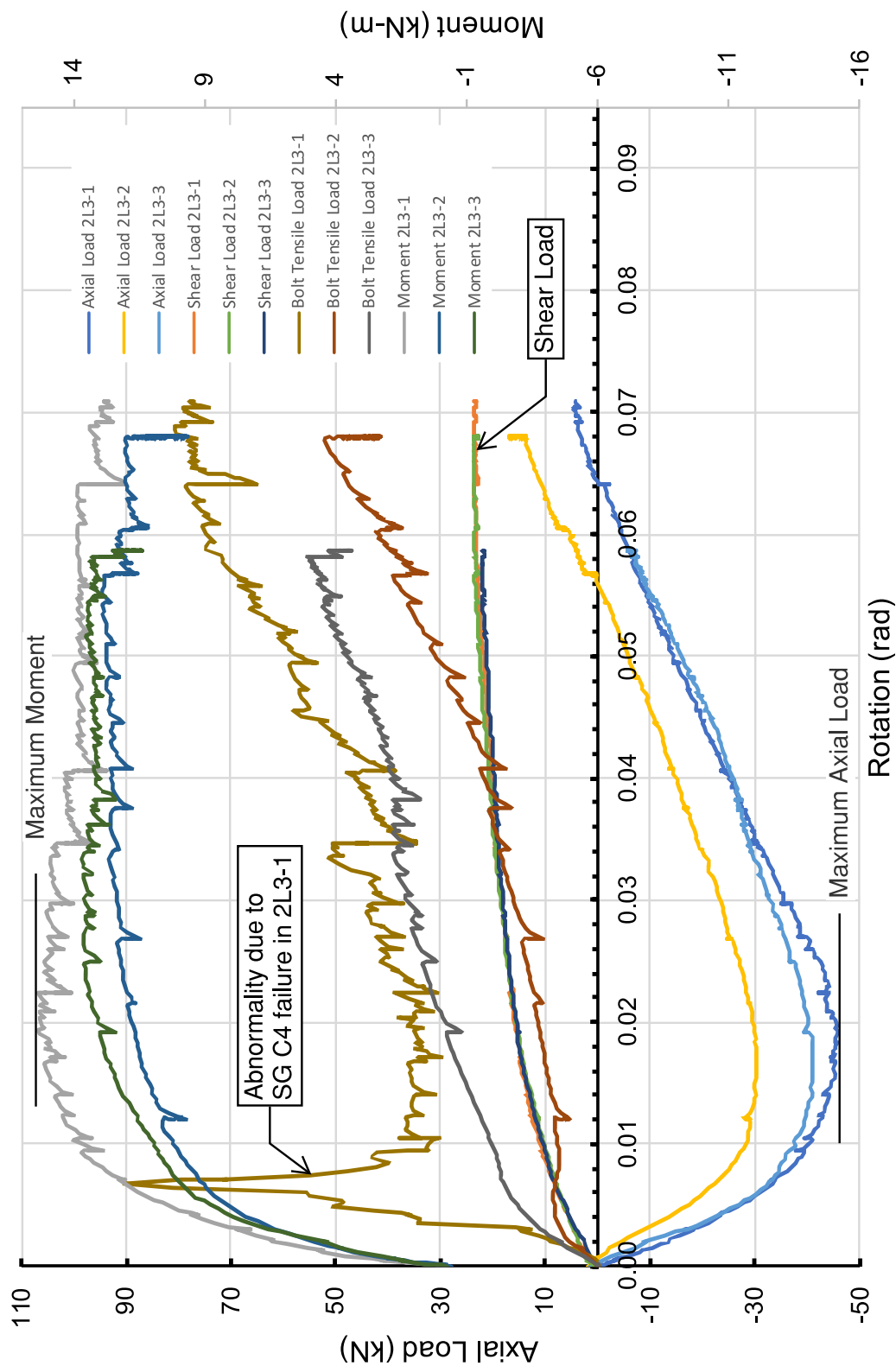


Figure 4.4-12: Load versus rotation for 2L3 series of tests with respect to DWT2 (Metric units).

4.4.2. Four-Bolt Double-Angle Tests

Three four-bolt tests were conducted with naming conventions of 2L4-1, 2L4-2 and 2L4-3. Every four-bolt test was halted before a rupture failure mode occurred due to binding between the beam flange and column flange. There were moderate levels of angle deformation, with no apparent bolt deformation. Figure 4.4-13, 4.4-14 and 4.4-15 show pictures before, during, and after testing, respectively. Figure 4.4-16 shows angle deformation immediately following a test. Figures 4.4-17, 4.4-18, 4.4-19 and 4.4-20 show enlargements of testing components following testing.



Figure 4.4-13: Typical 2L4 assembly before testing.



Figure 4.4-14: Typical LTB behavior of 2L4 series specimen during testing.



Figure 4.4-15: Typical 2L4 specimen post-test.



Figure 4.4-16: Typical underside view of specimen post-test showing angle deformation.



Figure 4.4-17: Typical post-test layout of 2L4 series specimen.

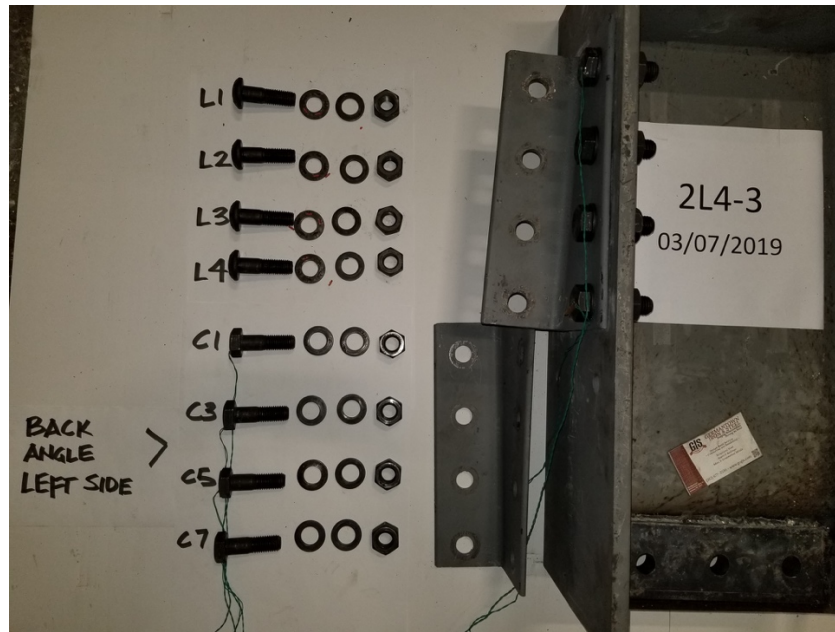


Figure 4.4-18: Typical left hand-side of a 2L4 series specimen following testing.

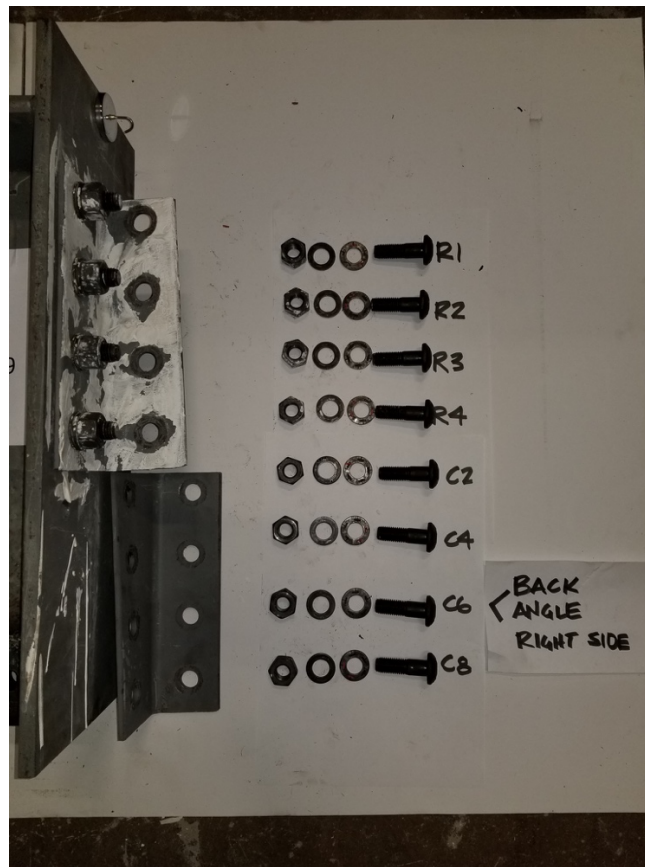


Figure 4.4-19: Typical right hand-side of a 2L4 series specimen following testing.



Figure 4.4-20: Plaster flake on specimen 2L4-1.

Specimens in the 2L4 series of tests underwent moderate levels of plastic deformation. The best example of the deformation that occurred is observable in Figure 4.4-16, in which the angle legs are prying away from the column face in a manner that was expected. However, no bolt hole deformation occurred and no localized block shear or tearing of the angles was imminent or observable. As discussed prior, it is likely that a slip-critical behavior of the connection reduced bearing of the bolts against their bolt holes, thereby reducing the observable deformations. In Figure 4.4-20, for example, the only visible flaking of plaster was around column bolt C4 (the bottom bolt on the plastered angle) and the web bolts. From this plaster flaking, it appears that center of rotation for the connection was somewhere around the third bolt of the connection.

Bolt hole deformations were so insignificant that they could not be accurately measured. Deformations of the bolts themselves were also insignificant, especially due to the double shear condition of the bolts at the beam web. Figure 4.4-21 shows the Force-Displacement plot of the 2L4 series of tests. Figures 4.4-22 and 4.4-23 show the load-rotation plots for 2L4 series of tests with respect to DWT1 in US and metric units, respectively. Figures 4.4-24 and 4.4-25 show the load-rotation plots for 2L4 series of tests with respect to DWT2 in US and metric units, respectively.

It is noteworthy that all tests shown in Figure 4.4-21 follow a similar curve. Maximum deflection for each test ranged from about 7 to 10 inches with approximately 21 kips (93 kN) of applied load, with the exception of test 2L4-1 Part 1, during which a computer failure interrupted data recording. Fortunately, this test had not progressed far enough into load application for plastic deformation to occur; the test was simply reset and carried to completion under the name 2L4-1 Part 2. However, a strain gage failure did occur which severely impacted the calculation of moment for 2L4-1 Part 2; for clarity this data was removed from Figures 4.4-22 through 4.4-25.

From Figures 4.4-22 through 4.4-25, the maximum moment developed at the double angle tests was approximately 30 kip-ft (40 kN-m) at a shear load of 7 kips (31 kN). Similar to the 2L3 series of tests, the 2L4 data show a compressive force axial force at the beginning stages of load application, but then develop tensile loads as would be expected under catenary action. Rotations were limited to just over 0.12 radians. The bolt axial loads, as expected, were all tensile.

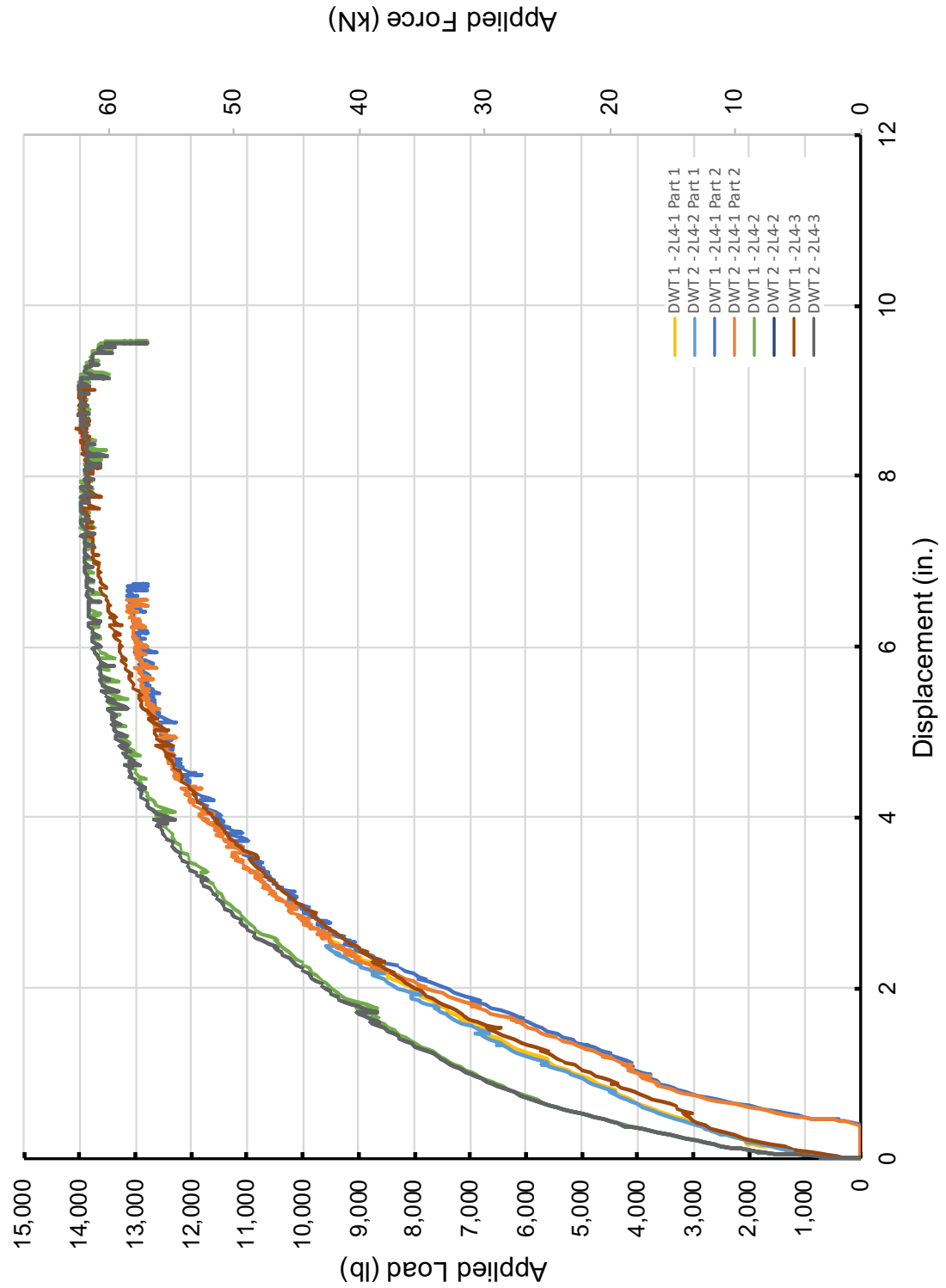


Figure 4.4-21: Force versus displacement for 2L4 series of tests.

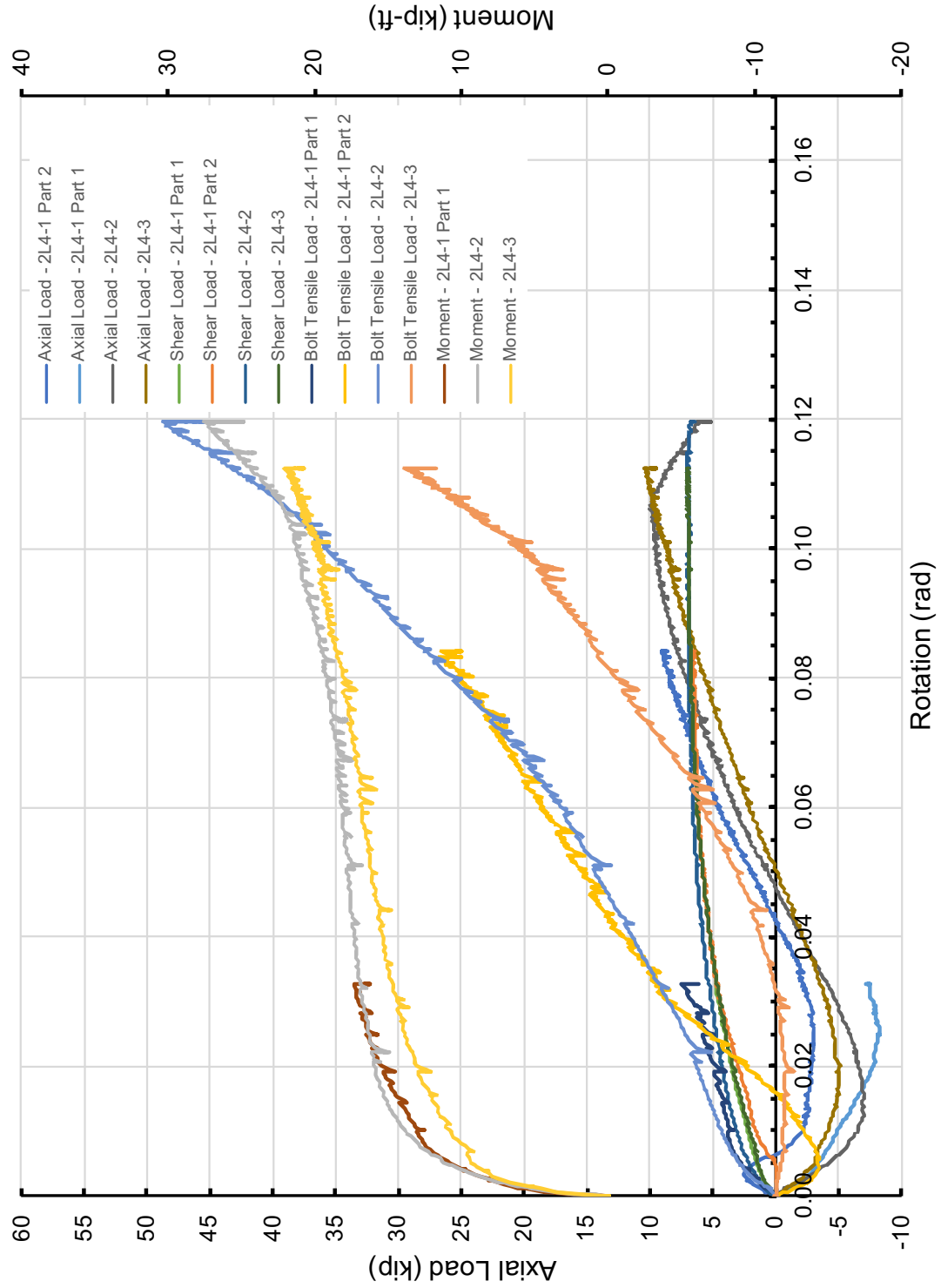


Figure 4.4-22: Load versus rotation for 2L4 series of tests with respect to DWT1 (US units).

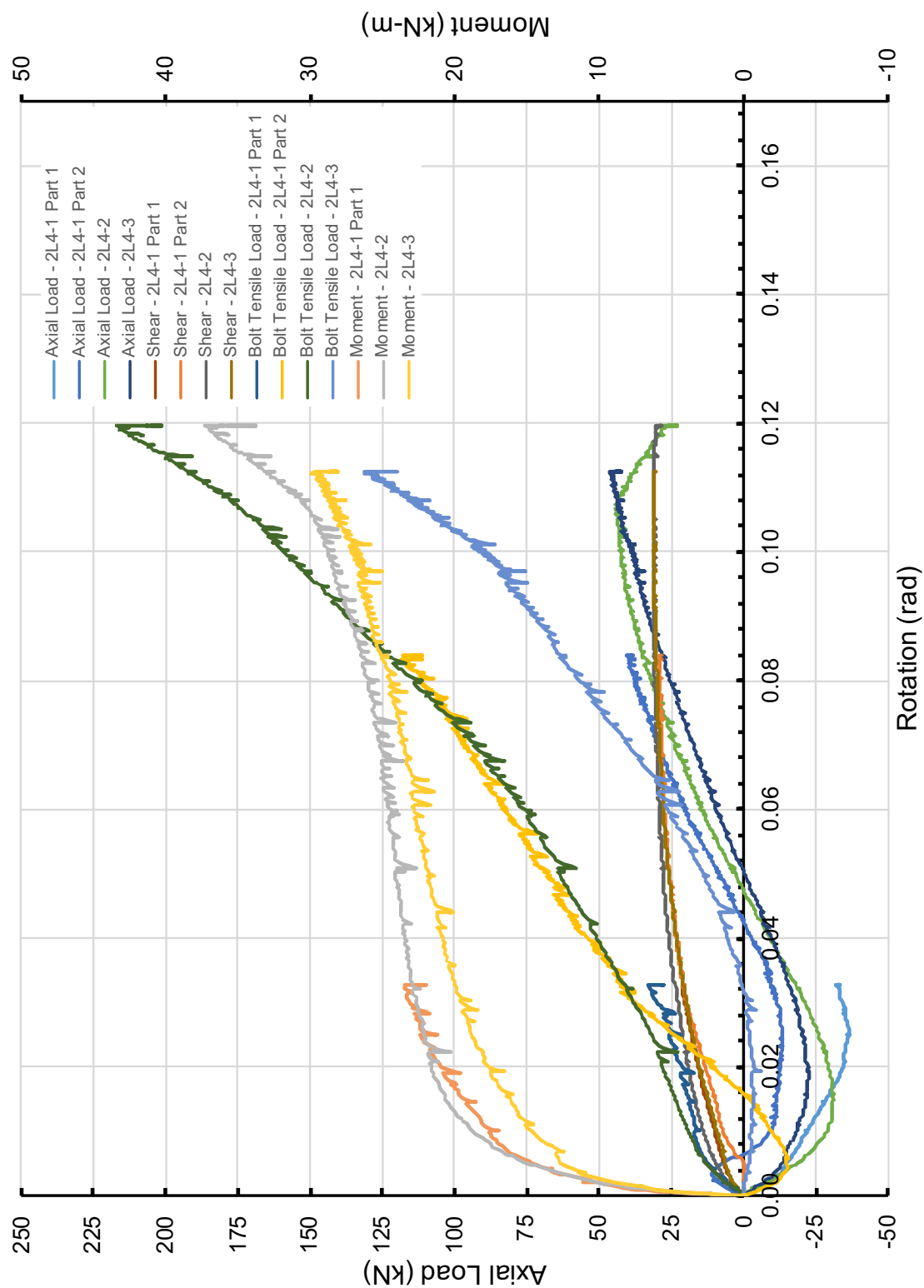


Figure 4.4-23: Load versus rotation for 2L4 series of tests with respect to DWT1 (Metric units).

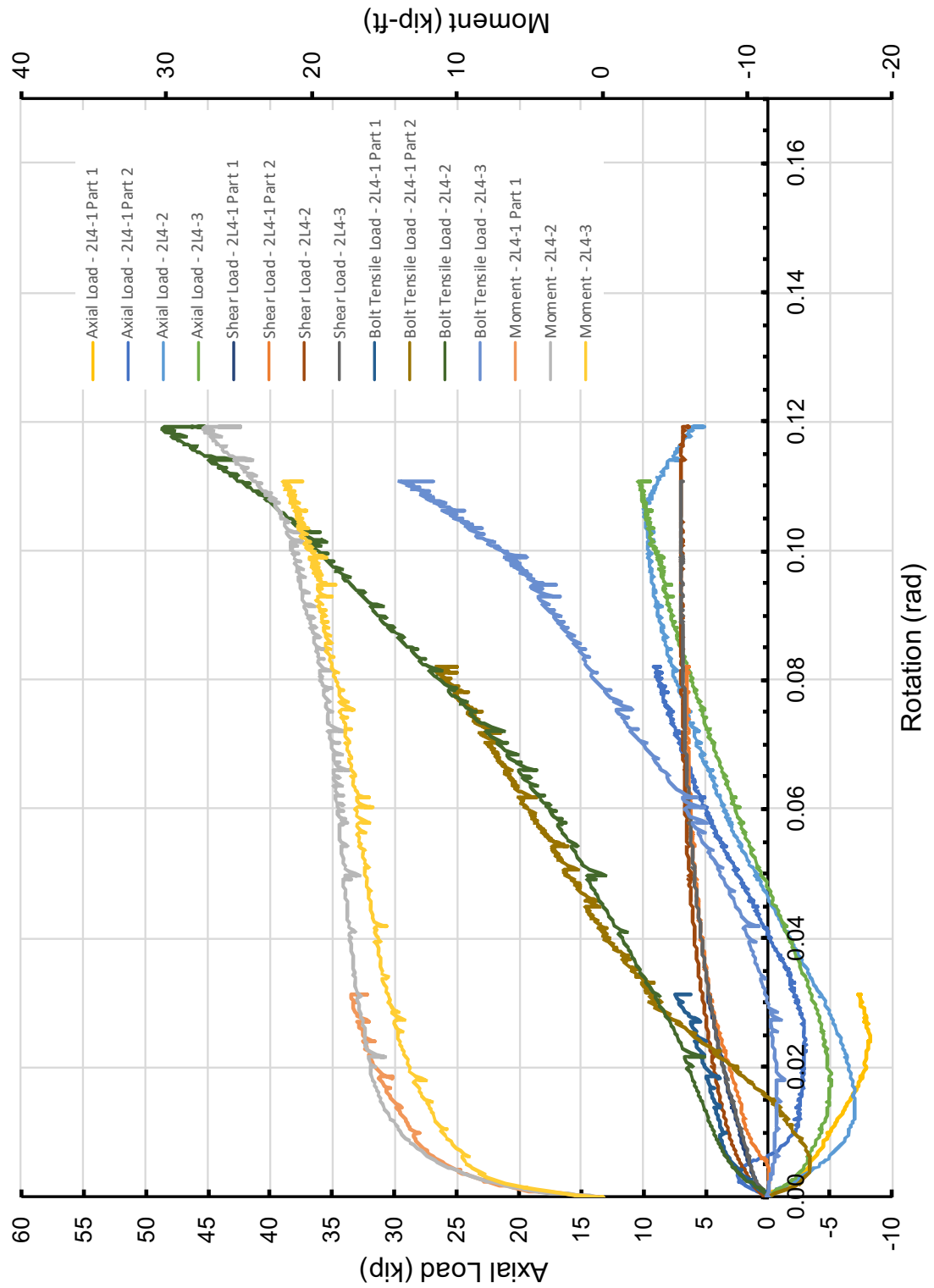


Figure 4.4-24: Load versus rotation for 2L4 series of tests with respect to DWT2 (US units).

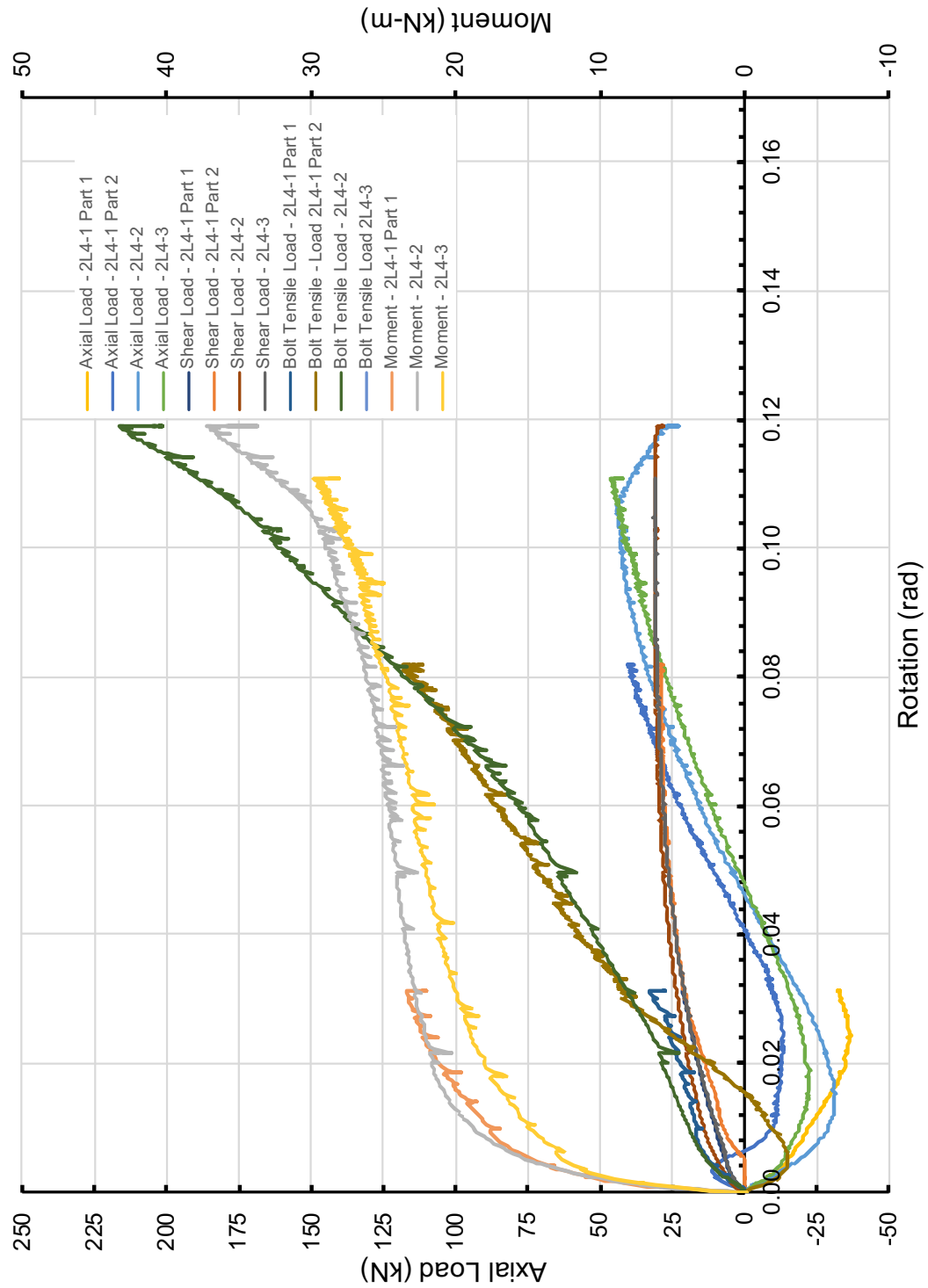


Figure 4.4-25: Load versus rotation for 2L4 series of tests with respect to DWT2 (Metric units).

4.4.3. Five-Bolt Double-Angle Tests

Three five-bolt tests were conducted with naming conventions of 2L5-1, 2L5-2 and 2L5-3. Every five-bolt test was halted before a rupture failure mode occurred due to binding between the beam flange and column flange. There were higher levels of angle deformation than three or four bolt tests, as expected, with no apparent bolt deformation. Figure 4.4-26, 4.4-27 and 4.4-28 show pictures before, during, and after testing, respectively. Figure 4.4-16 shows angle deformation immediately following a test. Figures 4.4-17, 4.4-18, 4.4-19 and 4.4-20 show enlargements of testing components following testing.



Figure 4.4-26: Typical 2L5 assembly before testing.

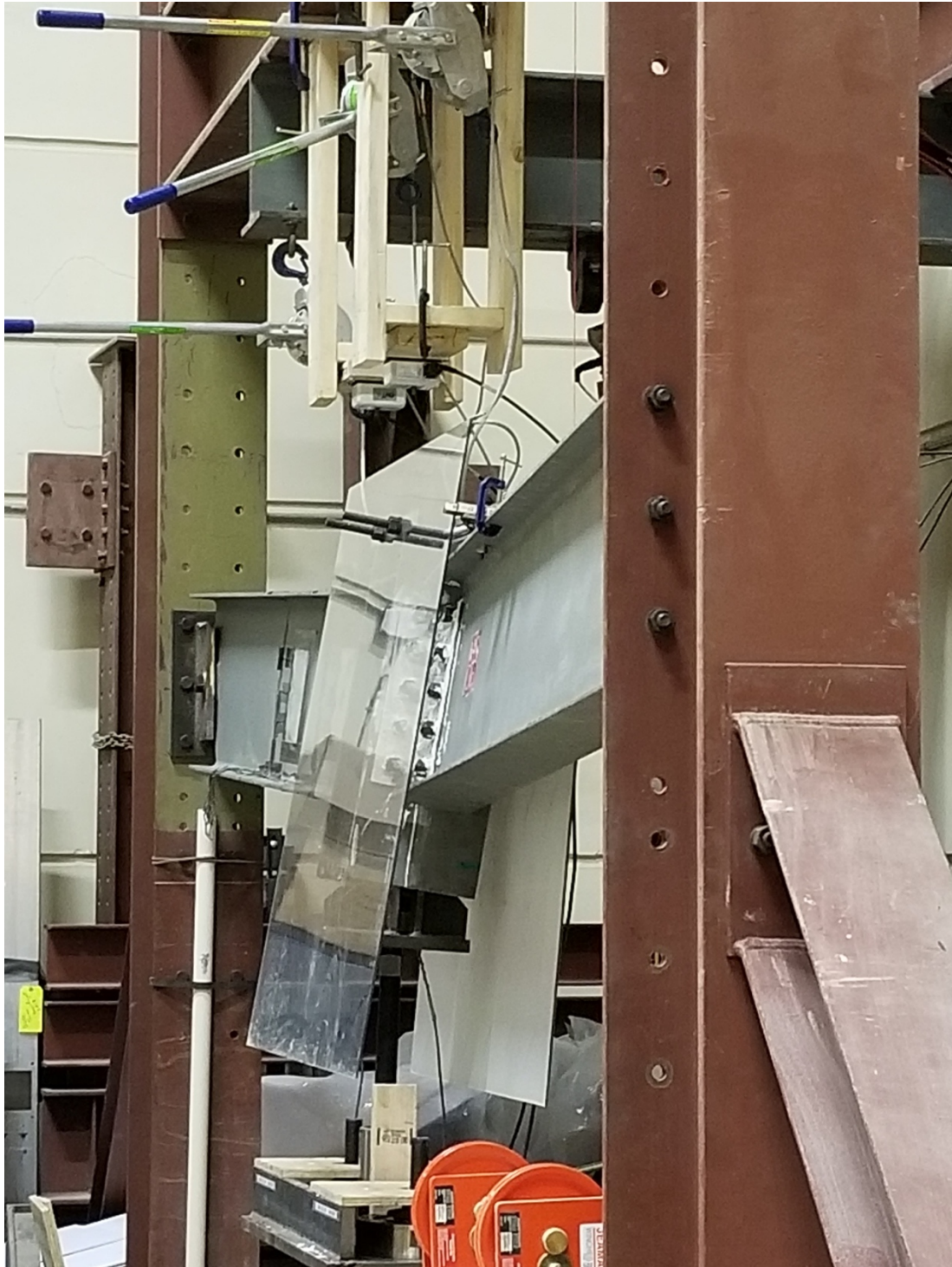


Figure 4.4-27: Typical LTB behavior of 2L5 series specimen during testing.



Figure 4.4-28: Typical 2L5 specimen post-test.

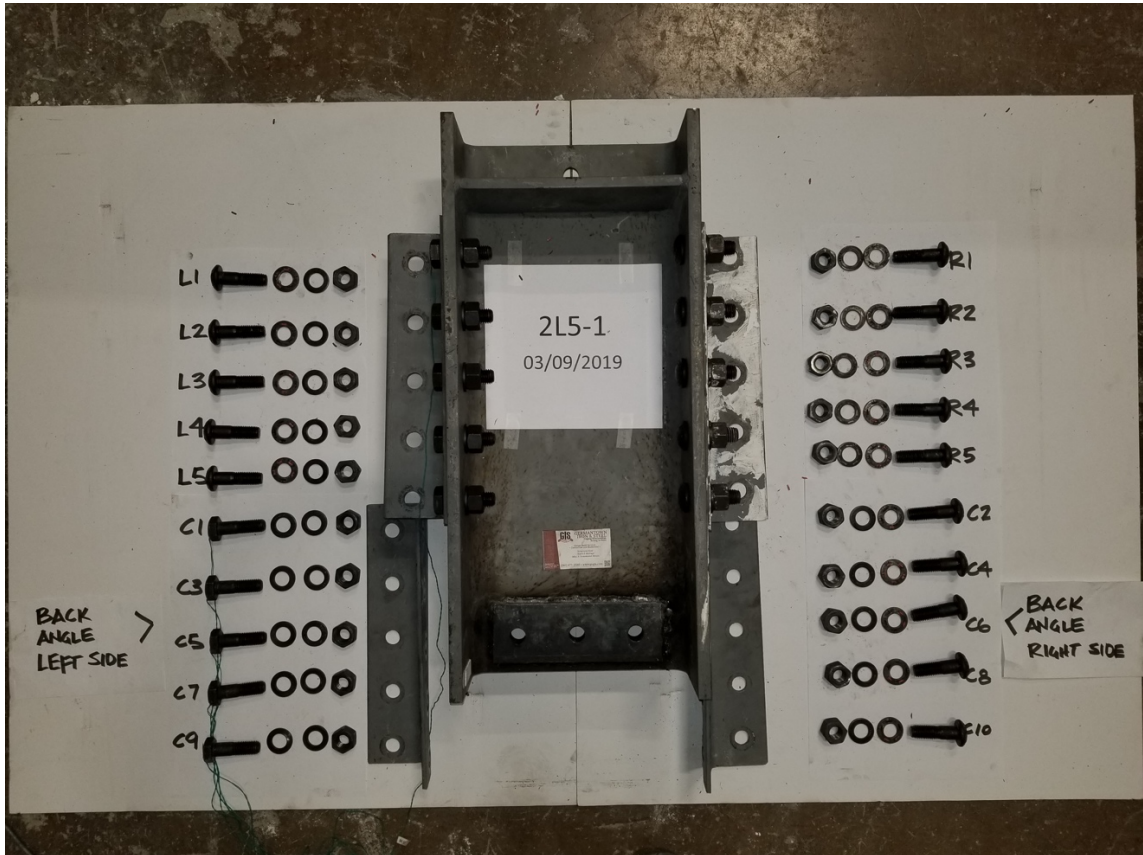


Figure 4.4-29: Typical post-test layout of 2L5 series specimen.

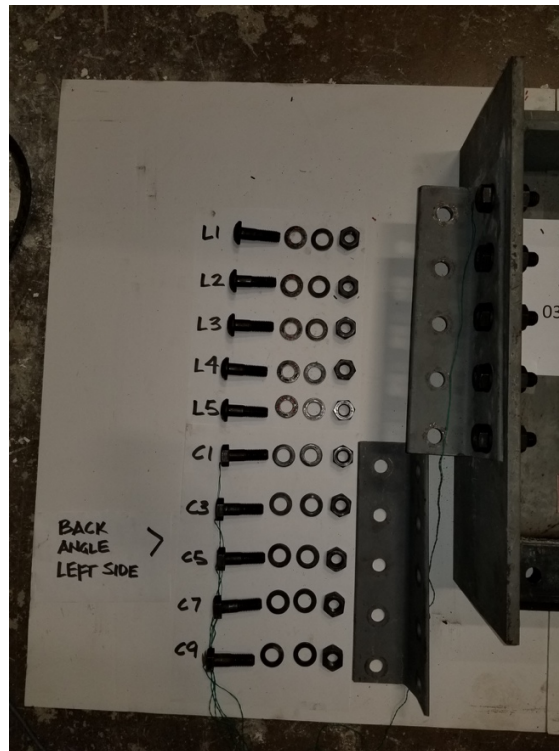


Figure 4.4-30: Typical left hand-side of a 2L5 series specimen following testing.

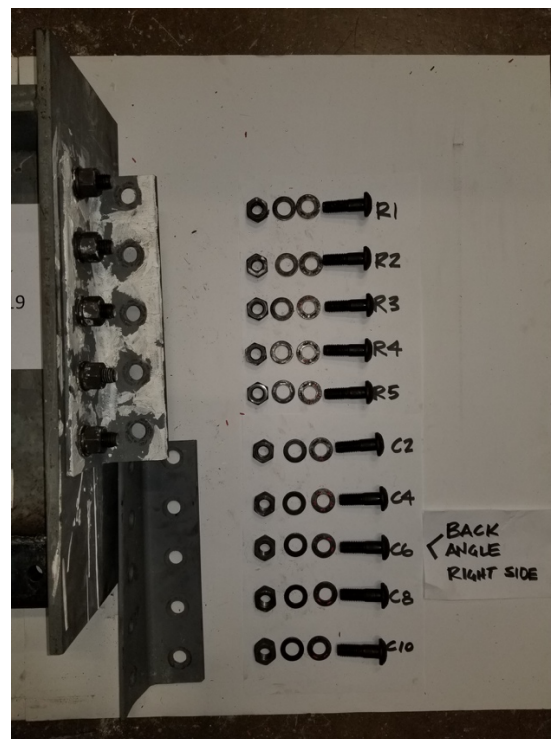


Figure 4.4-31: Typical right hand-side of a 2L5 series specimen following testing.



Figure 4.4-32: Plaster flake on specimen 2L5-1. Typical for 2L5 series of tests.

Specimens in the 2L5 series of tests underwent moderate levels of plastic deformation. No bolt hole deformation occurred and no localized block shear or tearing of the angles was imminent or observable. Plaster flaking is shown in Figure 4.4-32, indicating the unfolding of the angle and concentrations of stresses around the bolts. Unfortunately, the plaster flaking was damaged during the disassembly process for each test, making further visual judgment on stress concentrations difficult. However, in Figure 4.4-32 it is observable that movement of the beam web relative to the angle occurred by considering the increased gap between the plaster line on the beam web and the edge of the angle leg. This may indicate that the slip-critical capacity of the connection was overcome.

Bolt hole deformations were so insignificant that they could not be accurately measured, again, likely resulting from the possible slip-critical behavior of the connection. Deformations of the bolts themselves were also insignificant, especially due to the double shear condition of the bolts at the beam web. Figure 4.4-33 shows the Force-Displacement plot of the 2L5 series of tests. Figures 4.4-34 and 4.4-35 show the load-rotation plots for 2L5 series of tests with respect to DWT1 in US and metric units, respectively. Figures 4.4-36 and 4.4-37 show the load-rotation plots for 2L5 series of tests with respect to DWT2 in US and metric units, respectively.

It is noteworthy that all tests shown in Figure 4.4-33 follow a similar curve. Maximum deflection for each test was about 8 inches with approximately 21 kips (93 kN) of applied load. From Figures 4.4-34 through 4.4-37, the maximum moment developed at the double angle tests was approximately 35 kip-ft (47 kN-m) at a shear load of 10 kips (45 kN). Similar to the 2L3 and 2L4 series of tests, the 2L5 data show a compressive force axial force at the beginning stages of load application, but then develop tensile loads as would be expected under catenary action. Rotations were limited to just over 0.1 radians. The bolt axial loads, as expected, were all tensile.

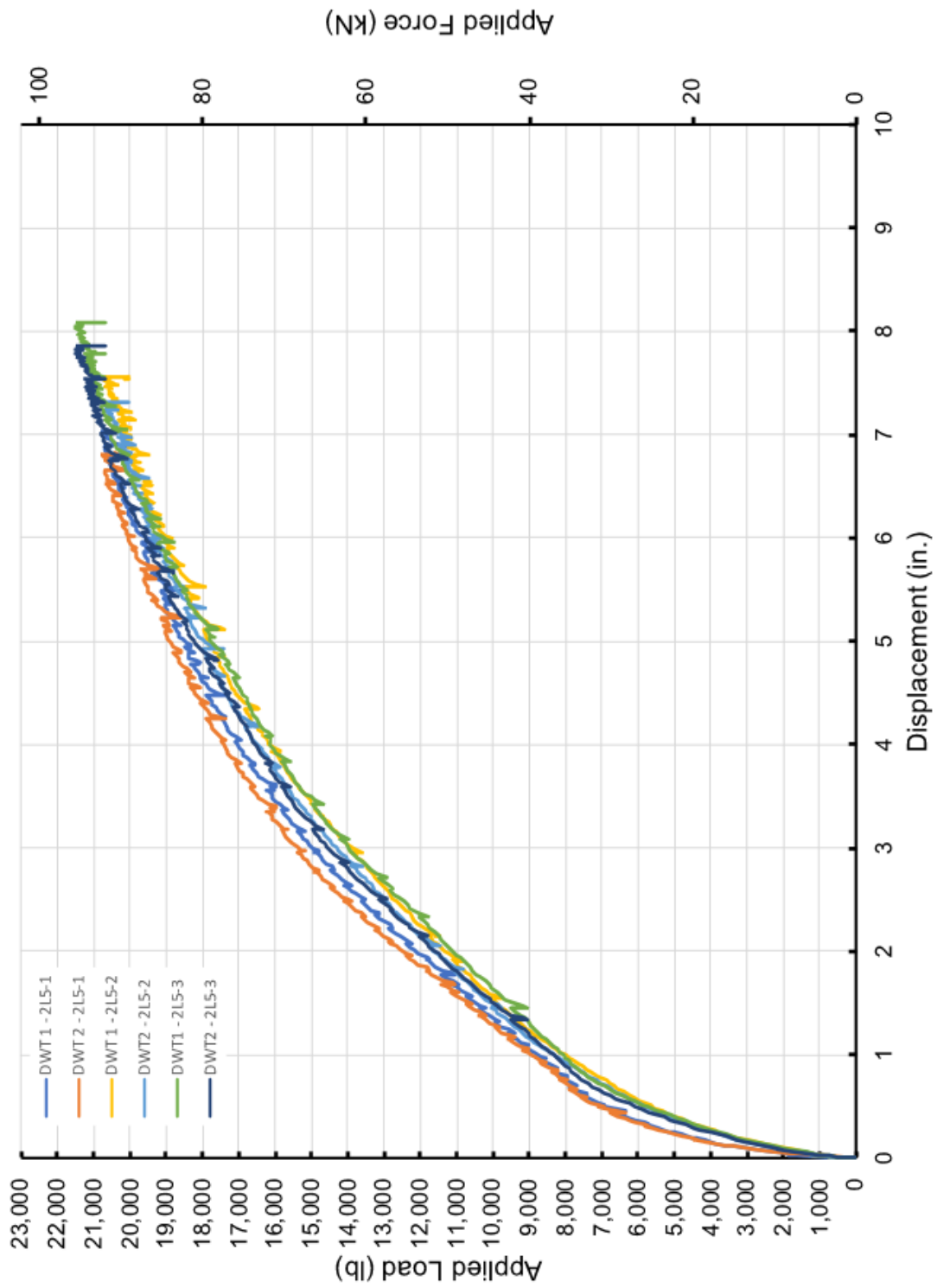


Figure 4.4-33: Force versus displacement for 2L5 series of tests.

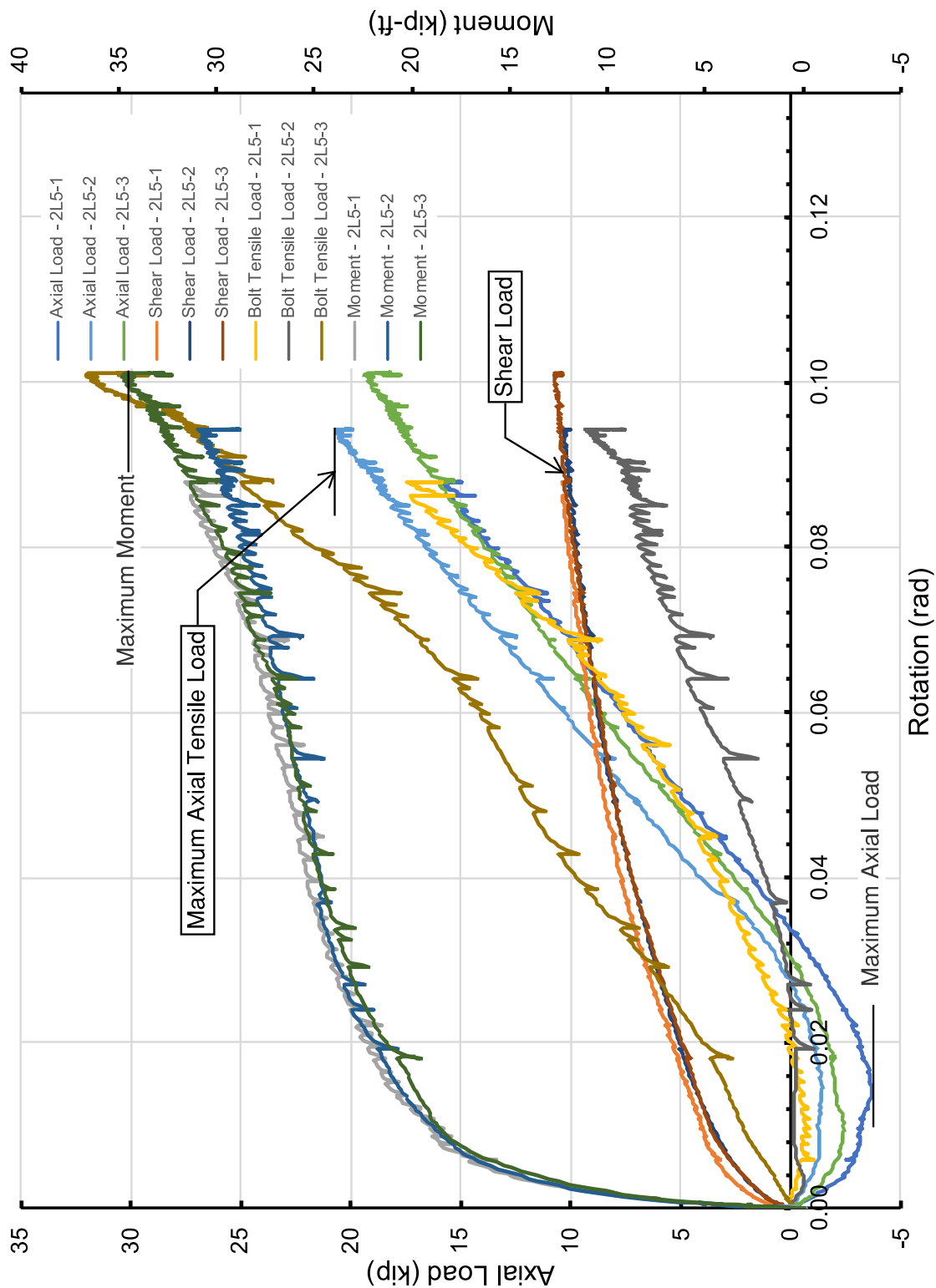


Figure 4.4-34: Load versus rotation for 2L5 series of tests with respect to DWT1 (US units).

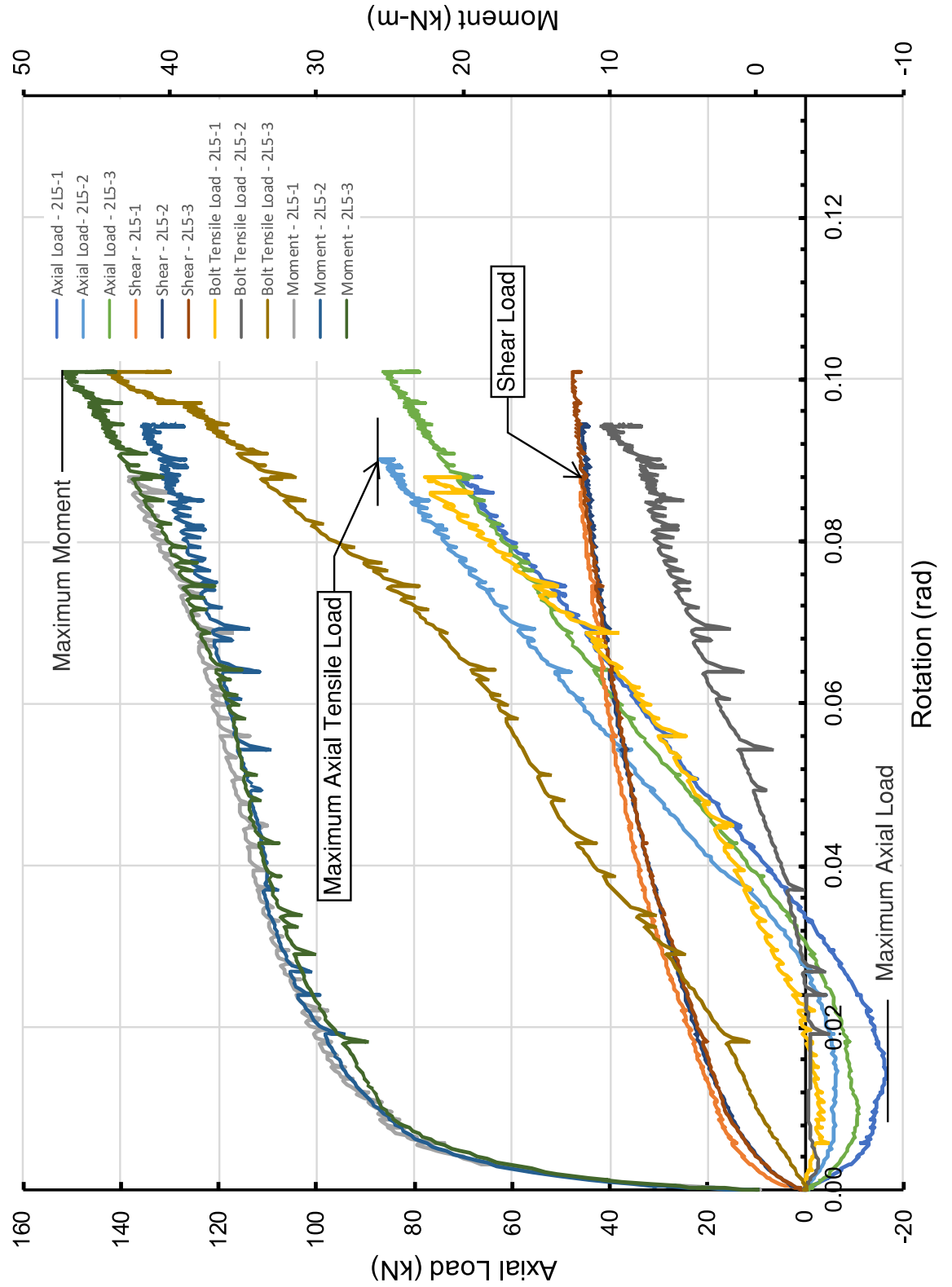


Figure 4.4-35: Load versus rotation for 2L5 series of tests with respect to DWT1 (Metric units).

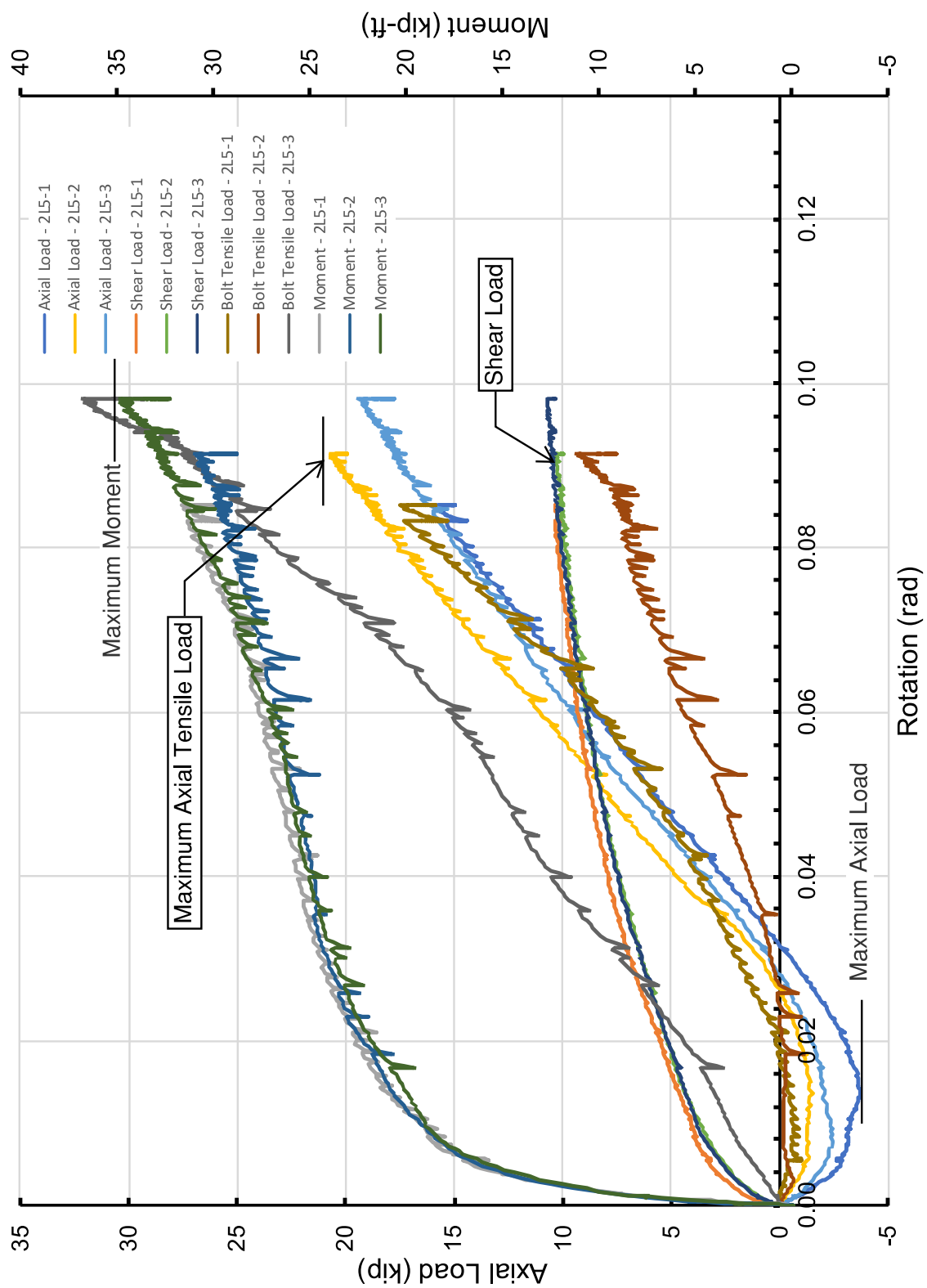


Figure 4.4-36: Load versus rotation for 2L5 series of tests with respect to DWT2 (US units).

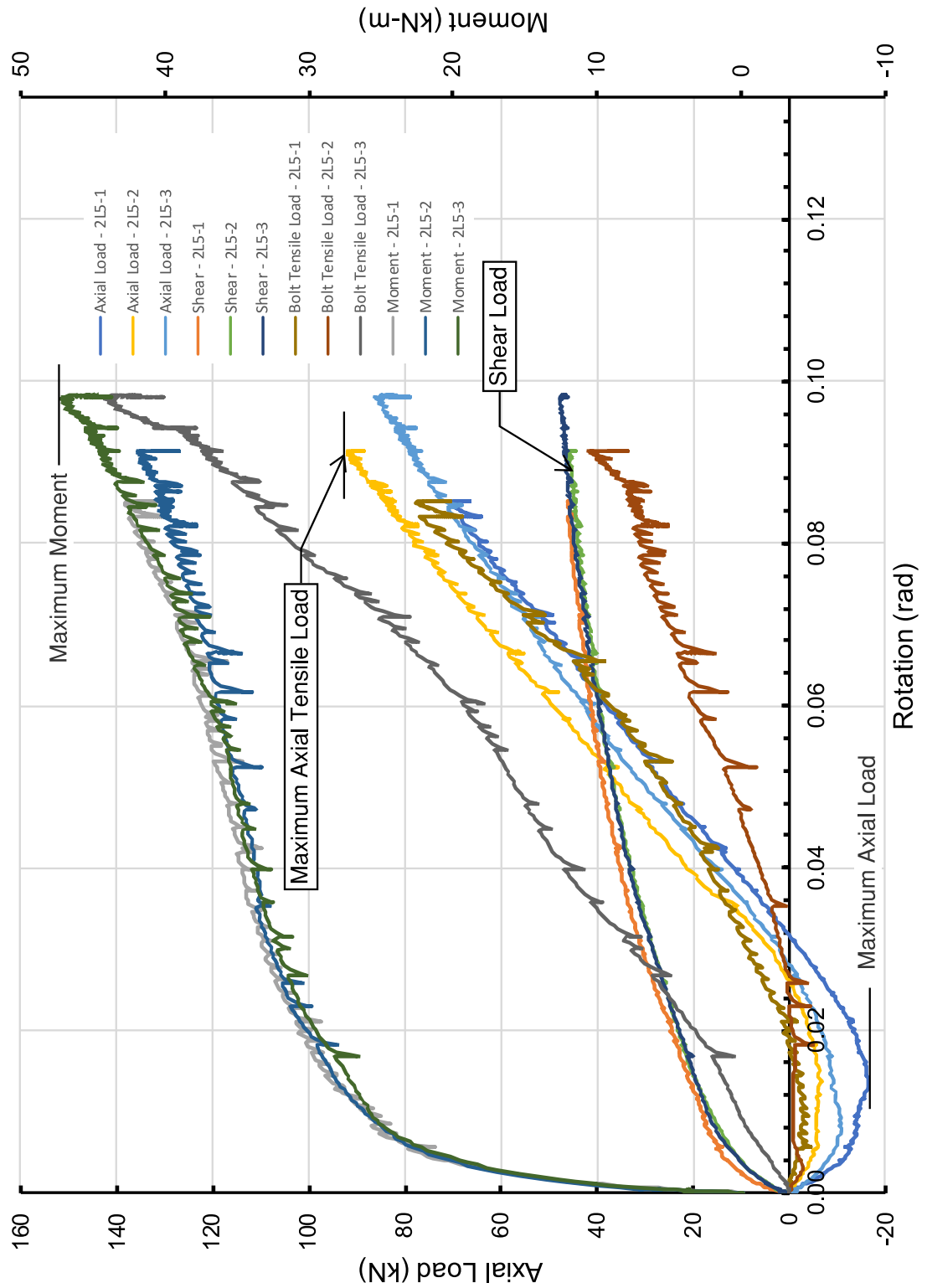


Figure 4.4-37: Load versus rotation for 2L5 series of tests with respect to DWT2 (Metric units).

4.5. Summary of Test Results

To summarize the results of testing, tables have been created for easy comparison across the various connection configurations and test runs. Table 4.5-1 lists the various test values at the point of maximum moment at the connection in US units, and Table 4.5-2 lists the various test values at the point of maximum moment at the connection in metric units. While maximum moment values are relatively consistent across the various test series, the shear and axial loads at the point of maximum moment vary greatly. This behavior is also observable in the graphs for each test in their respective sections. Each test underwent similar levels of LTB, with the 2L5 series of testing exhibiting the most dramatic LTB. It is possible that variations in the out-of-plane behavior of each specimen contributed to these differences. It is also remarkable that the shear values of these connections never overcome the capacity of a slip critical connection as detailed in Table 3.2-1, which validates the proposition that the connection behaved as a slip-critical connection with the corresponding lack of bolt-hole deformations.

Table 4.5-1: Test Values at Maximum Moment, US units.

| Test | Test Values at Maximum Moment | | | | Notes |
|-------|-------------------------------|-----------------------|-----------------------|--|--------------|
| | Moment, M (kip-ft) | Shear, V (kips) | Axial, P (kips) | Average Rotation, θ (radians) | |
| 2L3-1 | 11.35 | 3.76 | -9.89 | 0.07 | |
| 2L3-2 | 9.54 | 5.2 | -0.47 | 0.07 | |
| 2L3-3 | 10.12 | 4.98 | 6.71 | 0.06 | |
| 2L4-1 | 29.03 | 6.58 | 8.92 | 0.08 | 2L4-1 Part 2 |
| 2L4-2 | 27.44 | 6.76 | 6.30 | 0.12 | |
| 2L4-3 | 22.05 | 7.01 | 10.37 | 0.11 | |
| 2L5-1 | 31.59 | 10.37 | 15.85 | 0.09 | |
| 2L5-2 | 30.87 | 10.33 | 20.66 | 0.09 | |
| 2L5-3 | 34.77 | 10.74 | 9.26 | 0.1 | |

Table 4.5-2: Test Values at Maximum Moment, metric units.

| Test | Test Values at Maximum Moment | | | | Notes |
|-------|-------------------------------|---------------------|---------------------|--|--------------|
| | Moment, M (kN-m) | Shear, V (kN) | Axial, P (kN) | Average Rotation, θ (radians) | |
| 2L3-1 | 15.4 | 16.71 | -44.03 | 0.07 | |
| 2L3-2 | 12.94 | 23.14 | -2.07 | 0.07 | |
| 2L3-3 | 13.72 | 18.94 | -29.85 | 0.06 | |
| 2L4-1 | 39.36 | 29.22 | 39.66 | 0.08 | 2L4-1 Part 2 |
| 2L4-2 | 37.2 | 30.09 | 28.05 | 0.12 | |
| 2L4-3 | 29.89 | 31.19 | 46.15 | 0.11 | |
| 2L5-1 | 46.15 | 46.15 | 70.51 | 0.09 | |
| 2L5-2 | 45.94 | 45.95 | 91.92 | 0.09 | |
| 2L5-3 | 47.15 | 47.79 | 85.65 | 0.1 | |

A combination of the shear, axial and moment forces may have overcome the slip-critical capacity in specimen 2L5-2, however. By considering the moment arm as the distance from the top of the angle to the bottom bolt, the shearing force is calculated as:

$$V_{bolt} = \frac{(M)(d)}{2 \text{ bolts}} + \frac{P+V}{5} = \frac{(30.87 \text{ k-ft})\left(\frac{12 \text{ ft}}{\text{in}}\right)(12 \text{ in})}{2 \text{ bolts}} + \frac{10.33 \text{ k} + 20.66 \text{ k}}{5 \text{ bolts}} =$$

$$21.6 \text{ k/bolt},$$

where V_{bolt} is the shear force per bolt, M, V and P are the maximum moment and corresponding shear and axial force at that moment value per test, respectively. By exceeding the slip-critical capacity of a bolt, the connection would slip.

The plots for each test in the load versus displacement show a remarkably similar level of load application and displacement for each series of tests, which plateau. This indicates that the connections did reach a level of plastic deformation, albeit small in each series of testing. From the load versus rotation graphs for each series, it is noticeable that the maximum moment at the connection, the shear load, and the bolt tensile force all

increase up to the end of the test. Therefore, the connection still possessed additional capacity which is obvious as no failure mode had occurred.

4.6. Verification of Data Results

An evaluation of forces was performed using the calculated forces at the strain gages to verify that equations of equilibrium have been satisfied. The statics evaluation was made based on the measured forces of axial load, P , moment, M , and rotation, θ , over a range of data for each testing run. This range of data was selected where the individual tests for each series had similar slopes in their axial force trace, which means that each range of data was taken from different starting and ending rotations. To determine the reactions at the pin connection, the length from a set of strain gages to the pin was determined to be 38.0625 inches using the center line of strain gages. These values were used to evaluate the reactions at the pin; these reactions are shown in Figure 4.6-1.

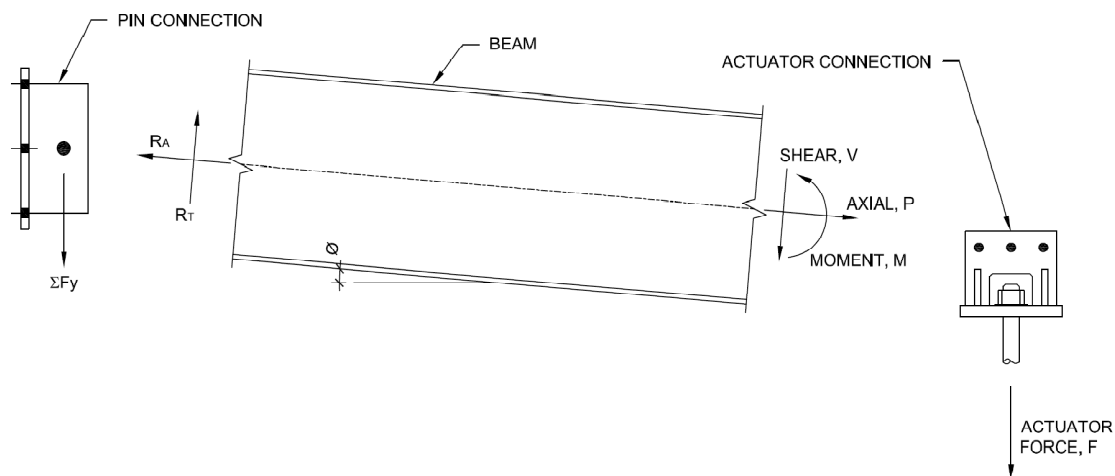


Figure 4.6-1: Free body diagram for statics evaluation as seen in Friedman (2009).

The sum of forces in the horizontal direction were taken to determine the internal axial force, R_a , being transmitted to the pin of the connection. Summing these forces gives:

$$\Sigma F_h = P - R_a = 0 \quad (4.6-1)$$

$$\therefore R_a = P. \quad (\text{kips}) \quad (4.6-2)$$

The sum of the moments at the pin location, M , may be used to calculate the transverse reaction at the pin, R_t . Summing the moments:

$$\Sigma M = 0 = M - R_t(38.0625 \text{ in}) \quad (4.6-3)$$

where

$$R_t = \frac{M}{38.0625 \text{ in}}. \quad (\text{kips}) \quad (4.6-4)$$

Based on the amount of rotation, these values were then transposed with respect to a global axis, with the vertical plane being the y-axis and the horizontal plane being the x-axis. Because the statics evaluation was compared to the actuator force applied to the connection, F , only the vertical components of these forces have been considered.

Therefore:

$$R_{a \text{ vertical}} = (R_a) \sin(\theta) \quad (\text{kips}) \quad (4.6-5)$$

and

$$R_{t \text{ vertical}} = (R_t) \cos(\theta). \quad (\text{kips}) \quad (4.6-6)$$

Determination of the sum of forces was accomplished by summation of all of the vertical components of axial and transverse forces. Thus,

$$\Sigma F_y = 0 = F - R_{a \text{ vertical}} - R_{t \text{ vertical}}. \quad (4.6-7)$$

The vertical load remaining, or “residual load”, was compared to the actuator force, F , to determine the percent difference:

$$\% \text{ Difference} = \frac{F}{\Sigma F_y}. \quad (4.6-8)$$

Equation (4.6-8) was used to compute the accuracy of measured results, as shown in Table 4.6-1.

Table 4.6-1: Static Check Percent Error for 2L Tests.

| Test | Average | Maximum | Minimum | Standard Deviation | Rotation Range |
|--------------|---------|---------|---------|--------------------|----------------|
| 2L3-1 | 37% | 46% | 15% | 7% | 0.03-0.07 |
| 2L3-2 | 47% | 52% | 31% | 4% | 0.03-0.07 |
| 2L3-3 | 41% | 47% | 23% | 5% | 0.03-0.06 |
| 2L4-1 Part 2 | 50% | 71% | 44% | 5% | 0.04-0.08 |
| 2L4-2 | 23% | 38% | 0% | 12% | 0.04-0.12 |
| 2L4-3 | 9% | 18% | 0% | 5% | 0.04-0.11 |
| 2L5-1 | 3% | 9% | 0% | 2% | 0.04-0.09 |
| 2L5-2 | 8% | 15% | 0% | 3% | 0.04-0.09 |
| 2L5-3 | 13% | 20% | 0% | 5% | 0.04-0.10 |

The values from Table 4.6-1 show that there is a significant difference between the expected forces at the connection from statics and those recorded experimentally.

Chapter 5: Discussion and Conclusion

5.1. Introduction

After review of existing literature and the commencement of physical testing, conclusions may be made with respect to the axial, shear and moment interaction of double-angle shear connections. The purpose of this project was to determine the extent to which standard, commonplace double-angle shear connections contribute to the inherent robustness of a structural steel system. An attempt to quantify the level of additional reserve strength was also included as part of the research.

5.2. Conclusions

Based on the testing, it can be established that double-angle shear connections do possess measurable flexural capacity due to the unfolding mechanisms of the angles. As expected, the shear capacity of the connections increased with depth, as did the developed moment and axial force at the connection. The levels of deformation also increased with depth, with three-bolt connections undergoing minimum amounts of angle unfolding, four-bolt connections deforming to a higher degree, and maximum deformations observed in five-bolt connections. The maximum measured moment was approximately 35 kip-ft during test 2L5-3, with a maximum rotation of approximately 0.12 radians on several 2L4 series tests. Ultimately, every double-angle connection, which were designed specifically for shear loads only, maintained strength even while subjected to unanticipated flexural and axial loads.

The LTB behavior of the assembly during each test suggests that compressive forces were effectively resisted through the connection, with the bolt pretensioning

increasing the frictional forces between the legs of the angle and the beam. This behavior is expected to be the cause of the compressive axial forces seen on the axial trace for tests in the 2L3 series; in other tests with deeper connections, the axial forces eventually showed evidence of a developed catenary force after the development of significant levels of deformation. While there was no failure of the system, the ductility of the connection in the form of angle unfolding suggests that the development of alternate load paths occurred effectively, thereby redistributing the load.

Two cases were considered in an attempt to qualitatively determine the overall robustness of the connections: a) structural integrity and b) functionality. Structural integrity represents a measure of inherent redundancy and ductility in the connection, while functionality will be considered as the ability of a connection to perform as it was designed during and after an event of unanticipated loading.

In the consideration of structural integrity, each double-angle connection was able to withstand unexpected loading. Load redistribution occurred during testing, enabling the connections to perform in a desirable manner instead of brittle failure. The transmission of flexural loads was accomplished through the friction between the faying surfaces of the angle heel and the beam web, and ultimately through the deformation of the angles. From a structural integrity standpoint, when the connections were subjected to loading outside of the original design, they successfully withstood the unanticipated loading and provided additional levels of strength.

Conclusions regarding the robustness of double-angle connections may not be made definitively as the connections did not fail. Therefore, the resistance to shear at the point of failure would need to be determined to make a conclusion. It is expected,

however, by the trends of the graphs presented in Chapter 4 that the connections would not be able to withstand design shear values as the developed shear asymptotically reaches a certain value that is below the design value for each test. Therefore, while the connections are able to resist some force, it is expected that they would fail below the design force and therefore the connections cannot be considered robust.

5.3. Comparisons of Test Results with Results in Literature

For the purposes of this section, “2L Report” refers to this capstone project report and its results.

In Chapter 2.2 of this “2L Report,” the work of Oosterhof and Driver (2015) was described. Oosterhof and Driver subjected varying configurations of double angles to a combination of axial, shear and moment force to determine response characteristics. It was noted, following testing, that plastic hinges developed in several locations throughout the angle as it deformed, with the most critical locations being on the inside edge of the row of column bolts, and on the edge of the “k-area” of the angle adjacent to the beam web. As the angles deformed, tears and eventually rupture would occur at these two locations. However, the connections tested were able to resist an interaction of axial, shear and moment. While the angles tested in the process of creating this “2L Report” did undergo levels of deformation, the identification of the location of plastic hinges is not clear and it is unknown if the failure of the angle material would have occurred at the locations of maximum deformation.

In Chapter 2.4 of this “2L Report,” Gong (2017) performed three tests on double-angle connections and single-angle connections with flange angles. It was found, through this testing, that the double-angle connections would fracture in locations similar to those

found in Oosterhof and Driver (2015), with tears forming adjacent to the column-line of bolts. It was also argued that in thinner angles which deform more significantly under catenary action, the bearing of the unfolding angle against the bolt head contributed to the formation of a plastic hinge or yield line along the angle. Gong (2017) also found that between double-angle connections and single-angle connection with flange angles, double-angle connections were able to withstand higher rotations before failure. From the testing performed for this “2L Report,” the bearing of the bolt head against the deforming angle did, from an observation standpoint, seem to impact the location of yield lines; in the photographs in each respective section, it may be noticed that flaking of the plaster of Paris did occur around the bolt heads in angles with higher levels of deformation.

In Chapter 2.5 of this “2L Report,” the work of Weigand and Berman (2016) were described. In their work, 17 full-scale bolted-bolted angle connection sub-assemblages were tested with variations made to the thickness, bolt sizes, and numbers of bolts. It was found that the angles typically underwent four phases in the unfolding process, with the first phase being characterized by large initial stiffness of the angles, the second phase showing slip of the beam’s web between the angles, the third phase showing high levels of deformation of the angle, and the fourth and ultimate phase showing complete angle degradation. Weigand and Berman (2016) note that a level of compression was initially developed in some of the horizontal force-displacement responses because of the connection’s predisposition toward the compressive side of the connection. This agrees with the behavior of the double-angle connections in this “2L Report,” with each test showing a significant level of compressive resistance at the onset of testing. While

Weigand and Berman (2016) did not fully pretension any bolts in their testing, the behavior of pretensioned bolts and the contribution to connection response is discussed.

5.4. Future Research

The testing in this project focused on a particular configuration of double-angle angles, which only varied in the number of bolts within the connection, and not variations in beam size, bolt size, bolt staggering, or other possible modifications. Furthermore, the connections in this test were assumed to be the point of failure, and not the beams or the columns, which were much stronger in comparison. Real structures differ from these assumptions, and there are numerous configurations of double angle connections that may be used in practice.

Lateral torsional buckling proved to be an issue during testing primarily as a result of a lack of restraint of out-of-plane column movement. In a real frame, the columns would be continuous instead of a short segment, and in turn would be far more restricted against behavior seen in this test.

Ultimately, future research should consider:

- Variation of angle thickness, leg lengths, bolt size, bolt hole size, and snug tight versus pretensioned bolts
- Consideration of other components as the weak link
- Compressive capacity of angles as shown in Figure 2.3-8.
- Inclusion of a floor system or other means of lateral bracing for the beams and the column
- Testing of a multi-bay and multi-story structure, or a complete three-dimensional frame

- Modification to connections to assist in arresting collapse, perhaps with novel materials like fiber reinforced polymers or high-strength steels.

References

- ACI Committee 318. (2014). *318-14: Building Code Requirements for Structural Concrete and Commentary*. American Concrete Institute.
- AISC. (2017). *Manual of Steel Construction 15th Edition*. Chicago: AISC.
- City of New York. (2014). *2014 NYC Construction Code*. Retrieved from NYC Buildings:
https://www1.nyc.gov/assets/buildings/apps/pdf_viewer/viewer.html?file=2014C_C_BC_Chapter_22_Steel.pdf§ion=conscode_2014
- Friedman, A. (2009). *Axial, Shear and Moment Interaction of WT Connections*. Master's thesis, Milwaukee School of Engineering.
- Gong, Y. (2017). Test, Modeling and Design of Bolted-Angle Connections Subjected to Column Removal. *Journal of Constructional Steel Research*, 139, 315-326.
- International Code Council. (2019). *International Building Code*. American National Standards Institute.
- Liu, J., Main, J., & Sadek, F. (2016). Modeling of Double-Angle Shear Connections for Evaluation of Structural Robustness. *6th Conference on Forensic Engineering*, (pp. 1081-1090). San Francisco, CA.
- Oosterhof, S. A., & Driver, R. G. (2015). Behavior of Steel Shear Connections under Column-Removal Demands. *ASCE Journal of Structural Engineering*, 141(4), [1]-[14].
- Owens, G., & Moore, D. (2006). Steelwork Connections - The Robustness of Simple Connections. *Canadian Journal of Civil Engineering*, 33, 357-372.

Shen, J., & Astaneh-Asl, A. (1999). Hysteretic Behavior of Bolted-Angle Connections.

Journal of Constructional Steel Research, 51, 201-218.

Van Buskirk, M. (2019). *Experimental Evaluation of Strain Distributions in Steel*

Member Systems Subjected to Unanticipated Loading. Master's thesis, Milwaukee School of Engineering.

Weigand, J. M., & Berman, J. W. (2016). Integrity of Bolted Angle Connections

Subjected to Simulated Column Removal. *ASCE Journal of Structural Engineering*, 142(3), [1]-[13].

Weigand, J., Liu, J., & Main, J. A. (2017). Modeling of Double-Angle Connections for

Robustness Evaluation of Steel Gravity Frames. *Eighth International Workshop on Connections in Steel Structures (Connections VIII)*. AISC.

A. Appendix – Double Angle Connection Calculations

Given:

All-bolted double-angle connection between a W18×35 beam with two 1/4-in. doubler plates flanking the web ($F_y = 36$ ksi) and a W12×53 column flange. Bolts used are 3/4-in. A325-X bolts in standard holes on one angle leg and horizontal short-slotted holes (HHSL) on the other angle leg. Conservatively, all bolt holes against the column flange will be taken as HSSL. Bolts at the beam web are 3/4-in. A325-N in standard holes.

Determine the capacity of the 2L4 x 3 1/2 x 1/4 three bolt connection based on the geometry as shown in Figure A-1. Assume the beams and columns are indefinitely strong compared to the connection. Capacities are presented as ultimate values only. Material properties sourced from material testing conducted by a laboratory are indicated with an asterisk next to the section designation. Reference Appendix B for Mill Certifications and material testing results.

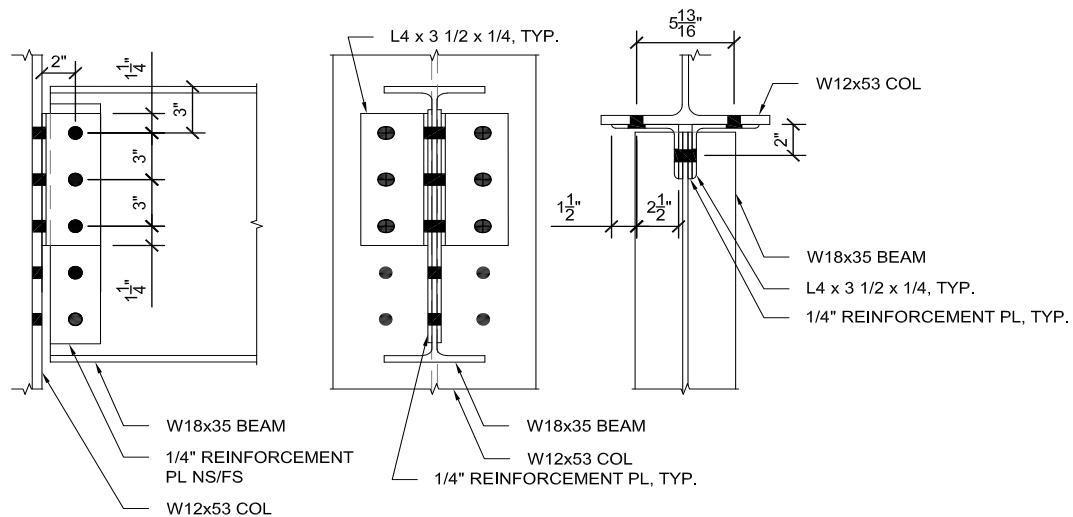


Figure A.1: Given Geometry.

Material Properties

| | | | |
|-------------------|-----------|--------------------------|--------------------------|
| W18x35* | ASTM A992 | $F_y = 52.9 \text{ ksi}$ | $F_u = 74.4 \text{ ksi}$ |
| W12x53 | ASTM A992 | $F_y = 50 \text{ ksi}$ | $F_u = 65 \text{ ksi}$ |
| L4 x 3 1/2 x 1/4* | ASTM A36 | $F_y = 58.4 \text{ ksi}$ | $F_u = 77.7 \text{ ksi}$ |

Geometric Properties:

Beam W18x35 $t_w = 0.3 \text{ in.}$ $d = 17.7 \text{ in.}$ $t_f = 0.425 \text{ in.}$

Column W12x53 $t_w = 0.345 \text{ in.}$

Angle L4 x 3 1/2 x 1/4 $t = 0.25 \text{ in.}$

Check bolt group through angle to beam connection for bolt bearing and tear-out

CASE I – Shear in beam-side connection

$$\text{Edge bolt, } L_c = L_{ev} - \frac{(d_b + 1/16 \text{ in.})}{2} = 1.25 \text{ in.} - \left(\frac{3/4 \text{ in.} + 1/16 \text{ in.}}{2} \right) = 0.84$$

$$\text{Non-Edge Bolt, } L_c = s - (d_b + 1/16 \text{ in.}) = 3 \text{ in.} - (3/4 \text{ in.} + 1/16 \text{ in.}) = 2.19 \text{ in.}$$

$$R_n = 1.2L_c t F_u \leq 2.4dt F_u]$$

$$R_n = [1.2(0.84 \text{ in.})(0.25 \text{ in.})(77.7 \text{ ksi}) + 2(1.2)(2.19 \text{ in.})(0.25 \text{ in.})(77.7 \text{ ksi})] \\ \leq 3[2.4(0.75 \text{ in.})(0.25 \text{ in.})(77.7 \text{ ksi})]$$

$$R_n = 121.6 \text{ k} \leq 104.9 \text{ k}$$

$$R_n = (2 \text{ angles})(104.9 \text{ k}) = 209.8 \text{ k}$$

$$4\text{-bolt capacity: } R_n = 279.8 \text{ k}$$

$$5\text{-bolt capacity: } R_n = 349.6 \text{ k}$$

CASE II – Tension in beam-side connection

$$\text{Edge bolt, } L_c = L_{ev} - \frac{(d_b + 1/16 \text{ in.})}{2} = 1.5 \text{ in.} - \left(\frac{3/4 \text{ in.} + 1/16 \text{ in.}}{2} \right) = 1.1 \text{ in.}$$

$$R_n = 1.2L_c t F_u \leq 2.4dt F_u$$

$$R_n = [1.2(3 \text{ bolts})(1.1 \text{ in.})(0.25 \text{ in.})(77.7 \text{ ksi})]$$

$$\leq [2.4(3 \text{ bolts})(0.75 \text{ in.})(0.25 \text{ in.})(77.7 \text{ ksi})]$$

$$R_n = 76.9 \text{ k} \leq 104.9 \text{ k}$$

$$R_n = (2 \text{ angles})(76.9 \text{ k}) = 153.8 \text{ k}$$

$$4\text{-bolt capacity: } R_n = 205.1 \text{ k}$$

$$5\text{-bolt capacity: } R_n = 256.4 \text{ k}$$

Check tensile yielding of angles

$$R_n = F_y A_g$$

$$R_n = (58.4 \text{ ksi})(8.5 \text{ in.})(0.25 \text{ in.})(2 \text{ angles}) = 248.2 \text{ k}$$

$$4\text{-bolt capacity: } R_n = 335.8 \text{ k}$$

$$5\text{-bolt capacity: } R_n = 423.4 \text{ k}$$

Check tensile rupture of angles

$$R_n = F_u A_e \text{ (U=1 per AISC D3.3; } A_e = A_n)$$

$$R_n = (77.7 \text{ ksi}) \left[(8.5 \text{ in.})(0.25 \text{ in.}) - (3 \text{ bolts}) \left(\frac{3}{4} \text{ in.} + \frac{1}{16} \text{ in.} \right) (0.25 \text{ in.}) \right] (2 \text{ angles})$$

$$= 235.5 \text{ k}$$

$$4\text{-bolt capacity: } R_n = 320.5 \text{ k}$$

$$5\text{-bolt capacity: } R_n = 405.5 \text{ k}$$

Check shear yielding of angles

$$R_n = 0.60 F_y A_{gv}$$

$$R_n = 0.60(58.4 \text{ ksi})(8.5 \text{ in.})(0.25 \text{ in.})(2 \text{ angles}) = 148.9 \text{ k}$$

$$4\text{-bolt capacity: } R_n = 201.5 \text{ k}$$

$$5\text{-bolt capacity: } R_n = 254.0 \text{ k}$$

Check shear rupture of angles

$$R_n = 0.60F_u A_{nv}$$

$$R_n = 0.60(77.7 \text{ ksi}) \left[(8.5 \text{ in.})(0.25 \text{ in.}) \right. \\ \left. - 3 \text{ bolts} \left(\frac{3}{4} \text{ in.} + \frac{1}{16} \text{ in.} \right) (0.25 \text{ in.}) \right] (2 \text{ angles}) = 141.3 \text{ k}$$

4-bolt capacity: $R_n = 192.4 \text{ k}$

5-bolt capacity: $R_n = 253.3 \text{ k}$

Check bolt group shear capacity on beam web (double shear, n thread condition)

$$R_n = 2F_n A_{nvb} = 2F_n (\pi r^2)$$

$$R_n = 2(3 \text{ bolts})(54 \text{ ksi})(\pi) \left(\frac{3}{8} \text{ in.} \right)^2 = 143.1 \text{ k}$$

4-bolt capacity: $R_n = 190.9 \text{ k}$

5-bolt capacity: $R_n = 238.6 \text{ k}$

Check bolt group shear capacity on column flange (single shear, x thread condition)

$$R_n = F_n A_{nvb} = F_n (\pi r^2)$$

$$R_n = (6 \text{ bolts})(68 \text{ ksi})(\pi) \left(\frac{3}{8} \text{ in.} \right)^2 = 180.2 \text{ k}$$

8-bolt capacity: $R_n = 240.3 \text{ k}$

10-bolt capacity: $R_n = 300.4 \text{ k}$

Check bolt group slip-critical shear capacity on beam web for SC(A) (two shear planes)

Per AISC Manual Table 7-3 ($\phi = 1.0$),

3-bolt capacity: $(3 \text{ bolts}) (19.0 \text{ k/bolt}) = 57 \text{ k}$

4-bolt capacity: 76 k

5-bolt capacity: 95 k

Check bolt group slip-critical shear capacity on column flange for SC(A) (one shear plane)

Per AISC *Manual* Table 7-3 ($\phi = 1.0$)

6-bolt capacity: (6 bolts)(9.49 k/bolt) = 57 k

8-bolt capacity: 76 k

10-bolt capacity: 95 k

Check bolt group slip-critical shear capacity on beam web for SC(B) (two shear planes)

Per AISC *Manual* Table 7-3 ($\phi = 1.0$),

3-bolt capacity: (1.67)(57 k) = 95 k

4-bolt capacity: 127 k

5-bolt capacity: 159 k

Check bolt group slip critical shear capacity on column face for SC(B) (one shear plane)

Per AISC *Manual* Table 7-3 ($\phi = 1.0$),

6-bolt capacity: (1.67)(57 k) = 95 k

8-bolt capacity: 127 k

10-bolt capacity: 159 k

Check block shear rupture of angle stem

$L_{eh} = 1.5$ in.

$L_{ev} = 1.25$ in.

$$R_n = 0.60F_uA_{nv} + U_{bs}F_uA_{nt} \leq 0.60F_yA_{gv} + U_{bs}F_uA_{nt}$$

CASE I – Shear in angle leg (L shaped failure path)

$$A_{gv} = (2 \text{ angles})(0.25 \text{ in.})(7.25 \text{ in.}) = 3.6 \text{ in}^2$$

$$A_{nv} = (2 \text{ angles}) \left[\left(3 \text{ in.} + 3 \text{ in.} + 1\frac{1}{4} \text{ in.} \right) - (2.5) \left(\frac{3}{4} \text{ in.} + \frac{1}{8} \text{ in.} \right) \right] (0.25 \text{ in.}) = 2.53 \text{ in}^2$$

$$A_{nt} = (2 \text{ angles}) \left[\left(1\frac{1}{2} \text{ in.} \right) - (0.5) \left(\frac{3}{4} \text{ in.} + \frac{1}{8} \text{ in.} \right) \right] (0.25 \text{ in.}) = 0.41 \text{ in}^2$$

$$R_n = 0.60(77.7 \text{ ksi})(2.53 \text{ in}^2) + 1.0(77.7 \text{ ksi})(0.41 \text{ in}^2)$$

$$\leq 0.60(58.4 \text{ ksi})(3.6 \text{ in}^2) + 1.0(77.7 \text{ ksi})(0.41 \text{ in}^2)$$

$$R_n = 149.81 \text{ k} \leq 158.0 \text{ k}$$

$$R_n = 149.81 \text{ k}$$

$$\text{4-bolt capacity: } R_n = 199.4 \text{ k}$$

$$\text{5-bolt capacity: } R_n = 249.1 \text{ k}$$

CASE II – Tension in angle leg (capacity for governing failure path provided)

U Shaped Failure

$$A_{gv} = (2 \text{ angles})(2)(0.25 \text{ in.})(1.5 \text{ in.}) = 1.5 \text{ in}^2$$

$$A_{nv} = (2 \text{ angles})(2) \left[\left(1 \frac{1}{2} \text{ in.} \right) - (0.5) \left(\frac{3}{4} \text{ in.} + \frac{1}{8} \text{ in.} \right) \right] (0.25 \text{ in.}) = 1.1 \text{ in}^2$$

$$A_{nt} = (2 \text{ angles}) \left[(3 \text{ in.} + 3 \text{ in.}) - (2) \left(\frac{3}{4} \text{ in.} + \frac{1}{8} \text{ in.} \right) \right] (0.25 \text{ in.}) = 2.13 \text{ in}^2$$

L Shaped Failure

$$A_{gv} = (2 \text{ angles})(0.25 \text{ in.})(1.5 \text{ in.}) = 0.75 \text{ in}^2$$

$$A_{nv} = (2 \text{ angles}) \left[\left(1 \frac{1}{2} \text{ in.} \right) - (0.5) \left(\frac{3}{4} \text{ in.} + \frac{1}{8} \text{ in.} \right) \right] (0.25 \text{ in.}) = 0.53 \text{ in}^2$$

$$A_{nt} = (2 \text{ angles}) \left[\left(3 \text{ in.} + 3 \text{ in.} + 1 \frac{1}{4} \text{ in.} \right) - (2.5) \left(\frac{3}{4} \text{ in.} + \frac{1}{8} \text{ in.} \right) \right] (0.25 \text{ in.}) = 2.53 \text{ in}^2$$

$$\text{3-bolt capacity: } R_n = 216.8 \text{ k (L shaped failure path)}$$

$$\text{4-bolt capacity: } R_n = 298.1 \text{ k (L shaped failure path)}$$

$$\text{5-bolt capacity: } R_n = 386.8 \text{ k (L shaped failure path)}$$

Check angle leg bolts at column flange for shear and tension interaction

Determine required shear stress based on lowest shear capacity for all previous checks.

Note that shear rupture values govern.

$$f_{v \min} = \frac{0.2R_n}{(n)A_b} = \frac{0.2(141.3 \text{ k})}{6(0.442 \text{ in}^2)} = 10.65 \text{ ksi}$$

$$f_{v \max} = \frac{R_n}{(n)A_b} = \frac{141.3 \text{ k}}{6(0.442 \text{ in}^2)} = 53.28 \text{ ksi}$$

4-bolt minimum shear stress: $f_{v \min} = 10.88 \text{ ksi}$

4-bolt maximum shear stress: $f_{v \max} = 54.4 \text{ ksi}$

5-bolt minimum shear stress: $f_{v \min} = 11.46 \text{ ksi}$

5-bolt maximum shear stress: $f_{v \max} = 57.3 \text{ ksi}$

$$F'_{nt} = 1.3F_{nt} - \frac{F_{nt}}{F_{nv}} f_{rv} \leq F_{nt}$$

Using minimum shear stress

$$F'_{nt} = 1.3(90 \text{ ksi}) - \frac{90 \text{ ksi}}{68 \text{ ksi}} (10.65 \text{ ksi}) \leq 90 \text{ ksi} = 102.9 \text{ ksi} \leq 90 \text{ ksi}$$

$$F'_{nt} = 90 \text{ ksi}$$

4-bolt minimum nominal tensile stress: $F'_{nt} = 90 \text{ ksi}$

5-bolt minimum nominal tensile stress: $F'_{nt} = 90 \text{ ksi}$

Using maximum shear stress

$$F'_{nt} = 1.3(90 \text{ ksi}) - \frac{90 \text{ ksi}}{68 \text{ ksi}} (53.28 \text{ ksi}) \leq 90 \text{ ksi} = 46.5 \text{ ksi} \leq 90 \text{ ksi}$$

$$F'_{nt} = 46.5 \text{ ksi}$$

4-bolt maximum nominal tensile stress: $F'_{nt} = 45 \text{ ksi}$

5-bolt maximum nominal tensile stress: $F'_{nt} = 41.2 \text{ ksi}$

Maximum tensile force per bolt based on lowest shear

$$R_n = F'_{nt} A_b$$

$$R_n = (90 \text{ ksi})(0.442 \text{ in}^2) = 39.8 \frac{\text{k}}{\text{bolt}}$$

Values are identical for 4-bolt and 5-bolt connections.

Maximum tensile force per bolt based on highest shear

$$R_n = F'_{nt} A_b$$

$$R_n = (46.5 \text{ ksi})(0.442 \text{ in}^2) = 20.6 \text{ k/bolt}$$

4-bolt available tensile strength per bolt: $R_n = 19.9 \text{ k/bolt}$

5-bolt available tensile strength per bolt: $R_n = 18.2 \text{ k/bolt}$

B. Material Tests and Mill Certifications

BAYOU STEEL GROUP

| | |
|--|---|
| BAYOU STEEL GROUP (LAPLACE) 138 HWY 3217 LAPLACE LOUISIANA 70068 Telephone (985) 652-4900 | MATERIAL CERTIFICATION REPORT INFRA METALS COMPANY (IL) MARSEILLES, IL 1600 BROADWAY MARSEILLES IL 61341 |
|--|---|

| | |
|---------------------------------------|---|
| Tested in Accordance With: ASTM A6 | Sales Order 184182-13 Date 05/18/2018 PO: CE-553225 Product Unequal Angles Cust 40006158 Ref. 81009272 Heat NO. L111448 Grade A3652950 Pieces 43 Cust.Mat. Length 40' 00" Weight 10664 Size U4X3-1/2X1/4X6.2 * LP |
|---------------------------------------|---|

| CHEMICAL ANALYSIS | | MECHANICAL PROPERTIES | | TEST 1 | | TEST 2 | | TEST 3 | |
|-------------------|-------|-----------------------|-----------|----------|-----------|----------|--------|----------|--------|
| | | IMPERIAL | METRIC | IMPERIAL | METRIC | IMPERIAL | METRIC | IMPERIAL | METRIC |
| C | 0.12 | YIELD STRENGTH | 56800 PSI | 392 MPa | 57000 PSI | 393 MPa | | | |
| Mn | 0.88 | TENSILE STRENGTH | 75500 PSI | 521 MPa | 75000 PSI | 517 MPa | | | |
| P | 0.014 | ELONGATION | 29 % | 29 % | 29 % | 29 % | | | |
| S | 0.025 | GAUGE LENGTH | 8 IN | 203 mm | 8 IN | 203 mm | | | |
| Si | 0.20 | BEND TEST DIAMETER | | | | | | | |
| Cu | 0.30 | BEND TEST RESULTS | | | | | | | |
| Ni | 0.12 | SPECIMEN AREA | | | | | | | |
| Cr | 0.26 | REDUCTION OF AREA | | | | | | | |
| Mo | 0.052 | IMPACT STRENGTH | | | | | | | |
| Cb | 0.010 | | | | | | | | |
| V | 0 | | | | | | | | |
| B | | | | | | | | | |
| Al | | | | | | | | | |
| Sn | 0.007 | | | | | | | | |
| N | | | | | | | | | |
| Ti | | | | | | | | | |

| IMPACT STRENGTH | IMPERIAL | METRIC | INTERNAL CLEANLINESS | | GRAIN SIZE | |
|-----------------|----------|--------|----------------------|--|-----------------|--|
| AVERAGE | | | SEVERITY | | HARDNESS | |
| TEST TEMP | | | FREQUENCY | | GRAIN PRACTICE | |
| ORIENTATION | | | RATING | | REDUCTION RATIO | |

This heat makes the following grades: A36-14, A52950-14, G40.21-CSA50W, CSA44W, A70936-13a, ASME SA36-2010, A57250-12a, A70950-13a, and the following AASHTO M270 Grades: 36, 50, and 345. Heat is free of Mercury contamination in the process. This material is Hot Rolled Carbon Steel.EN10204-3.1B.

I hereby certify that the material test results presented here are from the reported heat and are correct. All tests were performed in accordance to the specification reported above. All steel is electric arc furnace melted (billets), manufactured, processed, tested in the U.S.A with satisfactory results. No weld repair was performed on this heat.

Notarized upon request:
 Sworn to and subscribed before me on this 18th day of May, 2018

| | |
|-------------------------------|--|
| Signed _____ Notary Public | MARK EDWARDS, QUALITY ASSURANCE SUPERVISOR this report to the Sales Department 1-800-535-7692 (USA) |
|-------------------------------|--|

Customer Name

GERMANTOWN IRON & STEEL CORP

Customer PO#

6386-G8459-18

Invoice No

1411260

Shipper No

1379400

Heat Number

KN18104313

SOLD INFRA METALS CO
TO: 8 PENT HWY
 WALLINGFORD, CT 06492-

NUCOR
NUCOR STEEL KANKAKEE, INC.

CERTIFIED MILL TEST REPORT

Page: 1

SHIP INFRA METALS
TO: 1601 BROADWAY ST
 MARSELLES, IL 61341-

Ship from:
 MTR #: 0000254227
 Nucor Steel Kankakee, Inc.
 One Nucor Way
 Bourbonnais, IL 60914
 815-937-3131

Date: 9-Aug-2018
 B.L. Number: 565883
 Load Number: 303901

Material Safety Data Sheets are available at www.nucorbar.com or by contacting your inside sales representative.

NBMG-08 January 1, 2012

| LOT # HEAT # | DESCRIPTION | PHYSICAL TESTS | | | | | | CHEMICAL TESTS | | | | | | | | | |
|--------------------------------------|--|----------------------------|----------------------------|------------------|------|------------|----------------------|----------------------|--------------------|--------------|-------------|-------------|------|--|--|--|--|
| | | YIELD P.S.I. | TENSILE P.S.I. | ELONG % IN 8" | BEND | WT% DEF | C NI | Mn Cr | P Mo | S V | Si Cb | Cu Sn | C.E. | | | | |
| PO# => KN1810431301 KN18104313 | CE-554771 Nucor Steel - Kankakee Inc 1/4x3" Flat 20" NUCOR MULTIGRADE NUCOR MULTIGRADE | 54,440 375MPa 55,138 | 74,798 516MPa 75,070 | 25.1% 24.5% | | | .14 .14 CE4020 | .78 .21 CEA529 | .020 .045 TI | .040 .024 | .18 .001 | .27 .011 | | | | | |
| | NUCOR MULTIGRADE MEETS THE REQUIREMENTS OF: ASTM A36/A36M-08, A529/529M-05(2009) GR50(345) A572/572M-07 GR50(345), A709/709M-10 GR36(250) & GR50(345), CSA G40.21-04 GR44W(300W) & GR50W(350W) AASHTO M270/M270M-10 GR36(270) & GR50(345), ASME SA36/SA36M-07 MEETS REPORTING REQUIREMENTS OF EN10204 SEC 3.1 Melted 06/13/18 Rolled 06/21/18 | | | | | | | | | | | | | | | | |

I hereby certify that the material described herein has been manufactured in accordance with the specifications and standards listed above and that it satisfies those requirements:
 1.) Weld repairs and standards performed on this material.
 2.) Melted and Nonfused in the United States.
 3.) Mercury, Cadmium, or Alpha source material in any form have not been used in the production of this material.

QUALITY
 ASSURANCE: Caitlin Widdicombe

Caitlin Widdicombe

| | | | | |
|------------------------------|---------------------|-------------------|-------------------|--------------------|
| Customer Name | Customer PO# | Invoice No | Shipper No | Heat Number |
| GERMANTOWN IRON & STEEL CORP | 6386-G8459-18 | 1411260 | 1379400 | KN18106802 |

NUCOR
NUCOR STEEL KANKAKEE, INC.

Mill Certification

10/10/2018

MTR#:92984-
Lot #:KN1810680201
ONE NUCOR WAY
BOURBONNAIS, IL 60914 US
815-937-3131
Fax: 815-939-5599

Sold To: INFRA METALS CO
8 PENT HWY
WALLINGFORD, CT 06492 US

Ship To: INFRA METALS
1601 BROADWAY ST
MARSEILLES, IL 61341 US

| | | | |
|---------------------------|---|----------------------|--------------|
| Customer PO | CE-561049 | Sales Order # | 345921 - 5.1 |
| Product Group | Hot Roll - Merchant Bar Quality | Product # | 3016753 |
| Grade | Nucor Multigrade | Lot # | KN1810680201 |
| Size | 0.375" x 3.5" | Heat # | KN18106802 |
| BOL # | BOL-189841 | Load # | 92984 |
| Description | Hot Roll - Merchant Bar Quality Flat 3/8" x 3 1/2" Nucor Multigrade 20' 0" [240"] 2001-6000 lbs | Customer Part # | |
| Production Date | 09/23/2018 | Qty Shipped LBS | 5895 |
| Product Country Of Origin | United States | Qty Shipped EA | 66 |
| Original Item Description | | Original Item Number | |

I hereby certify that the material described herein has been manufactured in accordance with the specifications and standards listed above and that it satisfies those requirements.

Melt Country of Origin : United States

Melting Date: 09/13/2018

| | | | | | | | | | | |
|-------|--------|-------|-------|--------|--------|--------|--------|--------|-------|--------|
| C (%) | Mn (%) | P (%) | S (%) | Si (%) | Ni (%) | Cr (%) | Mo (%) | Cu (%) | V (%) | Sn (%) |
| 0.15 | 0.79 | 0.013 | 0.042 | 0.180 | 0.16 | 0.14 | 0.05 | 0.34 | 0.023 | 0.012 |

ASTM A529 S78.2 CE (%) : 0.39

ASTM A992 5.4 CE (%) : 0.36

Other Test Results

Yield (PSI) : 53300

Yield (PSI) : 53600

Tensile (PSI) : 74900

Tensile (PSI) : 74900

Elongation in 8" (%) : 28.8

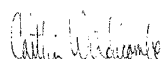
Elongation in 8" (%) : 28.3

Comments:

Nucor Multigrade meets the requirements of: ASTM A36/A36M-08, A529/529M-05(2009) GR50(345)A572/572M-07 GR50(345),A709/709M-10 GR36(250) & GR50(345), CSA G40.21-04 GR44W(300W) & GR50W(350W)AASHTO M270/M270M-10 GR36(270) & GR50(345),ASME SA36/SA36M-07

Meets reporting requirements of EN10204 SEC3.1

All manufacturing processes of the steel materials in this product, including melting, have occurred within the United States. Products produced are weld free. Mercury, in any form, has not been used in the production or testing of this material.


Caitlin Widdicombe, Chief Metallurgist

Customer Name

GERMANTOWN IRON & STEEL CORP

Customer PO#

6386-G8459-18

Invoice No

1411260

Shipper No

1379400

Heat Number

KN18106794

NUCOR

NUCOR STEEL KANKAKEE, INC.

Mill Certification

10/10/2018

MTR#:92984-

Lot #:KN1810679401

ONE NUCOR WAY

BOURBONNAIS, IL 60914 US

815-937-3131

Fax: 815-939-5599

Sold To: INFRA METALS CO
8 PENT HWY
WALLINGFORD, CT 06492 US

Ship To: INFRA METALS
1601 BROADWAY ST
MARSEILLES, IL 61341 US

| | | | |
|------------------------------|--|-------------------------|--------------|
| Customer PO | CE-561049 | Sales Order # | 345921 - 4.1 |
| Product Group | Hot Roll - Merchant Bar Quality | Product # | 3016727 |
| Grade | Nucor Multigrade | Lot # | KN1810679401 |
| Size | 0.375" x 3" | Heat # | KN18106794 |
| BOL # | BOL-189841 | Load # | 92984 |
| Description | Hot Roll - Merchant Bar Quality Flat 3/8" x 3" Nucor Multigrade 20' 0" [240"] 4001-8000 lbs | Customer Part # | |
| Production Date | 09/23/2018 | Qty Shipped LBS | 6125 |
| Product Country Of Origin | United States | Qty Shipped EA | 80 |
| Original Item Description | | Original Item Number | |

I hereby certify that the material described herein has been manufactured in accordance with the specifications and standards listed above and that it satisfies those requirements.

Melt Country of Origin : United States

Melting Date: 09/13/2018

| | | | | | | | | | | |
|-------|--------|-------|-------|--------|--------|--------|--------|--------|-------|--------|
| C (%) | Mn (%) | P (%) | S (%) | Si (%) | Ni (%) | Cr (%) | Mo (%) | Cu (%) | V (%) | Sn (%) |
| 0.16 | 0.77 | 0.012 | 0.040 | 0.190 | 0.17 | 0.14 | 0.05 | 0.34 | 0.023 | 0.013 |

ASTM A529 S78.2 CE (%) : 0.40

ASTM A992 5.4 CE (%) : 0.36

Other Test Results

Yield (PSI) : 53700

Yield (PSI) : 53700

Tensile (PSI) : 75200

Tensile (PSI) : 75100

Elongation in 8" (%) : 27.9

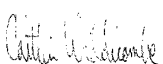
Elongation in 8" (%) : 31.3

Comments:

Nucor Multigrade meets the requirements of: ASTM A36/A36M-08, A529/529M-05(2009) GR50(345)A572/572M-07 GR50(345),A709/709M-10 GR36(250) & GR50(345), CSA G40.21-04 GR44W(300W) & GR50W(350W)AASHTO M270/M270M-10 GR36(270) & GR50(345),ASME SA36/SA36M-07

Meets reporting requirements of EN10204 SEC3.1

All manufacturing processes of the steel materials in this product, including melting, have occurred within the United States. Products produced are weld free. Mercury, in any form, has not been used in the production or testing of this material.


Caitlin Widdicombe, Chief Metallurgist

Page 1 of 1



Long Products Group
Structural and Rail Division

(260) 625-8100 (260) 625-8950 FAX
Quality Steel 100% EAF Melted
and Manufactured in the USA
Recycled content: PC = 75.0%, PI = 22.0%
ISO 9001:2015 and ABS Certified

CERTIFIED MILL TEST REPORT

Customer # 000002

Printed 11 / 07 / 2018
Produced 10 / 18 / 2018

Ship to:
Infra Metals Marseilles - "B"
1601 Broadway
Marseilles IL, 61341 US
Attn: Carl Janney

Bill to:
Infra-Metals Marseilles
8 Pent Highway
Wallingford CT, 06492 US
Attn: Michelle Calazza

GENERAL INFORMATION

Product Wide Flange Beam
Size W18X35
W460X52
Heat Number B156048
Condition(s) As-Rolled
Fine Grained
Fully Killed
No Weld Repair

SPECIFICATIONS

Standards
ASTM A6/A6M - 17a
» ASTM A992/A992M - 11
ASTM A572/A572M - 18
ASTM A709/A709M - 17e1
AASHTO M270/M270 - 15
CSA G40 21-13
ASTM A36/A36M - 14
SDI-MULTI meets the requirements of ASTM A992, A572-50, A529-50, A709-50, M270-50, A36
A709-36 M270-36 CSA330W, CSA345W, CSA350W

SHIPMENT DETAILS

BOL # 0000526110 - 6300 00 lbs
Bundle / ASN # Length pcs Cust PO | Recv PO | Job
060990672 30' 0" 3 CE-563141
060990668 30' 0" 3 CE-563141

CHEMICAL ANALYSIS (weight percent)

| C | Mn | P | S | Si | Cu | Ni | Cr | Mo | Sn | V | Nb/Cb | Al | N | B | *C1 | *C2 | *C3 | *PC | *I |
|-----|------|------|------|-----|-----|-----|-----|-----|------|------|-------|------|-------|-------|-----|------|-----|-----|------|
| .07 | 1.24 | .014 | .022 | .24 | .25 | .09 | .13 | .03 | .012 | .035 | .001 | .001 | .0141 | .0005 | .34 | .378 | .30 | .17 | 5.37 |

MECHANICAL TESTING

| Test | Yield (fy) | | Tensile (fu) | | fy / fu ratio | % Elong. {8" gage} | CHARPY IMPACT TESTS (available only when specified at time of order) | | | |
|------|------------|-----------|--------------|-----------|------------------|-----------------------|--|-------------------------------|------------|------------|
| | ksi / MPa | ksi / MPa | ksi / MPa | ksi / MPa | | | Temp F / C | Absorbed Energy Specimen 1 | Specimen 2 | Specimen 3 |
| 1 | 53 / 365 | 78 / 540 | 68 | 24 | 24 | 1 | | | | |
| 2 | 55 / 380 | 76 / 525 | 72 | 24 | 24 | 2 | | | | |
| 3 | | | | | | 3 | | | | |
| 4 | | | | | | 4 | | | | |
| | | | | | | 5 | | | | |
| | | | | | | 6 | | | | |
| | | | | | | 7 | | | | |

Notes: * Calculated Chemistry Values Carbon Equivalents (C1 C2 C3 PC) Corrosion Index (I) (ASTM G101) = 28.0(Cu) + 3.88(Mn) + 1.20(Cr) + 1.49(Si) + 1.72(P) + 2.28(Cu)(Ni) + 9.10(Ni)(P) + 33.38(Cu)²
CET (IV) = C + Mn/6 + (Cr + Mo + V)/5 + (Ni + Cu)/15 CEZ (AWS) = C + (Mn + Si)/6 + (Cr + Mo + V)/4 + (Ni + Cu)/15 CE3 (CEI) = C + (Mn/6) + (Si/24) + (Ni/40) + (Mo/4) + (V/14)
I hereby certify that the material described herein has been made to the applicable specification by the electric arc furnace/continuous cast process and tested in accordance with the requirements of American Bureau of Shipping Rules with satisfactory results.

Signed:

ABS CERTIFICATION

I hereby certify that the content of this report are accurate and correct. All tests and operations performed by this material manufacturer are in compliance with the requirements of the material specifications and applicable purchaser designated requirements.

State of Indiana, County of Whitley Sworn to and subscribed before me

this _____ day of _____

Signed **Todd Bashford**

Signed _____

Quality Manager

Notary Public

My commission expires _____

ASTM AG - 14.6 A signature is not required on the test report, however, the document shall clearly identify the organization submitting the report
Notwithstanding the absence of a signature, the organization submitting the report is responsible for the content of the report

Customer Name

GERMANTOWN IRON & STEEL CORP

Customer PO#

6386-G8459-18

Invoice No

1411260

Shipper No

1379400

Heat Number

B156048

Customer Name

GERMANTOWN IRON & STEEL CORP

Customer PO#

6386-G8459-18

Invoice No

1411260

Shipper No

1379400

Heat Number

kn18106802

NUCOR**NUCOR STEEL KANKAKEE, INC.****Mill Certification**

9/27/2018

MTR # K1-308117
 NUCOR STEEL KANKAKEE, INC.
 One Nucor Way
 Bourbonnais, IL 60914-4127
 (815) 937-3131
 Fax (815) 939-5599

| | | | |
|---------------|--------------------------------------|-----------------|-----------------|
| Customer P O | 5391755 | Sales Order | 346227 1 |
| Product Group | Merchant Bar Quality | Part Number | 5350035024010W0 |
| Grade | NUCOR MULTIGRADE | Lot # | KN1810680202 |
| Size | 1/2x3-1/2" Flat | Heat # | KN18106802 |
| Product | 1/2x3-1/2" Flat 20' NUCOR MULTIGRADE | B L. Number | K1-569471 |
| Description | NUCOR MULTIGRADE | Load Number | K1-308117 |
| Customer Spec | | Customer Part # | |

I hereby certify that the material described herein has been manufactured in accordance with the specifications and standards listed above and that it satisfies those requirements

Roll Date: 9/23/2018 Melt Date: 9/13/2018 Qty Shipped LBS. 6,074 Qty Shipped Pcs: 51

Melt Date: 9/13/2018

| | | | | | | | | | | | |
|--------|--------|--------|--------|-------|-------|-------|-------|--------|---------|--------|--------|
| C | Mn | P | S | Si | Cu | Ni | Cr | Mo | V | Cb | Sn |
| 0.15% | 0.79% | 0.013% | 0.042% | 0.18% | 0.34% | 0.16% | 0.14% | 0.048% | 0.0231% | 0.001% | 0.012% |
| CE4020 | CEA529 | | | | | | | | | | |
| 0.36% | 0.39% | | | | | | | | | | |

CE4020 C E CSA G4020 AASHTO M270
 CEA529 A529 CARBON EQUIVALENT

Roll Date: 9/23/2018

Yield 1 54,176psi

Tensile 1. 76,106psi

Elongation 29.13% in 8"(% in 203.3mm)

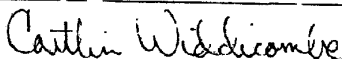
Yield 2 53,975psi

Tensile 2. 76,027psi

Elongation 28.75% in 8"(% in 203.3mm)

Specification Comments: NUCOR MULTIGRADE MEETS THE REQUIREMENTS OF ASTM A36/A36M-08, A529/529M-05(2009) GR50(345) A572/572M-07 GR50(345) A709/709M-10 GR36(250) & GR50(345), CSA G40.21-04 GR44W(300W) & GR50W(350W) AASHTO M270/M270M-10 GR36(270) & GR50(345), ASME SA36/SA36M-07 MEETS REPORTING REQUIREMENTS OF EN10204 SEC 3.1

1. ALL MANUFACTURING PROCESSES OF THE STEEL MATERIALS IN THIS PRODUCT, INCLUDING MELTING, HAVE OCCURRED WITHIN THE UNITED STATES.
2. ALL PRODUCTS PRODUCED ARE WELD FREE
3. MERCURY, IN ANY FORM, HAS NOT BEEN USED IN THE PRODUCTION OR TESTING OF THIS MATERIAL.



Caitlin Widdicombe

Division Metallurgist

MAI METALLURGICAL ASSOCIATES, INC.

Tensile Test Report (Page 1 of 2)

MAI Report No: 219-1-119 **Date:** February 28, 2019
Client: Milwaukee School of Engineering **Contact:** Dr. Christopher Rabel
P.O. No: Verbal **Date Rec'd:** February 11, 2019
Description: ASTM A36 I-Beam and ASTM A992 Angles and Wyes

| Property | I-Beam Flange | I-Beam Web | ASTM A36 | ASTM A992 |
|-------------------------|---------------|------------|--------------------|--------------------|
| Test Bar Dimensions | | | | |
| Width, inch | 0.497 | 0.503 | 0.50 | 0.50 |
| Thickness, inch | 0.386 | 0.300 | Material Thickness | Material Thickness |
| Gage Length, inches | 2.0 | 2.0 | 2.0 | 2.0 |
| Tensile Strength, psi | 74,300 | 74,400 | 58,000 - 80,000 | 65,000 min. |
| Yield Strength, psi (1) | 51,400 | 54,400 | 36,000 min. | 50,000 - 65,000 |
| Yield/Tensile Ratio | 0.69 | 0.73 | Not Specified | 0.85 max. |
| Elongation, % | 33 | 31 | 21 min. | 18 min. |

| Property | Wye Stem 1 | Wye Flange 1 | ASTM A36 | ASTM A992 |
|-------------------------|------------|--------------|--------------------|--------------------|
| Test Bar Dimensions | | | | |
| Width, inch | 0.504 | 0.501 | 0.50 | 0.50 |
| Thickness, inch | 0.376 | 0.580 | Material Thickness | Material Thickness |
| Gage Length, inches | 2.0 | 2.0 | 2.0 | 2.0 |
| Tensile Strength, psi | 73,300 | 72,200 | 58,000 - 80,000 | 65,000 min. |
| Yield Strength, psi (1) | 57,600 | 51,900 | 36,000 min. | 50,000 - 65,000 |
| Yield/Tensile Ratio | 0.80 | 0.72 | Not Specified | 0.85 max. |
| Elongation, % | 36 | 38 | 21 min. | 18 min. |

| Property | Wye Stem 2 | Wye Flange 2 | ASTM A36 | ASTM A992 |
|-------------------------|------------|--------------|--------------------|--------------------|
| Test Bar Dimensions | | | | |
| Width, inch | 0.496 | 0.503 | 0.50 | 0.50 |
| Thickness, inch | 0.378 | 0.568 | Material Thickness | Material Thickness |
| Gage Length, inches | 2.0 | 2.0 | 2.0 | 2.0 |
| Tensile Strength, psi | 72,400 | 72,100 | 58,000 - 80,000 | 65,000 min. |
| Yield Strength, psi (1) | 55,900 | 51,000 | 36,000 min. | 50,000 - 65,000 |
| Yield/Tensile Ratio | 0.77 | 0.71 | Not Specified | 0.85 max. |
| Elongation, % | 36 | 38 | 21 min. | 18 min. |

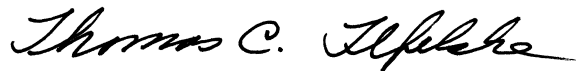
| Property | Angle 1 | Angle 2 | ASTM A36 | ASTM A992 |
|-------------------------|---------|---------|--------------------|--------------------|
| Test Bar Dimensions | | | | |
| Width, inch | 0.502 | 0.503 | 0.50 | 0.50 |
| Thickness, inch | 0.250 | 0.247 | Material Thickness | Material Thickness |
| Gage Length, inches | 2.0 | 2.0 | 2.0 | 2.0 |
| Tensile Strength, psi | 77,500 | 77,900 | 58,000 - 80,000 | 65,000 min. |
| Yield Strength, psi (1) | 56,800 | 60,000 | 36,000 min. | 50,000 - 65,000 |
| Yield/Tensile Ratio | 0.73 | 0.77 | Not Specified | 0.85 max. |
| Elongation, % | 34 | 31 | 21 min. | 18 min. |

(1): at 0.2% offset

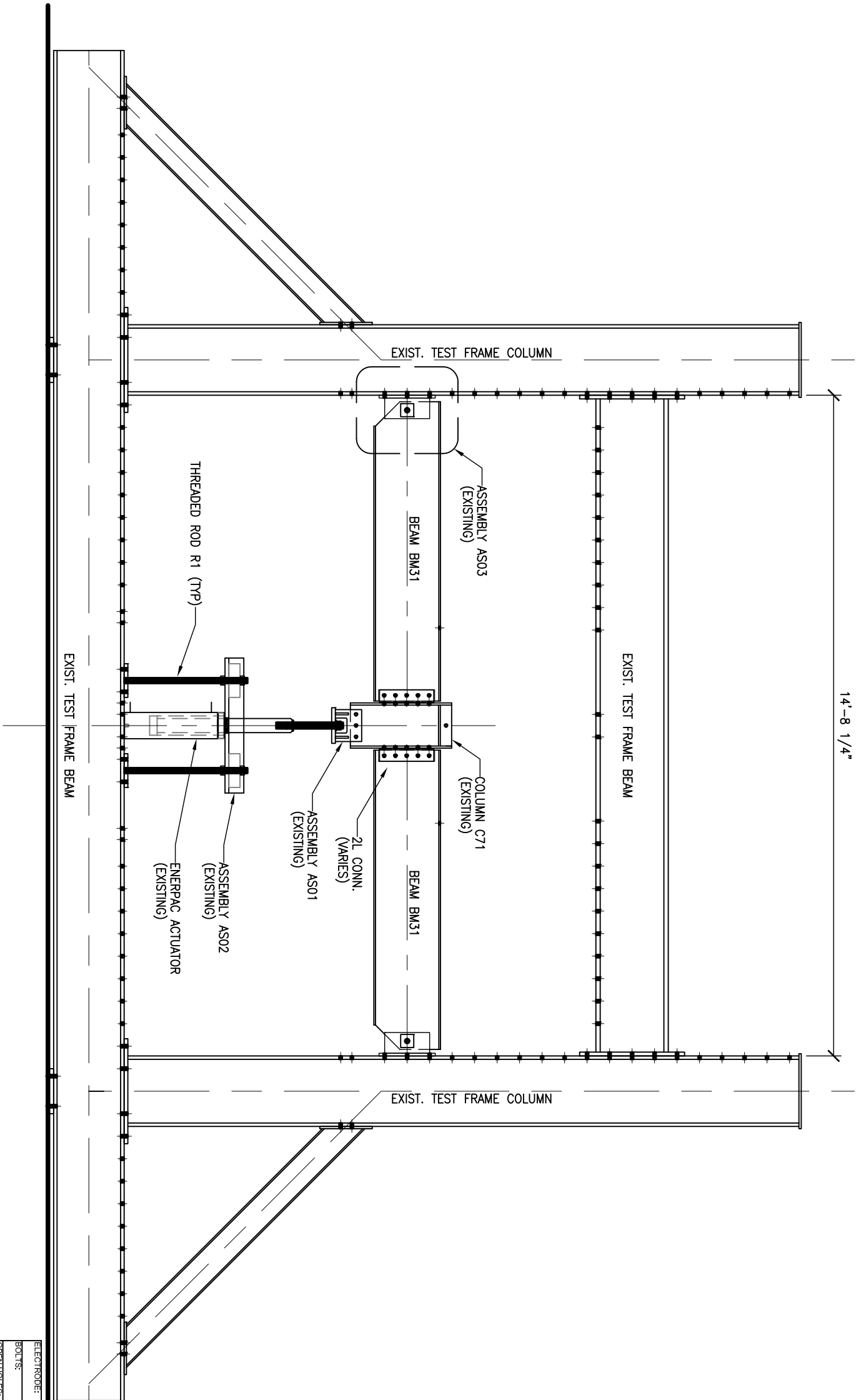
Notes: The tensile properties of all of the samples are in conformance with both ASTM A36, "Standard Specification for Carbon Structural Steel," and ASTM A992, "Standard Specification for Structural Steel Shapes."

The stress-strain curves for these samples are provided as separate Excel spreadsheets.

Respectfully submitted,



Thomas C. Tefelske,
President



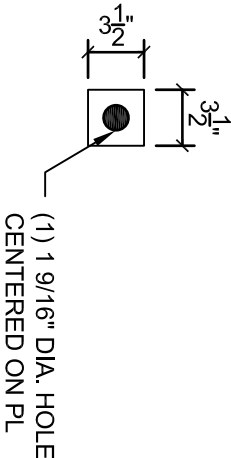
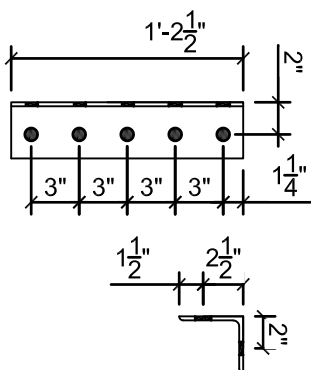
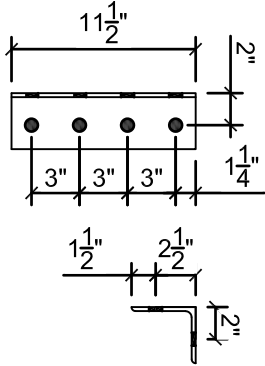
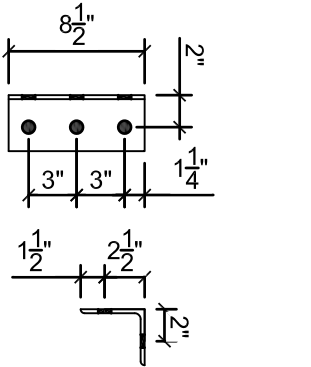
EXPERIMENTAL SETUP – 2L TEST

SCALE: 3/8" = 1'-0"

| | | |
|-------------|-------------|------------------------------------|
| ELECTRODE: | | E70XX |
| BOLTS: | | 3/4" A325 |
| OPEN HOLES: | | 13/16" |
| PAINT: | | PRIMER ONLY |
| REVISION | DESCRIPTION | DATE |
| | B | RELEASED FOR FABRICATION 9/20/2018 |
| | | |
| | | |

VANBUSKIRK - MORACHE
MSOE THESIS TEST SPECIMEN
AE-8900 2018-2019

| | | | |
|------------------------|-----------|----------|--|
| SHEET: | | | |
| TEST ASSEMBLY | | | |
| ANGLE CONNECTION FRAME | | | |
| DRAWN | DATE: | JOB NO.: | |
| MAM | 8/20/2018 | AE-8900 | |
| CHECKED | DATE: | SHEET: | |
| MLV | 8/20/2018 | 2 | |
| APPROVED | DATE: | REV.: | |
| CHR | 9/07/2018 | B | |

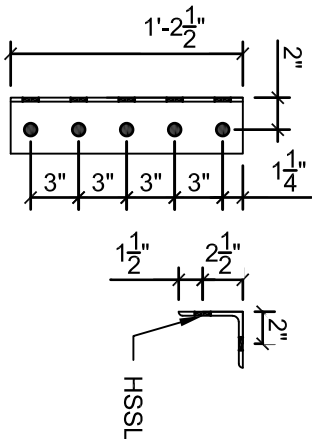
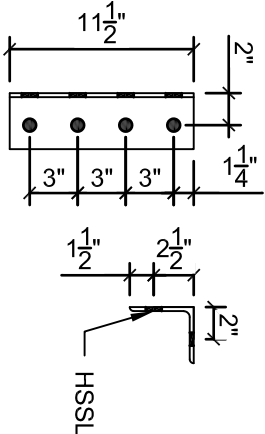
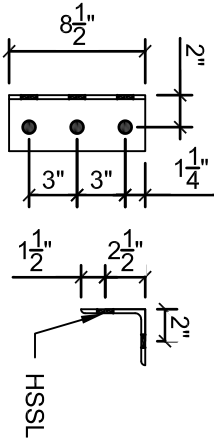


(6) ANGLES L11

(6) ANGLES L21

(6) ANGLES L31

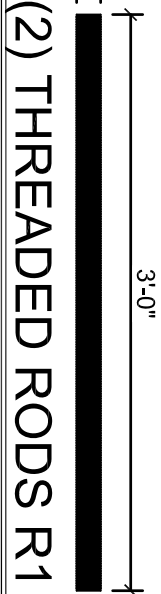
(2) PLATES PL81



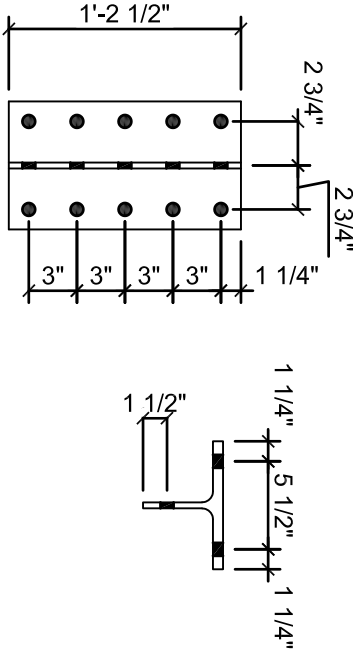
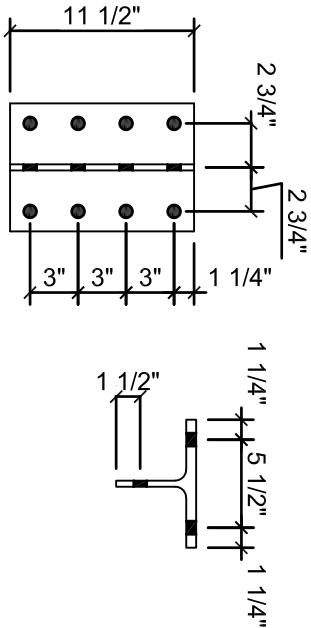
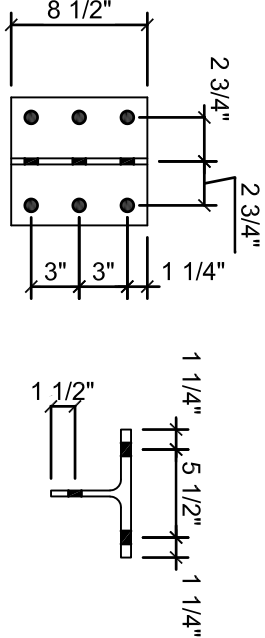
(6) ANGLES L12

(6) ANGLES L22

(6) ANGLES L32



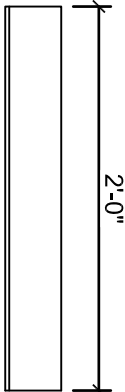
(2) THREADED RODS R1



(6) TEES WT11

(6) TEES WT21

(6) TEES WT31



(2) ANGLES L41



(2) TEES WT41

| BILL OF MATERIALS | | | | | | |
|-------------------|-----|------------------------------|------|--------|---------|------------|
| MARK | QTY | SHAPE | FEET | INCHES | GRADE | REMARKS |
| L11 | 6 | L4 x 3 1/2 x 1/4" | 0 | 8 1/2 | A36 | |
| L12 | 6 | L4 x 3 1/2 x 1/4" | 0 | 8 1/2 | A36 | |
| L21 | 6 | L4 x 3 1/2 x 1/4" | 0 | 11 1/2 | A36 | |
| L22 | 6 | L4 x 3 1/2 x 1/4" | 0 | 11 1/2 | A36 | |
| L31 | 6 | L4 x 3 1/2 x 1/4" | 1 | 2 1/2 | A36 | |
| L32 | 6 | L4 x 3 1/2 x 1/4" | 1 | 2 1/2 | A36 | |
| L41 | 2 | L4 x 3 1/2 x 1/4" | 2 | 0 | A36 | |
| | | | | | | |
| WT11 | 6 | WT5x22.5 | 0 | 8 1/2 | A992 | |
| WT21 | 6 | WT5x22.5 | 0 | 11 1/2 | A992 | |
| WT31 | 6 | WT5x22.5 | 1 | 2 1/2 | A992 | |
| WT41 | 2 | WT5x22.5 | 2 | 0 | A992 | |
| | | | | | | |
| PL81 | 2 | PL 1/2" x 3 1/2" | 0 | 3 1/2 | A36 | |
| | | | | | | |
| R1 | 2 | 1 1/2" DIA - 12 THREADED ROD | 3 | 0 | A193 B7 | (2) NUTS |
| | | | | | | |
| | | FIELD BOLTS | | | | |
| | | | | | | |
| | 475 | 3/4" DIA A325X | 0 | 2 1/2 | | DTI WASHER |

| | |
|-------------|--------------------------|
| ELECTRODE: | E70XX |
| BOLTS: | 3/4" A325 |
| OPEN HOLES: | 13/16" |
| PAINT: | PRIMER ONLY |
| REVISION: | DIMENSIONAL ADJUSTMENTS |
| B | RELEASED FOR FABRICATION |
| | |
| | |

VANBUSKIRK - MORACHE
MSOE THESIS TEST SPECIMEN
AE-8900 2018-2019

SHEET:
TEST ASSEMBLY
CONNECTION MATERIAL

| | | |
|-----------|-----------|----------|
| DRAWN: | DATE: | JOB NO.: |
| MAM | 8/20/2018 | AE-8900 |
| CHECKED: | DATE: | SHEET: |
| MLV | 8/20/2018 | 4 |
| APPROVED: | DATE: | REV.: |
| CHR | 9/07/2018 | B |

Architectural Engineering

Capstone Report Approval Form

Master of Science in Architectural Engineering -- MSAE

Milwaukee School of Engineering

This capstone report, entitled “Experimental Evaluation of Axial, Shear, and Moment Forces of Double Angle Connections when Subjected to Unanticipated Loading,” submitted by the student Max A. Morache, has been approved by the following committee:

Faculty Advisor: _____ Date: _____

Dr. Christopher Raebel, Ph.D.

Faculty Member: _____ Date: _____

Dr. Todd Davis, Ph.D.

Faculty Member: _____ Date: _____

Mr. Adam Friedman